2018

USING THE FROG EPIDERMIS TO UNCOVER DESMOSOME FUNCTION AND REGULATION IN THE DEVELOPING EMBRYO

Navaneetha Krishnan Bharathan
Virginia Commonwealth University

USING THE FROG EPIDERMIS TO UNCOVER DESMOSOME FUNCTION AND REGULATION IN THE DEVELOPING EMBRYO

A dissertation submitted in partial fulfillment of the requirements for the degree of Doctor of Philosophy at Virginia Commonwealth University

by

NAVANEETHA KRISHNAN BHARATHAN
Bachelor of Technology, SRM University, 2011
Master of Science, Virginia Commonwealth University, 2014

Director: AMANDA J. DICKINSON, Ph.D.
ASSOCIATE PROFESSOR
DEPARTMENT OF BIOLOGY
DEPARTMENT OF HUMAN AND MOLECULAR GENETICS

Virginia Commonwealth University
Richmond, Virginia
April 2014

ACKNOWLEDGEMENT

Working on this project only brought me closer to loving the world of scientific research. During the four years I spent working on this project, I had a lot of amazing experiences inside and out of the lab. It was peppered with moments of extreme doubt and depression but fortunately, I had the help of so many people to get me though these episodes.

First, I have to thank my mentor, Dr. Amanda Dickinson, who has been the most supportive boss one could ask for. Amanda has helped me with my scientific endeavors whether it has been me performing some out-of-the-box experiments, being involved with science communication, or a multitude of other pursuits. Somehow, intentionally or not, she always knows when to provide words of encouragement. Her advice has helped me become a better critical thinker and scientific writer. Most importantly, however her actions have molded me to become a more empathetic person to everyone around me.

Next, I thank Dr. Jim Lister, who has been involved the longest in my scientific career at VCU, first as my mentor during my M.S. project, and now as my committee member. His subtle jokes and Vulcan salutes will always provide a quiet chuckle from time to time.

I thank Dr. Rita Shiang, both for her valuable advice as a committee member, and as an extraordinary advisor. I am grateful for her constant support and empathy through my education at VCU.

I thank my committee member, Dr. Gregory Walsh, who leads me down a whole new train of thought with a simple question.

I thank my committee member, Dr. Daniel Conway, whose suggestions and guidance have inspired me to love the world of cell adhesion.

I would be remiss if I did not thank the greatest lab members one could ask for. Nathalie Houssin and Stacey Wahl have answered way too many of my questions. Allyson Kennedy, whose laugh can be heard three doors down, thank you. I thank Brent Wyatt, who, even through his silence, is a great source of encouragement. I thank Deb Pridgen Howton, without whom I never would have learned so much about our beloved frogs. I thank all the people who have passed through our lab including Nadine, Jatin, and Skyler. I am very grateful to Morgan van Driest and Joey Thompson who helped me with my experiments.

Next, I thank my dad without whom I would not be here. His struggles in the last two decades have all been to give me a better life. He is one of the most helpful humans on the planet, and I hope I am at least half the person he is.

I thank my mom, who isn't here with us, but has always tolerated and accepted my breaking away from tradition. I especially thank Drs. Shiang and Lister, whose actions during my mother's passing have made me take immense pride in being a member of the VCU community.

I thank my twin, my sister Harini, who is one of the kindest people I know. Her parcels of chocolates and messages of support are the best indicators of her love.

I am grateful to the Spencers, who have been a second family here in Richmond. They have made my life here more enjoyable and full.

I thank Maciej Gonek, for being an amazing friend and great source of laughter when he loses at mini-golf.

I give an honorable mention to Dave Brohawn, only because he asked me to.

I cannot go without thanking, my partner, best friend and fellow scientist, Sam Spencer, who is simply the most amazing individual. She has provided me with a great appreciation of music from the 80s and her dark sense of humor can bring me to tears. Our conversations about science gives me countless perspectives and for all these, I thank her.

Finally, Dr. Michael Crichton, for Jurassic Park, which, despite some scientific inaccuracies, sparked my love for genetics, I thank you.

TABLE OF CONTENTS

LIST OF TABLES

LIST OF FIGURES

LIST OF ABBREVIATIONS

AJ – Adherens junction

CA-JNK – Constitutively-active JNK

CMO – Control morpholino

CT – C-Terminal region

D. rerio – Danio rerio

DP-NTP – Desmoplakin-N-terminal Peptide

Dsc – Desmocollin

Dsg – Desmoglein

Dsp – Desmoplakin

EGFP – Enhanced Green Fluorescent Protein

EGTA – Ethylene glycol-bis(β-aminoethyl ether)-N,N,N',N'-tetraacetic acid

H. sapiens – Homo sapiens

hpf – Hours post fertilization

IF – Immunofluorescence

JNK – c-Jun N-terminal kinase

K5/ K14 – Keratin 5/ Keratin 14

M. musculus – Mus musculus

MCC – Multiciliated cell

MeOH – Methanol

mGFP – Membrane-Green Fluorescent Protein

MO – Morpholino

ORF – Open Reading Frame

PCR – Polymerase Chain Reaction

Pg – Plakoglobin

Pkp - Plakophilin

PNA – Peanut Agglutinin

PRD – Plakin Repeat Domain

RT-PCR – Reverse Transcription PCR

SH – Src homology domain

SR – Spectrin Repeat domain

SSC – Small secretory cell

TEM – Transmission Electron Microscopy

TJ – Tight junction

WT – Wild-type

X. laevis – *Xenopus laevis*

X. tropicalis – *Xenopus tropicalis*

ABSTRACT

USING THE FROG EPIDERMIS TO UNCOVER DESMOSOME FUNCTION AND REGULATION IN THE DEVELOPING EMBRYO

By Navaneetha Krishnan Bharathan, Ph.D.

A dissertation submitted in partial fulfillment of the requirements for the degree of Doctor of Philosophy at Virginia Commonwealth University

Virginia Commonwealth University, 2018

Major Director: Dr. Amanda J. Dickinson
Assistant Professor, Department of Human and Molecular Genetics

The desmosome is one of the major cell adhesion junctions found in the epithelia, heart, and hair follicle. Described as a "rivet" that hold cells together, it provides these tissues with the integrity to withstand the tremendous forces they face in everyday life. Defects in this junction can lead to devastating diseases where patients are susceptible to skin infections and cardiovascular defects. Limited treatments exist for diseases of the desmosome, and strategies do not target all symptoms. Therefore, delineating the function and regulation of desmosomes is of paramount importance for the development of prevention and treatment strategies. The *Xenopus laevis* has been utilized for the study of embryonic development and tissue movements. This study takes advantage of the frog model to study a key desmosomal protein, desmoplakin (Dsp), in the

epidermal development of the embryo. First, *Xenopus* embryonic epidermis has junctional desmosomes as early as the blastula stages. Desmosomes numbers per junction increase as the embryo develops. Dsp is present in many epidermally-derived structures in the embryo at varying levels. *Xenopus* embryos deficient in desmoplakin have phenotypic defects in epidermal structures and the heart, mimicking mammalian models. Embryos with reduced Dsp exhibit an increased susceptibility to epidermal damage under applied mechanical forces. Assays also reveal a potential role for desmosomes in radial intercalation, a process through which cells move from the inner to the outer epidermal layers. Embryos with reduced Dsp exhibit a slight reduction in intercalation and defects in intercalating cell types, including multiciliated cells and small secretory cells. Finally, c-Jun N-terminal kinase (JNK) may have a potential role in the regulation of desmosome assembly and adhesion. Embryos with deficient Dsp display a partial recovery of mechanical integrity when treated with a JNK inhibitor.

CHAPTER 1: THE ROLE AND REGULATION OF DESMOSOMES IN THE *XENOPUS LAEVIS* EMBRYONIC EPIDERMIS

INTRODUCTION

Desmosomes or *macula adherens* are junctional complexes that mediate cell-cell adhesion, along with tight junctions and adherens junctions. Their strong adhesion confers the mechanical integrity to withstand stresses experienced by the skin and heart (Collins and Garrod, 1994; Garrod, 1993). Desmosome function has largely been investigated in the context of cell adhesion and disease. As a consequence, little is known regarding the regulation of desmosomes during development *in vivo* and their function in morphogenesis. The current study makes use of the vertebrate frog model, *Xenopus laevis*, to investigate desmosome function and regulation during embryonic development.

XENOPUS LAEVIS AS A MODEL ORGANISM

The African clawed frog, *Xenopus laevis*, is an allotetraploid aquatic amphibian species of the order Anura. Over the last 100 years, this species along with the related diploid species, *Xenopus tropicalis*¸ have been extensively utilized for biological research and medical applications. For example, these organisms have been used to study various aspects of cellular and developmental biology including gastrulation, cell movements, and signaling pathways (Tandon et al., 2017).

Xenopus laevis possesses many characteristics that have led to its emergence as a model organism. First, many embryos (500-2000+) can be obtained in a single clutch, providing statistical power to experiments. Second, the egg size is relatively larger (1-1.3mm) than other aquatic vertebrates including X. tropicalis (0.7-0.8mm) and the zebrafish, *Danio rerio* (0.7mm) (Hirsch et al., 2002; Kimmel et al., 1995). The large egg size allows one to easily manipulate the embryo by microinjection of morpholinos, mRNA, plasmid constructs, or protein. Over the last decade, the genetic manipulation toolkit has expanded to include I-SceI meganuclease, Transcription Activator-Like Effector Nucleases (TALENs), and CRISPR/ Cas, thus making it possible to create genetically manipulated organisms (Ishibashi et al., 2012; Joung and Sander, 2013; Lei et al., 2012; Sater and Moody, 2017; Tandon et al., 2017). Third, fate maps for the embryonic blastomeres are well-characterized in *X. laevis*, allowing one to study tissue-specific functions of a gene or protein (Dale and Slack, 1987; Moody, 1987; Moody and Kline, 1990). Additionally, external fertilization and detailed staging of early embryonic development make this organism well-suited for the study of organogenesis and use in chemical drug screening (Dickinson, 2016; Harland and Grainger, 2011; Nieuwkoop and Faber, 1967; Schmitt et al., 2014).

X. tropicalis is a diploid organism with 2n=20 chromosomes, while *X. laevis* is an allotetraploid organism with 2n=36 chromosomes. Based on protein-coding gene phylogeny, the ancestors of *X. laevis* and *X. tropicalis* are believed to have diverged around 48-65 Mya (Evans et al., 2004; Hellsten et al., 2007; Matsuda et al., 2015; Session et al., 2016). The ancestor of *X. laevis*, now thought to be extinct, had 18 chromosomes (2n) (Evans, 2008), and a whole genome duplication (allotetraploidization) event around 17 Mya led to the emergence of *X. laevis* (Chain and Evans, 2006; Evans et al., 2004; Hellsten et al., 2007; Hughes and Hughes, 1993; Session et al., 2016).

The allotetraploidization of *X. laevis* resulted from the convergence of two 18-chromosome species. The genetic contribution of both ancestral species appears to be cytologically distinct from each other, forming bivalents instead of quadrivalents during meiosis (Tymowska and Kobel, 1972; Uno et al., 2013). Recently, these two "subgenomes" were designated "L" (Long) and "S" (Short) for their relative differences in chromosome length(Matsuda et al., 2015). Each of the 9 pairs of chromosomes in the L subgenome are found to be homologous to those in the S subgenome based on similarities in chromosome morphology and banding patterns as well as comparative phylogenetic mapping (Krylov et al., 2010; Matsuda et al., 2015; Tymowska and Kobel, 1972; Uno et al., 2013). Further genetic analysis revealed large deletions in the S subgenome. Genes already present in multiple copies are more likely to be retained, such as Hox clusters. However, genes involved in DNA repair and metabolic enzymes, for example, are lost, suggesting deletion due to selection pressure (Session et al., 2016).

Despite the allotetraploidy of *X. laevis*, development and sequencing of the inbred J strain has made it a more tractable model (Gantress et al., 2003; Pearl et al., 2012; Session et al., 2016).

DEVELOPMENT OF THE EMBRYONIC EPIDERMIS

The epidermis or skin plays pivotal roles in regulating body temperature as well as protection from dehydration and infection. The human epidermis arises as a bi-layer from the embryonic surface ectoderm sometime after neurulation (4 weeks) (Breathnach and Wyllie, 1965; Holbrook and Odland, 1975). The outer protective layer of cells is called the periderm, and functions as the embryonic epidermis *in utero* until about 5 months (Haslam et al., 2014). The periderm is marked by expression of simple epithelial keratins K8/K18 (Jackson et al., 1981; Moll et al., 1982). The inner or basal layer is considered the epidermis proper, expressing K5/K14 (Lourenco et al., 2008). This basal layer eventually gives rise to the remaining layers.

At around 8 weeks, adherens junction proteins including E-cadherin, P-cadherin, α catenin, and α actinin are expressed in the bi-layer (Fujita et al., 1992; Hentula et al., 2001; Lourenco et al., 2008). Tight junctions are also visible between peridermal cells and ZO-1 and occludin expression have been demonstrated (Pummi et al., 2001). During this time, the basal layer undergoes mitosis and gives rise to the intermediate cell layer which matures into the spinous layer expressing K1/K10 (Dale et al., 1985). This layer arises from asymmetric cell divisions and a spindle shift in the basal layer from lateral to perpendicular (Lechler and Fuchs, 2005).

Between 9-20 weeks, the number of desmosomes in the spinous layer increases as it proliferates (Dale et al., 1985; Holbrook and Odland, 1975). By 21-24 weeks post-coitus, the spinous cells proliferate and migrate outward, giving rise to the granular and cornified layers (Holbrook, 1983). The granular layer expresses transglutaminase and involucrin, while the cornified layer is marked by filaggrin and loricrin expression (Koster and Roop, 2007). Finally, keratinization proceeds as the cornified layer becomes flattened and the periderm is shed into the amniotic fluid (Holbrook and Odland, 1980). This process leads to the formation of the stratum

corneum that functions as a barrier (Liu et al., 2013). This final configuration of the stratified epidermis is maintained through adulthood.

The *Xenopus* epidermis also develops from a bi-layered ectoderm (Chalmers et al., 2003; Itoh et al., 1988). The single-layered 32-cell stage embryo develops an inner layer through asymmetrical division (Chalmers et al., 2003). As the embryo progresses into the 1024-cell stage, the number of layers increases and eventually thins out to two layers at the animal cap, forming the prospective epidermis (Haslam et al., 2014).

As the embryos progresses through gastrulation (st. 12-15), specialized cell types are specified in both layers. The outer layer eventually forms mucus-secreting goblet cells. During neurulation (st. 19), the specified cell types of the inner layer integrate into the goblet cells of the outer layer (Deblandre et al., 1999). The inner basal layer is maintained in a proliferative state, similar to the mammalian embryonic epidermis. The *Xenopus* epidermis remains as a bi-layer until metamorphosis.

During metamorphosis, the basal layer proliferates further and gives rise to the five-layered adult skin (Duellman and Trueb, 1994; Itoh et al., 1988). *Xenopus* epidermis can also become keratinized (stratum corneum) like that of mammals, although to a lesser extent. However, this corneal layer is not present in fish, marking the evolutionary transition from aquatic to terrestrial life (Fox, 1986; Schempp et al., 2009). Together, these similarities make the *Xenopus* epidermis a suitable model for the study of embryonic development in general.

The specialized cell types in the *Xenopus* embryonic epidermis include the multiciliated cells, ionocytes, and small secretory cells. These cells move from the inner to the outer epidermal layer through a process known as radial intercalation. While these cell types are not present in the mammalian epidermis, they are found in other epithelia (Billett and Gould, 1971). For example,

multiciliated cells are found lining the human airways (Hayes et al., 2007). Ionocyte-like cells are found in transporting epithelia of the mammalian kidney (Oliver, 1944; Wall, 2005). These features validate the use of *Xenopus* embryonic epidermis as a model for radial intercalation and the development of specialized epithelia.

RADIAL INTERCALATION IN THE *XENOPUS* EPIDERMIS

Radial intercalation is a process by which cells in adjacent layers throughout a multilayered tissue exchange places with each another (Walck-Shannon and Hardin, 2014). This process is known to occur in *Drosophila melanogaster* mesoderm to facilitate spreading, eventually forming a monolayer (Clark et al., 2011; McMahon et al., 2010; McMahon et al., 2008). Deep cells in the zebrafish embryo undergo radial intercalation to drive epiboly (Kane et al., 2005). In the gastrulating *Xenopus* embryo, these movements occur in the chordamesoderm (Wilson and Keller, 1991).

The *Xenopus* embryonic epidermis also undergoes radial intercalation. The outcome of these movements is the incorporation of specialized cell types into the outer epidermal layer at two separate timepoints. Development of these cell types in the bi-layered ectoderm occurs through four major steps. First, precursors of ionocytes and multiciliated cells are specified in the inner layer of the ectoderm during gastrulation. At the same time, the outer layer is specified into goblet cells. Second, ionocytes and multiciliated cells intercalate into the outer layer beginning at neurulation. Third, these cells fully differentiate once they have been apically "docked" into their final position (Deblandre et al., 1999). Finally, small secretory cells intercalate into the outer layer during a second wave of intercalation (Cibois et al., 2014; Dubaissi et al., 2014). Many factors are involved in the specification, intercalation, and differentiation of each of the cell types.

Lateral inhibition through the Notch pathway restricts the fate of precursors in the inner layer (Deblandre et al., 1999; Drysdale and Elinson, 1992). Cells expressing the Notch ligand, Delta-1, adopt the differentiated cell fate while repressing this fate in neighboring cells where it activates the Notch receptor (Bray, 2006; Deblandre et al., 1999). This mechanism results in an organized spacing pattern of these cells.

The specification of the different cell types is controlled by many factors. In multiciliated cell specification, Notch pathway inhibition leads to activation of Multicilin, a transcriptional regulator that is necessary and sufficient for the multiciliated cell fate (Stubbs et al., 2012). Gmnc (geminin coiled-coil domain containing) has been identified as an upstream activator of multicilin (Zhou et al., 2015). Multicilin in turn activates FoxJ1, a master regulator of motile ciliogenesis (Stubbs et al., 2008). Additionally, the transcription factor, Rfx2, targets genes involved in cilia assembly, motility, and planar polarization of directional beating (Chung et al., 2014; Chung et al., 2012). Other factors that are expressed in ciliated cell precursors, such as Sox7, may also play roles in differentiation (Fawcett and Klymkowsky, 2004). The differentiated multiciliated cell facilitates mucus-clearance from the epidermis and might also help in oxygen uptake through the skin before hatching (Billett and Gould, 1971; Deblandre et al., 1999; Mueller and Seymour, 2011).

Ionocytes are also specified by Notch inhibitory signaling through another target, FoxI1e. This transcription factor can activate genes encoding proton-pump subunits and anion antiporters such as pendrin and ae1. Additionally, expression of grainyhead-like transcription factor *ubp1* can regulate the formation of alpha- and beta-subtypes (Quigley et al., 2011). Ionocytes are required for ionic regulation of the embryo and also have non-autonomous roles in proper development of cilia in multiciliated cells (Dubaissi and Papalopulu, 2011).

Multiciliated cells and ionocytes are specified during gastrulation and intercalate during neurulation (st. 15-19). However, small secretory cells intercalate sometime after embryonic hatching (st. 32). Development of these cells is controlled by Foxa1. The Lectin Peanut Agglutinin (Lectin PNA) binds the carbohydrate sequence Gal-β(1-3)-GalNAc present in vesicular secretions and can be used to identify these cells. Mass spectrometry analysis of this material revealed glycosylated Otoglein-like protein which may contribute to the protective mucus layer on the epidermis (Dubaissi et al., 2014). Together, all these specialized cell types are thought to work in concert to provide resistance to bacterial infections (Stubbs et al., 2006).

ADHERENS AND TIGHT JUNCTIONS

The intercellular junctions in epithelial and endothelial tissues comprise the tight junctions (*zonula occludens*), adherens junctions (*zonula adherens*), the desmosomes (*macula adherens*), and gap junctions. The first three junctions help maintain an adhesive tissue. In the skin, adherens junctions play a vital role in intercellular adhesion. However, they also mediate intracellular signaling, cell polarity, and cell sorting (Gottardi et al., 2001; Niessen and Gottardi, 2008; Perrais et al., 2007; Wang and Margolis, 2007; Wei et al., 2005). Tight junctions serve as a semi-permeable barrier in the skin where they protect against trans-epidermal water loss (Furuse et al., 2002; Hadj-Rabia et al., 2004; Niessen, 2007). Tight junctions also function as a paracellular barrier, restricting flow based on size and charge (Larre et al., 2014). Also similar to adherens junctions, tight junctions can participate in signaling pathways (Gonzalez-Mariscal et al., 2014; Zihni et al., 2014).

THE DESMOSOME AND ITS COMPONENTS

The desmosome appears as an electron dense structure in an electron micrograph and consists of 3 main families of proteins - cadherins, armadillo proteins, and the plakins (**Fig. 1.1**). The desmosomal cadherins, desmogleins (Dsg) and desmocollins (Dsc), form the transmembrane components of the desmosome. In humans and mice, four desmoglein genes (Dsg 1-4) and three desmocollin genes (Dsc 1-3) have been identified. Furthermore, all three desmocollins are alternatively spliced into two distinct isoforms (a and b) (Collins et al., 1991; Parker et al., 1991). Depending on tissue type and availability, the desmosomal cadherins can form homo- or hetero-dimers in a *cis*- fashion and bind to apposing cadherins in a *trans*- fashion (Delva et al., 2009; Green and Simpson, 2007).

The desmosomal cadherins are made up of several functional domains. At the N-terminus, there are extracellular subdomains including four extracellular cadherin domains (EC1-4) which are required for dimerization (Pokutta and Weis, 2007). The presence of a cell adhesion recognition (CAR) site contributes to adhesion. At the C-terminal region of desmogleins and the "a" isoform of desmocollins, there is an intracellular cadherin-like sequence (ICS) domain. In the desmocollin "b" isoform, this domain is truncated and has additional unique amino acids. The ICS domain enables binding to the armadillo protein, plakoglobin (Pg) (Mathur et al., 1994; Roh and Stanley, 1995; Troyanovsky et al., 1994).

The armadillo family of proteins, among others, include β-catenin, α-catenin, p-120 catenin, plakoglobin (γ-catenin), and the plakophilins. They are named for the presence of distinctive armadillo repeats of a ~42 amino acid motif (Peifer et al., 1994; Peifer et al., 1992). In the desmosome, plakoglobin (Pg) and plakophilin (Pkp) are present and attach to the cytoplasmic tail of the desmogleins and desmocollins (Kowalczyk et al., 1994; Mathur et al., 1994).

Plakoglobin is analogous to β-catenin in the adherens junction (Butz et al., 1992; McCrea et al., 1991). It has also been found to associate with both desmosomes and adherens junctions (Cowin et al., 1986). Additionally, plakoglobin has some overlapping roles with β-catenin, and can bind to TCF/ LEF factors (Simcha et al., 1998; Zhurinsky et al., 2000). In humans, there are three plakophilin genes (Pkp 1-3) which have differential expression in epithelial and cardiac tissues. For example, Pkp1 is expressed in the suprabasal layers of the multi-layered epidermis, whereas Pkp2 is expressed more ubiquitously in simple, stratified, and complex epithelia, as well as cardiomyocytes (Hatzfeld, 2007; Hatzfeld et al., 1994; Kapprell et al., 1988; Mertens et al., 1996; Mertens et al., 1999; Schmidt et al., 1997). Plakophilin 3 is expressed in most simple and stratified epithelia and is expressed in all epidermal layers (Bonne et al., 1999). All three plakophilins have two alternatively spliced isoforms (a and b) (Mertens et al., 1996; Muhmer et al., 2014; Schmidt et al., 1997). Plakophilins are found to associate with desmosomal cadherins, plakoglobin, desmoplakin, and even the intermediate filaments, indicating that they are important desmosomal proteins (Hatzfeld, 2007)

The plakin family of desmosomal proteins include desmoplakin (Dsp), epiplakin (Epi), periplakin (Ppl), envoplakin (Evpl), plectin, and BPAG (bullous pemphigoid antigen) to name a few. Proteins in this family bind to the underlying cytoskeleton mainly to intermediate filaments (IF). Through this interaction, they tether the IF to cell-cell or cell-matrix junctions (Green et al., 1992; Stappenbeck et al., 1993). Some plakins have also been found to interact with actin and microtubules (Roper et al., 2002). Plakins have characteristic domains which enable them to dimerize (such as the alpha-helical coiled-coil domain) and to attach to intermediate filaments (such as the plakin repeat domains (PRD)) (Jefferson et al., 2004; Leung et al., 2002). At the N-

terminal region, Dsp, for example, has a plakin domain comprising spectrin repeats (Virata et al., 1992).

The intermediate filaments comprise several cytoskeletal proteins including epithelial keratins, mesenchymal vimentin, muscle desmin, and the nuclear lamins (Conway and Parry, 1988; Herrmann and Aebi, 1998). They are so named because their average diameter (10nm) lies between the diameters of the other two major cytoskeletal proteins, actin microfilaments (7nm) and microtubules (25nm). Most IFs have a 45nm central α-helical rod domain flanked by non-α-helical domains. The epithelial keratins are made up of Type I (acidic) and Type II (basic) keratins that form heterodimers. The first step is the formation of a coiled-coil dimer of the Type I and Type II keratins stabilized by a cysteine cross-link (Hatzfeld and Weber, 1990). This step is followed by anti-parallel association of dimers forming a tetramer, called a protofilament (Steinert et al., 1993). These units further dimerize and tetramerize to form the keratin filament (Aebi et al., 1988; Goldie et al., 2007; Herrmann et al., 2009). Humans have over 60 epithelial keratins which are expressed in a cell-type specific manner. For example, K5/ K14 are expressed in the proliferating basal layer of the epidermis, while K1/K10 are expressed in the differentiated suprabasal layers (Fuchs and Green, 1980; Roop et al., 1987). Each keratin is vital to normal embryonic development, with little compensation by the remaining keratins. For example, K14 knockout mice have postnatal lethality with extensive blistering (Chan et al., 1994). K1/ K10 double knockout mice also have postnatal lethality probably due to loss of nuclear integrity during differentiation (Wallace et al., 2012). Together, these proteins provide integrity to the cell and mechano-transduction, i.e., generation of molecular signals in response to a mechanical stimulus (Brooke et al., 2012; Green and Simpson, 2007).

In an electron micrograph, the desmosome appears as a highly organized electron-dense structure. The electron-dense nature of the plaque is indicative of negatively-charged polar groups. The desmosome consists of 3 main families of proteins: cadherins, armadillo proteins, and plakins. The desmosomal cadherins, desmogleins (Dsg) and desmocollins (Dsc), form the transmembrane components of the desmosome. In humans and mice, four desmoglein genes (Dsg 1-4) and three desmocollin genes (Dsc 1-3) have been identified (Green and Simpson, 2007). These cadherins can form homo- or hetero-dimers in a *cis*- fashion and bind to opposing cadherins in a calcium-dependent *trans*- arrangement (Chitaev and Troyanovsky, 1997; Marcozzi et al., 1998; Syed et al., 2002). Intracellularly, the cadherin tails interact with armadillo proteins, plakoglobin and plakophilin (Kowalczyk et al., 1994; Mathur et al., 1994). The armadillo proteins in turn interact with plakin family proteins, most notably, desmoplakin (Hatzfeld, 2007; Hatzfeld et al., 2000). The plakin proteins tether the desmosome to the underlying cytoskeletal intermediate filaments such as keratin (Green et al., 1992; Stappenbeck et al., 1993) (**Fig. 1.1**). Desmoplakin is a protein that is unique to and present in all desmosomes. Studies have revealed a reduction of desmosome number and size in desmoplakin knockout models (Gallicano et al., 1998). Therefore, in the current study, desmoplakin is used as a proxy to determine the role of desmosomes.

HUMAN DISEASES OF THE DESMOSOME

In mammals, desmosomes are predominantly found in various epithelia, the heart, and hair follicle. They have been described as rivet-like structures facilitating cell-cell adhesion (Alberts, 1994). Along with underlying intermediate filaments, this complex also provides mechanical integrity to the skin and heart which are regularly subjected to physical forces (Green et al., 1998; Russell et al., 2004). Perturbations of the desmosome and its components have been implicated in human disease. Not surprisingly, these diseases have manifestations in the epithelia, the heart, and

hair, either separately or in combination (Brooke et al., 2012). Some of the most devastating desmosomal diseases are auto-immune. Pemphigus Foliaceus and Pemphigus Vulgaris present with acantholysis and blistering of the skin and mucosal membranes, respectively (Payne et al., 2004). Auto-antibodies are directed against DSG1 in Pemphigus Foliaceus and both DSG1 and DSG3 in Pemphigus Vulgaris leading to disease symptoms (Amagai et al., 1991; Ding et al., 1997; Ishii et al., 1997). Studies in mice suggest that Pemphigus vulgaris sera may cause endocytosis of Dsg3, possibly through steric hindrance, which might contribute to morphological symptoms such as the acantholysis observed in Pemphigus vulgaris patients (Amagai et al., 1995b; Calkins et al., 2006; Jolly et al., 2010; Tsunoda et al., 2003).

Desmosomal proteins can also be targeted by infectious pathogens. Infectious diseases such as Bullous impetigo and its generalized form, Staphylococcal Scalded Skin generally affect children under 5 years of age and immunocompromised individuals (Hanakawa et al., 2002; Hanakawa et al., 2003; Melish and Glasgow, 1970; Nishifuji et al., 2008). In these diseases, DSG1 is targeted by the causative Exfoliative toxins (ET), which are glutamate-specific serine proteases that cleave DSG1 (Hanakawa et al., 2002; Hanakawa et al., 2003).

Desmosomal diseases can also be inherited in an autosomal dominant or recessive manner (Celentano and Cirillo, 2017; McGrath, 2005). Plakophilin 1 (PKP1) was the first desmosomal protein to be linked to hereditary skin disease. Complete loss of PKP1, which is normally found in the suprabasal layer, is found to result in ectodermal dysplasia/ skin fragility syndrome (McGrath et al., 1997). Autosomal dominant mutations in DSG1 can lead to striate palmoplantar keratoderma in the palms of the hand and soles of the feet due to haploinsufficiency (Hunt et al., 2001; Kljuic et al., 2003b). On the other hand, DSG4 mutations lead to defects in hair follicle differentiation with hypotrichosis restricted to scalp, chest, arms, and legs (Kljuic et al., 2003a).

The severity of inherited desmosomal diseases is emphasized by the propensity for ventricular arrhythmias and sudden cardiac death (Delmar and McKenna, 2010). For instance, plakophilin 2 mutations are implicated in arrhythmogenic right ventricular cardiomyopathy, a disease which accounts for 10% of cardiac-related deaths in teens (Gerull et al., 2004; Thomason et al., 2010; van Tintelen et al., 2006).

Inherited mutations in desmoplakin (DSP) are also diverse, resulting in diseases with varying degrees of severity. Autosomal dominant mutations in DSP leading to haploinsufficiency result in SPPK, like patients with DSG1 mutations (Armstrong et al., 1999; Whittock et al., 1999). These mutations are found in the plakin (N-terminal) domain of DSP. A recessive mutation in desmoplakin causes a frameshift in the tail region, perturbing interaction with intermediate filaments (IFs). Patients display dilated cardiomyopathy, woolly hair, and keratoderma – known as Carvajal syndrome - and affected individuals experience heart failure within the teens (Carvajal-Huerta, 1998). Another desmoplakin recessive disease with compound heterozygous mutations termed skin fragility / woolly hair syndrome is reported with similar findings but without the dilated cardiomyopathy (Whittock et al., 2002). These cases reveal that desmosomal diseases are often associated with symptoms in the epithelia, heart and hair. Additionally, these examples highlight the variability in phenotypes when different regions of the same protein are mutated. To design effective therapies, it is important to understand how desmosomal components, including the various functional domains, contribute to proper development and functioning.

USING ANIMAL MODELS TO STUDY DESMOSOME FUNCTION

The prevalence of desmosomal diseases and birth defects has prompted the need for animal models to understand disease pathology. Currently, the mouse model, *Mus musculus*, is the most

popular *in vivo* model used to study desmosome function. Desmosomes are first detected in the blastocyst stage (32- to 64-cell) in the mouse embryo (Ducibella et al., 1975; Fleming et al., 1991; Magnuson et al., 1977). These proteins are expressed after adherens junctions are formed, alluding to desmosomes being dispensable during the initial cleavage stages. In the embryos of the teleost fishes, *Fundulus heteroclitus* and zebrafish (*Danio rerio*), desmosomes begin to appear during mid-gastrula stages (~st. 12.5) (Slanchev et al., 2009; Trinkaus and Lentz, 1967). It is possible that the relatively late appearance of desmosomes in these fishes might be because of the presence of the protective vitelline membrane which may provide structural integrity to the embryo.

Several mouse models illustrate the important roles of desmosomal proteins during the early stages of life (Green and Simpson, 2007). For example, Desmoglein 2 ablation is lethal in the mouse embryo, dying shortly after implantation (Eshkind et al., 2002). Similarly, Desmocollin 3 knockout mice die within the first 2 days of development (Den et al., 2006). Some desmosomal components appear to be dispensable in the early embryo (younger than E10) but reveal important roles after this stage. For example, plakoglobin knockout mice die by E11 due to cardiac abnormalities. Of those that survive until birth, skin fragility is observed (Bierkamp et al., 1996). Targeted ablation of Desmoglein 3 in mice leads to runting, hair loss, and suprabasilar acantholysis (loss of cohesion) in the epidermis (Koch et al., 1997). Skin defects are also observed in Desmocollin 1 knockout mice but acantholysis is instead present in the granular layer in conjunction with hyperproliferation (Chidgey et al., 2001). These studies indicate that desmosomal proteins have a significant role in the early embryo.

DESMOPLAKIN STRUCTURE AND FUNCTION

In humans and mice, desmoplakin has a tripartite domain structure. The N-terminal plakin domain associates with plakoglobin and plakophilin, linking desmoplakin to the desmosomal complex (Al-Jassar et al., 2011; Kowalczyk et al., 1997; Kowalczyk et al., 1999). This domain consists of six spectrin repeats and a Src homology domain (SH3) with unrestricted flexibility which is believed to impart adaptability to mechanical forces (Al-Jassar et al., 2013; Al-Jassar et al., 2011). The rod domain facilitates dimerization of desmoplakin (Green et al., 1990). This domain contains a heptad repeat and is thought to form a coiled-coil dimer which interacts with intermediate filaments (Garrod and Chidgey, 2008; Green et al., 1990; Green et al., 1992). Finally, the C-terminal plakin repeat domain associates with, and is essential for intermediate filament attachment (Choi et al., 2002; Green et al., 1990). This C-terminal tail domain contains three globular subdomains in *H. sapiens* desmoplakin, designated A, B and C, each consisting of 4.6 repeats of a 38-amino acid motif (Green et al., 1990). The periodicity of amino acids in this domain allow interaction with intermediate filaments (Bornslaeger et al., 1996; Choi et al., 2002; Fontao et al., 2003). Together, these domains are critical to proper functioning of desmoplakin, but they have not been analyzed in the *X. laevis* homologs.

Several studies in mice have attempted to determine the role of desmoplakin during embryonic development. Embryos homozygous for a desmoplakin deletion mutation do not survive beyond E6.5 (Gallicano et al., 1998). Most notably, $Dsp^{-/-}$ embryos are significantly smaller, although E-cadherin labelling remain unaffected in the developing endoderm and ectoderm. Keratin 8 (K8) also appear disorganized within the cell, with a collapse of keratin networks to the cell periphery. There is also a >10X reduction in desmosome number and >2X reduction in desmosome size. Since the early lethality was suspected to be due to defects in extra-

embryonic tissues such as the visceral endoderm and the trophectoderm, a tetraploid rescue model was developed (Gallicano et al., 2001). Here, the embryo proper that is homozygous for the *dsp* mutation is cultured along with wild-type tetraploid cells, the latter of which eventually develops into extra-embryonic tissues (Dragatsis et al., 1998; Kupriyanov and Baribault, 1998). These embryos are still significantly smaller with fewer desmosomes. They also have an increased lifespan and survive until E12.5. However, the heart is severely deformed with collapsed epicardial and myocardial layers. The neuroepithelial folds are also greatly reduced usually preceded by defective neural tube closure. Most importantly, the embryonic epidermis displays intercellular separation and detachment from the underlying mesoderm. Interestingly, vasculature development is also perturbed despite no desmosomes being present normally within these tissues. However, desmoplakin is expressed in another junction, the complexus adherents, present in endothelial cells, possibly accounting for this phenotype (Schmelz and Franke, 1993; Schmelz et al., 1994). In an effort to understand epidermis-specific roles of desmoplakin, conditional knockout mice under the Keratin 14 promoter were also examined. There is no defect in the differentiation of the epidermal layers. However ,the epidermis is fragile in these embryos, experiencing intercellular separation under an applied mechanical stress (Vasioukhin et al., 2001).

Desmoplakin has also been implicated in other cellular processes and signaling pathways. For instance, desmoplakin can function as a microtubule organizing center in mouse epidermis. Ninein, a centrosomal protein required for microtubule anchoring is recruited to the desmosomes by Dsp (Delgehyr et al., 2005; Lechler and Fuchs, 2007; Mogensen et al., 2000). There is some evidence for the desmoplakin-intermediate filament connection as a regulator of cellular response to mechanotransductive signals (Broussard et al., 2017). Although no inherited mutations of desmosomal proteins have been found to be oncogenic, downregulation of Dsp can influence

tumorigenesis and invasion. Decreased invasion and increased adhesion are observed when desmosomal components are introduced into normally non-adhesive fibroblasts (Tselepis et al., 1998). Dsp-knockdown keratinocytes exhibit increased proliferation associated with increased phosphor-ERK1/2 and phosphor-Akt levels (Wan et al., 2007). Furthermore, increased tumor invasion is observed in a desmoplakin-deficient mouse model of pancreatic neuroendocrine tumors (Chun and Hanahan, 2010).

REGULATION OF THE DESMOSOMAL COMPLEX AND HYPERADHESION

Embryonic development occurs through the coordination of various processes including cell division, migration, intercalation, and cell death. Maintaining tissue adhesion and integrity during morphogenesis would require precise regulation of desmosome dynamics, for example, through control of transcription and post-translational modifications. Transcription factors associated with regulation of desmosomal gene expression include AP-2, Oct-2, NF-kB, Lef-1, HoxC, and C/EBP (Adams et al., 1998; Bazzi et al., 2009; Johnson et al., 2014; Marsden et al., 1997; Potter et al., 2001). Protein Kinase C alpha (PKCα), EGFR, lipid raft clusters, and plakophilins are documented as regulators of desmosomal assembly and adhesive strength (Bass-Zubek et al., 2008; Garrod et al., 2005; Kimura et al., 2007; Klessner et al., 2009; Miravet et al., 2003; Stahley et al., 2014; Tucker et al., 2014; Wallis et al., 2000; Yin et al., 2005). Furthermore, desmosomal components can regulate signaling pathways. For example, plakoglobin can regulate Wnt/ β-catenin (Chidgey and Dawson, 2007; Conacci-Sorrell et al., 2002; Miravet et al., 2002), p38MAPK (Spindler et al., 2014), and Hippo signaling (Chen et al., 2014). Recent studies also suggest regulation of biochemical and mechanotransductive signaling by desmoplakin (Broussard

et al., 2017; Yang et al., 2012). However, not much is known about the downstream effectors of these signaling pathways.

Cadherins in both adherens junctions and desmosomes require calcium for homophilic binding and maintenance of adhesion at cell contacts. However, desmosomes have a unique property of achieving insensitivity to calcium chelators (such as EGTA) when they mature and are termed "hyperadhesive" (Garrod and Kimura, 2008). Cells with calcium-insensitive desmosomes are in a stronger adhesive state (Kimura et al., 2007). Molecular modeling of the crystal structure of the EC domains of desmosomal cadherins suggests that the Ca^{2+} ion is trapped, making it isolated from calcium chelators (Garrod et al., 2005). Hyperadhesive desmosomes are thought to identified by the presence of an electron-dense midline between apposing desmosome halves under electron microscopy, although direct evidence is yet to be demonstrated.

Hyperadhesive desmosomes were first detected in the stratified epithelia of the *Rana pipiens* (frog) adult skin and cat and rat esophagi as being resistant to EDTA-mediated dissociation (Borysenko and Revel, 1973). In keratinocyte and simple epithelial cell culture, desmosomes begin to assemble when calcium (1.8 - 2mM) is added to the growth medium in as soon as 15 min. (Mattey and Garrod, 1986; Watt et al., 1984). The addition of calcium is also followed by stratification of the monolayer within 24h. Only when confluency is reached are desmosomes demonstrated to achieve hyperadhesion (Wallis et al., 2000). Hyperadhesive desmosomes are also found in the developing mouse embryo. For instance, the first epidermal desmosomes that assemble are sensitive to disruption by calcium chelation but switch to a hyperadhesive nature between E12.0-14.0 (Kimura et al., 2012).

There are many mechanisms found to regulate the adhesive state of the desmosome. Since wound healing is a dynamic process requiring some cell movements, it is not surprising that

desmosomes need to switch from their hyperadhesive state upon wounding. Wallis and colleagues observed the switch to a calcium-sensitive state upon scratch wounding of monolayers (Wallis et al., 2000). Importantly, Protein Kinase C α (PKCα) activation is increased after wounding and is thought to be responsible for the switch from a resistant to calcium-sensitive state. Plakophilin 1 overexpression in keratinocytes transforms desmosomes to a hyperadhesive state (Tucker et al., 2014). Since it is known that Dsp-IF interaction is crucial for maintaining adhesive strength in epithelial sheets, the function of Dsp in hyperadhesion was also explored (Huen et al., 2002). A phosphorylation-deficient mutant of Dsp (S2849G) with increased IF binding leads to increased cohesiveness of cell sheets (Hobbs and Green, 2012). Importantly, being able to modulate the adhesive state of the desmosome might be an effective therapeutic strategy for some desmosomal diseases. Overexpression of Plakophilin 1 or PKC inhibition in keratinocytes induces hyperadhesion and abrogates Pemphigus vulgaris sera-induced loss of adhesion (Cirillo et al., 2010; Tucker et al., 2014). Therefore, being able to identify regulators of desmosomes is beneficial to alleviate the pathophysiology of certain desmosomal diseases.

C-JUN N-TERMINAL KINASE

The c-Jun N-terminal kinase or JNK, also known as stress-activated MAP kinase (SAPK) is a member of MAPK signaling pathways through which cells respond to extracellular stimuli. These stimuli can include UV radiation, pH fluctuations, and heat, as well as chemical stimulation including cytokines, growth factors, and hormones (Davis, 2000; Weston and Davis, 2002).

The MAPK signaling cascade contains at least three MAP kinases in series. MAPKKKs phosphorylate MAPKKs, which phosphorylate MAPKs such as JNK. JNK is activated by dual phosphorylation on Threonine and Tyrosine residues by MKK4 and MKK7 (Davis, 2000; Derijard

et al., 1995; Lin et al., 1995; Moriguchi et al., 1997; Tournier et al., 1997; Yan et al., 1994). MKK4 and MKK7 are known to be activated by ASK1, MLK2, and MEKK2-5 (Blank et al., 1996; Deacon and Blank, 1997; Ellinger-Ziegelbauer et al., 1997; Gerwins et al., 1997; Hirai et al., 1997; Ichijo et al., 1997). However, all these proteins can be differentially regulated. For example, treatment of cells with tumor necrosis factor (TNF) leads to activation of MKK7 but not MKK4 (Takekawa et al., 1997; Tournier et al., 2001; Wang et al., 1996). In contrast, both MKK4 and MKK7 can be activated by environmental stresses. The JNK signaling cascade is thought to be coordinated, in part, by JNK interacting proteins (JIP) that act as scaffolds for JNK cascade elements (Gupta et al., 1996; Kukekov et al., 2006; Xu et al., 2005).

JNK regulates activator protein-1 (AP-1) transcriptional activity through the phosphorylation of various effectors. For example, JNK phosphorylates the transactivation domain of c-Jun on Ser-63 and Ser-73 leading to its stabilization and increased transcriptional activity (Pulverer et al., 1991; Smeal et al., 1991). JNK can also phosphorylate other transcription factors including Junb, JunD, c-Fos, and ATF2 (Ip and Davis, 1998). Together, these proteins constitute the AP-1 transcription factors that regulate stress-responsive genes.

Some of the major effects of the JNK pathway are inflammatory responses and regulation of apoptosis and cell survival. JNK can mediate opposing responses through isoform- or cell-specific mechanisms. For example, JNK1 and JNK2 differentially affect fibroblast proliferation through either promoting or reducing c-Jun stability (Sabapathy et al., 2004). JNK can also have opposite effects on apoptosis, either promoting it by phosphorylating Bim and Bmf, or suppressing it through its effects on Bcl-2 and Bcl-x_L (Donovan et al., 2002; Ferrer et al., 2005; Kharbanda et al., 2000; Lei and Davis, 2003; Yamamoto et al., 1999).

In mammals, there are three JNK genes, JNK1, JNK2, and JNK3, all of which can undergo differential splicing, resulting in a total of 10 isoforms. JNK1 and JNK2 are expressed ubiquitously, while JNK3 is largely restricted the brain, heart, and testis (Bogoyevitch and Kobe, 2006; Davis, 2000). *Xenopus* is also predicted to have all 3 JNK genes, but there is limited expression data at the tissue level (Bagowski et al., 2001). *In situ* hybridization reveals expression of JNK1 in head and dorsal regions of the *Xenopus* embryo after neurulation (Garriock et al., 2005; Yamanaka et al., 2002). Several animal models reveal the importance of JNK *in vivo* during embryogenesis. Single knockout $Jnk1^{-/-}$ and $Jnk2^{-/-}$ mice are viable, with defects in apoptotic and immune responses (Constant et al., 2000; Dong et al., 2000; Dong et al., 1998; Tournier et al., 2000). However, $Jnk1^{-/-}/Jnk2^{-/-}$ double knockout mice exhibit embryonic lethality with decreased apoptosis in the hindbrain, increased apoptosis in the forebrain, and exencephaly (Kuan et al., 1999; Sabapathy et al., 1999).

JNK is also known to regulate embryonic morphogenesis *in vivo*. In *D. melanogaster*, JNK activity positively regulates dorsal closure through DJun and expression of decapentaplegic (related to mammalian BMP-4) in leading edge cells of the dorsal epidermis (Glise and Noselli, 1997; Hou et al., 1997; Kockel et al., 1997; Riesgo-Escovar and Hafen, 1997; Sluss and Davis, 1997). In *Xenopus* embryos, both activation and inhibition of JNK can lead to convergent extension defects (Yamanaka et al., 2002). JNK isoforms are also important for proper development of the epidermis *in vivo*. For example, JNK1-deficient mice exhibit reduced epidermal proliferation and differentiation resulting in a thinner epidermis. However, mice deficient in JNK2 have epidermal hyperplasia, suggesting opposite roles for JNK1 and JNK2 in epidermal development (Weston et al., 2004).

JNK activity is dysregulated in a variety of human diseases affecting many organs. Strong JNK activity has been observed in neurons and the hippocampus in patients with Alzheimer's disease (Shoji et al., 2000; Thakur et al., 2007; Zhu et al., 2001). Furthermore, liver samples from patients with nonalcoholic fatty liver disease are found to have elevated JNK activity (Ferreira et al., 2011). Unsurprisingly, JNK activity is also elevated in diseases with abnormal inflammatory responses including inflammatory bowel disease and rheumatoid arthritis (Mitsuyama et al., 2006; Mun et al., 2009; Schett et al., 2000). Similarly, JNK is activated in psoriatic skin, probably leading to abnormal epidermal proliferation and differentiation (Takahashi et al., 2002). Besides these instances, many cancers including retinoblastoma, melanoma nevi, and colorectal, breast, and ovarian cancers, exhibit altered JNK activity (Chen et al., 2011; Gulmann et al., 2009; Jorgensen et al., 2006; Odegaard et al., 2007; Wang et al., 2010). Therefore, understanding the role of JNK in mediating cellular processes will facilitate the development of therapeutic strategies.

SIGNIFICANCE

Work in the past decade has delineated novel functions of desmosomes in both adhesive and nonadhesive contexts. However, in the context of the whole embryo, much is unknown regarding regulation and function of the desmosomal complex during morphogenesis. The present study reveals roles for desmosomes in epidermal homeostasis and morphogenesis. Furthermore c-Jun N-terminal kinase (JNK) may have a potential role in regulation of desmosome assembly and stability. Notably, this study validates the frog as a tractable vertebrate model to study desmosome regulation and function in the developing embryo.

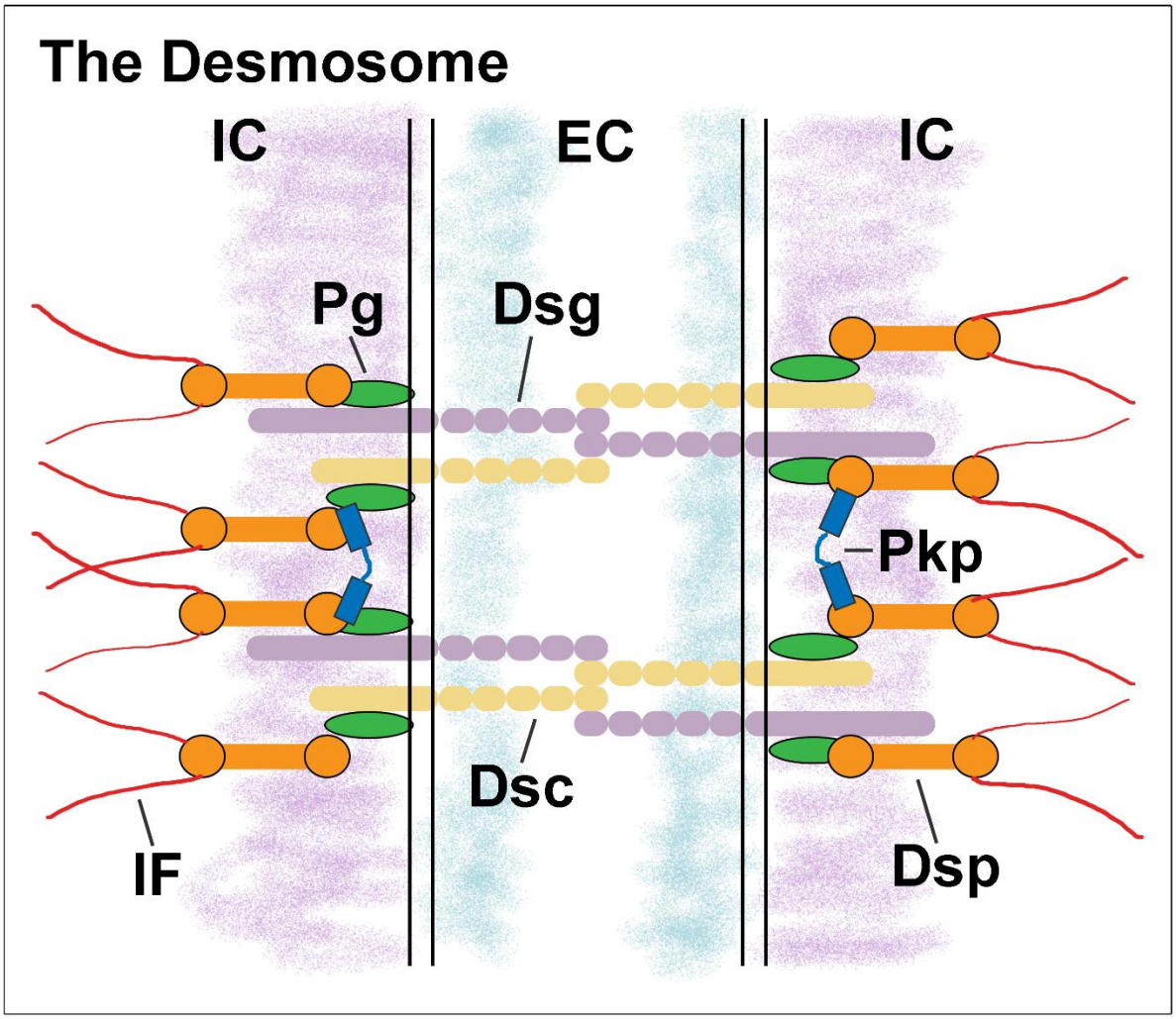

Figure 1.1: The desmosome and its components.
Schematic of a desmosome (adapted from (Garrod, 2010; Green and Simpson, 2007; Staehelin and Hull, 1978; Stahley and Kowalczyk, 2015)). EC=Extracellular space; IC=Intracellular space; Dsg=Desmoglein; Dsc=Desmocollin; Dsp=Desmoplakin; Pg=Plakoglobin; Pkp=Plakophilin; IF=Intermediate Filament.

MATERIALS AND METHODS

A. *XENOPUS* ADULTS AND EMBRYOS

Xenopus laevis embryos were obtained and cultured using standard methods (Sive et al., 2000) approved by the VCU Institutional Animal Care and Use Committee (IACUC protocol number 5AD20261). Embryos were staged according to Nieuwkoop and Faber (Nieuwkoop and Faber, 1967).

B. BIOINFORMATICS ANALYSIS TO COMPARE DESMOPLAKIN EXONIC SEQUENCES

The following full length desmoplakin exonic sequences of the longest isoforms were retrieved from NCBI: *Homo sapiens* Desmoplakin isoform I (NM_004415.3) and *Mus musculus* Desmoplakin (NM_023842.2). *Xenopus laevis* exonic sequences for *dsp.L* (XB-GENE-866134) and *dsp.S* (XB-GENE-17346609) were both obtained from Xenbase (http://www.xenbase.org). To estimate percent identity, pairwise sequence alignments were performed against *X. laevis dsp.L* using the EMBOSS Water tool (Smith Waterman algorithm) (https://www.ebi.ac.uk/) and DNAfull scoring matrix (Li et al., 2015; McWilliam et al., 2013; Rice et al., 2000).

C. BIOINFORMATICS ANALYSIS TO COMPARE DESMOPLAKIN PROTEIN SEQUENCES

The following full length Desmoplakin (Dsp) protein sequences of the longest isoforms were retrieved from NCBI: *Homo sapiens* Desmoplakin I (NP_004406) and *Mus musculus* Desmoplakin (NP_076331) were used for the analysis. To obtain *Xenopus laevis* Dsp.L (XB-GENE-866134) and *X. laevis* Dsp.S (XB-GENE-17346609) protein sequences, coding DNA sequences obtained from Xenbase Genome build Version 9.1 (*X. laevis*) (http://www.xenbase.org) were translated using the ExPASy Translate tool (Gasteiger et al., 2003). To obtain percent identity and similarity, pairwise sequence alignments were performed against *X. laevis* Dsp.L using the EMBOSS Water tool (Smith Waterman algorithm) (EMBL-EBI) with the BLOSUM62 scoring matrix (Li et al., 2015; McWilliam et al., 2013; Rice et al., 2000).

D. DETERMINING DESMOPLAKIN DOMAINS IN *XENOPUS LAEVIS*

To determine coordinates of domains, previously characterized domain coordinates in human DSPI protein was used as a reference (Al-Jassar et al., 2011; Green et al., 1990; Virata et al., 1992). The LALIGN tool (EMBL-EBI) was used to align the amino acid sequence for each human DSP domain with the full-length protein of *M. musculus* Dsp and *X. laevis* Dsp.L and Dsp.S to locate the corresponding regions (Li et al., 2015; McWilliam et al., 2013). This was done using the BLOSUM50 scoring matrix. To obtain percent identity and similarity for each domain, pairwise sequence alignments were performed against corresponding domains in *X. laevis* Dsp.L. The EMBOSS Water tool (Smith Waterman algorithm) (EMBL-EBI) was used with the BLOSUM62 scoring matrix (Li et al., 2015; McWilliam et al., 2013; Rice et al., 2000).

E. MULTIPLE SEQUENCE ALIGNMENT OF DESMOPLAKIN PROTEIN

Multiple sequence alignment of desmoplakin protein sequences of *X. laevis* (Dsp.L and Dsp.S), human, and mouse was performed with Clustal Omega (EMBL-EBI) using the HHalign algorithm (Goujon et al., 2010; McWilliam et al., 2013; Sievers et al., 2011). The threshold for shading (using the BOXSHADE tool) in the Clustal Omega generated sequence alignment was set to 50% using the BLOSUM62 scoring matrix.

F. TEM TO EXAMINE DESMOSOME ULTRASTRUCTURE AND LOCALIZATION IN THE EPIDERMIS

Embryos were fixed with 2% glutaraldehyde (MP Biomedicals, 198595) in 0.1M sodium cacodylate buffer (Electron Microscopy Services, 12300) at 4°C overnight. They were then rinsed in 0.1M cacodylate buffer three times (30 min. each). Embryos were incubated in 0.1M cacodylate buffer for up to 3 days at 4°C and then fixed in 2% osmium tetroxide in 0.1M cacodylate buffer for one hour. They were then rinsed in 0.1M cacodylate buffer three times (15 min. each). They were dehydrated in graded ethanol series (50%, 70%, 80%, 95%) for 5-10 minutes each followed by dehydration in 100% ethanol three times (10-15 min. each). Embryos were then incubated in propylene oxide (EMS, 20401) three times (10–15 min. each). They were then infiltrated with a 50/50 mix of propylene oxide and Poly/Bed 812 resin mix (Polysciences, 08792-1) overnight. This was followed by infiltration with pure EMbed 812 resin (EMS, 14120) mix overnight. Embryos were then embedded in flat molds and placed in 60˚C oven for 2 days. Embryos were sectioned on Leica EM UC6i Ultramicrotome (Leica Microsystems) into 700-900Å thick sections on grids and stained with 5% Uranyl acetate (EMS, 22400) and Reynold's Lead Citrate (Lead Nitrate (EMS,

17900), Sodium Citrate (EMS, 21140)). Grids were imaged on JEOL JEM-1230 TEM (JEOL USA, Inc.) with the Gatan Orius SC1000 digital camera (Gatan Inc., Pleasanton, CA).

G. MORPHOLINOS

Two splice-site blocking desmoplakin (Dsp) morpholinos, DspMO1 (5'-ACAGTTACTACTTACTCTATGCTGC-3') and DspMO2 (5'–TTGATGCAGAGCAAAGTTCAAACCT-3') with fluorescein tags were designed and purchased from Genetools (**Table 1.1**). A standard control morpholino (CMO) provided by Genetools was used as a control for all experiments. 34 ng of DspMO1 was injected per embryo and 17-25ng DspMO2 was injected per embryo. Targeted injections were accomplished with 3-5 ng per blastomere. Microinjections were carried out using a FemtoJet microinjector (Eppendorf) and a SteREO Discovery.V8 (Zeiss) stereoscope.

To determine if the MOs caused splicing defects in embryos, RT-PCR was performed as described previously (Dickinson and Sive, 2009). RNA from 10 embryos was extracted using TRIzol (Invitrogen) followed by lithium chloride precipitation. cDNA was prepared using the High-capacity cDNA Reverse Transcription kit and specific primers (Applied Biosystems) (**Table 1.2**). cDNA was then diluted 1:25 and the following PCR program was performed using Apex™ Hot Start Taq DNA Polymerase Master Mix: (1) 95°C for 5 min., (2) (95°C for 30s, 61°C for 30s, 72°C for 30s) X 40, (3) 72°C for 5 min. Samples were run on a 3% agarose gel to identify distinct banding patterns.

H. CRISPR

CRISPR gRNA sequences were designed against exons 8 (DspCRISPR1) and 19 (DspCRISPR2) in *dsp.L* (these correspond to exons 8 and 17 in *dsp.S*, respectively) using the CHOPCHOP tool (http://chopchop.cbu.uib.no/). sgRNA adaptor sequences and scaffold (loop-sequence oligo) were designed as previously described (Shah et al., 2016) (**Table 1.3**).

The PCR reaction to create a 120 bp product containing gene-specific sequence, T7 primer sequence and loop-specific oligo was as follows: (1) 98°C for 30s, (2) (98°C for 10s, 61°C for 10s, 72°C for 15s) X 45, (3) 72°C for 5 min. The PCR product was then purified using the DNA Clean & Concentrator Kit (Zymo Research, D4014). The Ambion MEGAscript T7 kit (Thermo Fisher Scientific, AM1333) was used for *in vitro* transcription and RNA was preferentially precipitated using the lithium chloride precipitation solution (Thermo Fisher Scientific, AM9480). To create F0 mosaic mutants, embryos were co-injected with 1ng gRNA and 1.5ng Cas9 protein (PNA-Bio, CP01) at the one-cell stage. Wild-type embryos were used as controls.

The T7 endonuclease I assay was used to detect mutations induced by CRISPR/ Cas9 (Mashal et al., 1995). Genomic DNA was extracted by incubating embryos in 35µl of alkaline lysis buffer (25 mM NaOH (Fisher Scientific, BP359), 0.2 mM Na^{2+}-EDTA (OmniPur, 4050)) at 95°C for 40 minutes. The samples were then cooled to 4°C and then 35µl of neutralization buffer (40 mM Tris-HCl (Sigma-Aldrich, T3253)) was added. The target region was then amplified with specific primers (**Table 1.4**). The PCR reaction was: 1. 98°C for 30s, 2. (98°C for 5s, 61°C for 10s, 72°C for 20s) X 36, 3. 72°C for 2min. PCR products were purified with the DNA Clean and Concentrator kit (Zymo Research, D4014), eluted into nuclease-free water, and quantified using the NanoDrop Lite spectrophotometer (Thermo Fisher Scientific). Purified PCR product (200ng) was used in the following protocol: 1. 95°C for 5 min., 2. 95°C-85°C @ -2°C/s, 3. 85°C-25°C @

-0.1°C/s. Then, 1µl of T7 endonuclease I (NEB, M0302) was added and incubated at 37°C for 15 min. Samples were run on a 3% agarose gel to identify presence of mutations.

I. MECHANICAL STRESS ASSAYS

Impact Assay: Embryos were vertically dropped from a height of 15 cm using a transfer pipette (Fisher Scientific, 13-711-7M) onto a 150 X 15mm petri dish lined on the bottom with 5mm of 2% agarose (Bioline, 41025). Images were taken on both left and right lateral sides of the embryos before and after the assay was performed. This was replicated in a blind manner to avoid any handling bias while pipetting embryos. Differences were compared statistically using a Student's t-test.

Rotational Assay: Embryos were placed in 50ml plastic polypropylene tubes (USA Scientific, 1500-1811) with 15 ml 0.1 X MBS (Modified Barth's Saline). The tubes were then rotated using a RKVSD vertical rotating mixer (ATR Biotech) at 55 rpm for a total of 25 rotations. Embryos were then scored as being intact or damaged based on whether the epidermis was intact or not. Differences were compared statistically using a Student's t-test.

J. CONSTITUTIVELY-ACTIVE JNK AND DOMINANT-NEGATIVE DESMOPLAKIN

The previously validated constitutively-active JNK1, MKK7-JNK1A1 (pcDNA3-flagMKK7B2Jnk1a1) (referred here as CA-JNK) construct was obtained from Addgene (ID: 19726) (courtesy of Roger Davis) and cloned into pCS2+ for expression in *X. laevis* embryos (Houssin et al., 2017). The dominant-negative desmoplakin (DP-NTP) construct fused with either

EGFP or mCherry (in pCS2+) was generously provided by Dr. Daniel Conway (Bornslaeger et al., 1996; Huen et al., 2002).

K. CHEMICAL TREATMENTS

To inhibit JNK, embryos were treated with 100µM SP600125 (Sigma-Aldrich, S5567) (Bennett et al., 2001). DMSO was used as the control treatment at a final concentration of 1% in 0.1X MBS.

L. IMMUNOFLUORESCENCE, ANTIBODIES AND FLUORESCENT LABELING

Embryos were fixed in 4% Paraformaldehyde (PFA) or Dent's fixative (80% methanol, 20% DMSO) and then labeled whole or after vibratome sectioning. For sectioning, embryos were embedded in 5% low-melt agarose (SeaPlaque GTG Cambrex) and sectioned using a 5000 Series Vibratome into 150-200µm sections. All antibodies were diluted in 1X PBT. Primary antibodies used were mouse anti-desmoplakin I+II (abcam, ab16434, diluted 1:75), mouse anti α-tubulin (Developmental Studies Hybridoma Bank (DSHB), AA4.3, 1:50), rabbit anti-phospho-Histone H3 (Ser10) (Millipore, 06-570, 1:1000), mouse anti-cytokeratin type II (DSHB, 1h5, 1:25), anti-β-catenin (Invitrogen, 71-2700, 1:500), and mouse anti-E-cadherin extracellular domain (DSHB, 5D3, 1:25). Secondary antibodies used were anti-mouse Alexa Fluor 568 (Molecular Probes, A11004, 1:500), anti-rabbit Alexa Fluor 488 (Molecular Probes, A11008, 1:500), anti-mouse Alexa Fluor 488 (Molecular Probes, A11029, 1:500), anti-rabbit Alexa Fluor 568 (Molecular Probes, A11036, 1:500), anti-mouse Alexa Fluor Plus 647 (Molecular Probes, A32728, 1:500) and anti-rabbit Alexa Fluor 405 (Molecular Probes, A31556, 1:500). To label small secretory cells, a Lectin PNA-Alexa Fluor 488 conjugate (Molecular Probes, L21409, 1:1000) was utilized.

Rhodamine phalloidin (Life Technologies, R415, 1:50) was used to label F-actin. Embryos fixed in PFA were washed three times in 1X PBT (1h each). Embryos fixed in Dent's fix were incubated in 90% MeOH for 10 min., then in 100% MeOH for 10 min. They were then stored at -20°C overnight in 100% MeOH. Embryos were then incubated in a MeOH: PBT (1X) dilution series into 1X PBT. Embryos (fixed in either PFA or Dent's fix) were then incubated in the primary antibody or fluorescent label at 4°C overnight. They were then washed three times in 1X PBT (1h each) and incubated in secondary antibody at 4°C overnight. This was repeated for multiple labels. Embryos were then washed three times in 1X PBT (1h each) and were mounted in 90-100% glycerol for confocal imaging.

For Cleaved Caspase-3 labeling (anti-rabbit, Cell Signaling, 9661, 1:1000), embryos were fixed in 4% PFA (2-3h at RT), embryos and then were washed in PBT and blocked in 1% goat serum/ 1% Triton PBT overnight (Kennedy and Dickinson, 2012). They were incubated in antibody on a nutating mixer at 4°C for 2 days.

M. CONFOCAL MICROSCOPY

Imaging was performed with the Nikon Eclipse Ni-U/ C2 confocal microscope. Step size was maintained at 0.5µm and size of stack was set between 6-12µm. Finally, maximum intensity projections of these stacks were obtained. The NIS-Elements AR 4.50.00 software was used for imaging and processing, including increasing intensity of images where allowed. Additional image processing was performed in Adobe Photoshop Creative Cloud. Brightness of images was increased or decreased to the same level in all images in an experiment.

N. ANALYSIS OF KERATIN RETRACTION IN DSP MORPHANTS

To determine the effect of morpholino-mediated loss of Dsp on keratin organization, additional image analysis was performed using the NIS-Elements AR 4.50.00 software. Maximum intensity projections of confocal images on Keratin-labeled embryos was generated. Using information from an Intensity Profile chart in a linear cross-section, intensity values were obtained for membrane junctions on opposite sides of a cell. These Border Intensity values (BI) were averaged (Avg_{BI}). The coordinates of the 2 borders where intensity was recorded were also noted. Three equidistant points between the two border coordinates above were placed within the cell on the same linear cross-section. Intensity values were calculated at these three points also. These Intracellular Intensity values (ICI) were averaged (Avg_{ICI}). A ratio of (Avg_{BI}/Avg_{ICI}) was obtained for eight random cells in an image (representative of one embryo). Statistical analysis of differences between intensity ratios of Dsp morphants and control morphants was performed using a Student's t-test.

O. BIOTIN LABELING OF THE SUPERFICIAL LAYER

Embryos were incubated from st. 19 (21hpf) to st. 20 (22hpf) in a 2mg/ml solution of EZ-Link Sulfo-NHS-LC-Biotin for 1h (Thermo Fisher Scientific, 21335). Embryos were then transferred to 0.1X MBS to develop for another 4-5h until st. 24 (26hpf). Embryos were then fixed in 4% PFA overnight at 4°C. Embryos were then washed three times in 1X PBT for 1h each and blocked with 1%BSA at RT for 1h. Embryos were labeled with Streptavidin, conjugated to Alexa Fluor 568 (Life Technologies, S11226, 1:500) overnight followed by three washes in 1X PBT for 30 min. each. They were mounted in 90% glycerol and imaged using a confocal microscope.

P. SURFACE AREA MEASUREMENT OF INTERCALATED CELLS

To measure the surface area of intercalated cells, confocal images were processed in Adobe Photoshop CC 2017. Under Image Adjustments, threshold was set such that intercalated cells were visible as distinct cells from the biotin-labeled cells. A scale bar was calibrated for each image. Using the Magic Wand Tool, individual cells were automatically selected and areas were calculated. These measurements were exported to Microsoft Excel and statistical analysis was performed.

Q. EGTA-INDUCED CELL DISSOCIATION

Embryos were treated with either 100µM SP600125 (20µl of 10mM stock in DMSO) or 20µl DMSO in 0.1 X MBS at 15°C from st. 32–41. DMSO was used as the control treatment at a final concentration of 1%. Whole embryos were washed for 1 hour in calcium-free 0.1 X MBS. This was followed by a 4mM EGTA treatment for 30 min. Embryos were then fixed in Dent's fix, labeled for desmoplakin and imaged as described above.

R. STATISTICAL ANALYSIS

Chi-square (χ^2) test for independence was used to determine statistically significant differences in phenotype prevalence. Pooled data from replicates was used for length and phenotype analysis. Mann-Whitney test (GraphPad Prism) was used to determine statistically significant differences in surface areas of intercalating cells. Student's t-test was used to determine statistical significance in the remaining comparisons. All data is representative of at least two independent experiments.

Table 1.1: Morpholino sequences used for injections.

Morpholino	Sequence (5' –> 3')	Subgenome Homolog	Exon/ Intron junction	Match with target site (bp/ bp)
DspMO1	ACAGTTACTACTTACTCTATGCTGC	*dsp.L*	E4/ I4	25/ 25
		dsp.S	E4/ I4	19/ 25
DspMO2	TTGATGCAGAGCAAAGTTCAAACCT	*dsp.L*	E14/ I14	25/ 25
		dsp.S	E12/ I12	22/ 25

Table 1.2: Primers used to genotype morphants.

Morpholino	Forward Primer (5' –> 3')	Reverse Primer (5' –> 3')	Wild-type fragment size (bp)
DspMO1	TAAATATGGAGATGCAAGTCAGC	CAAGATCCCATCGATAGTCAGC	422
DspMO2	CCTGGCACTACTGCATGATC	AACAGCCAGTTCTCTTGTTTCTC	388

Table 1.3: CRISPR gRNA sequences and mismatches.

gRNA	**gRNA sequence + <u>PAM</u> (5' –> 3')**	**Subgenome Homolog**	**Exon**	**Target site with mismatches (in BOLD) (5' –> 3')**
DspCRISPR1	GGTGCTGGTTCATGATAAGC**<u>TGG</u>**	*dsp.L*	8	GGTGCTGGTTCATGATAAGC
		dsp.S	8	GGTGCTGGTTCATGATAAGC
DspCRISPR2	GGTCGCATCTGACAGTTTGA**<u>TGG</u>**	*dsp.L*	19	GGTCGCATCTGACAGTTTGA
		dsp.S	17	G**A**TCGCATCTGACAGTTTGA

Table 1.4: Primers for CRISPR mutation analysis with T7 endonuclease I assay.

gRNA	Primers	Primer sequence (5' –> 3')	Wild-type fragment size (bp)	Approx. fragment sizes if cleaved (bp)
DspCRISPR1	dsp.L Forward	AAACTGATGAGTGAGCTGGAG	237	68, 169
	dsp.L Reverse	CTTGACAAGACCACTAAACCC		
	dsp.S Forward	AAACTGATGAGTGAGCTGGAG	380	68, 312
	dsp.S Reverse	ATTTTCTTTCAGGTGGACATCG		
DspCRISPR2	dsp.L Forward	GGGAATTAGAGAAACAAAGCAAGC	382	111, 271
	dsp.L Reverse	GCATTTTCTACCAGTGGCTG		
	dsp.S Forward	GTGGGAATTAGAGAAGCAAAGC	325	113, 212
	dsp.S Reverse	ACCTTTGCTATGTGTGTAGGG		

RESULTS

SECTION 1: DEVELOPMENT AND STRUCTURE OF THE EMBRYONIC DESMOSOME IN *XENOPUS LAEVIS*

Although the desmosomal structure has been reported in *Xenopus laevis* adult and tadpoles (Borysenko and Revel, 1973), it has not been examined at earlier developmental stages. Further, studies of the desmosomal complex in *Xenopus* have widely focused on plakoglobin but not other crucial desmosomal proteins (DeMarais and Moon, 1992; Karnovsky and Klymkowsky, 1995; Kofron et al., 2002; Kofron et al., 1997). Therefore, the goal of this section is to determine if and when desmosomes and desmoplakin, a critical desmosomal protein, are present in the *X. laevis* embryo.

A. TEM ANALYSIS OF DESMOSOMES REVEALED CONSERVED ULTRASTRUCTURE AND INCREASING NUMBERS DURING DEVELOPMENT

While others have demonstrated that desmosomes exist in the adult and tadpole epidermis of *X. laevis* (Borysenko and Revel, 1973), these structures have not been identified in the early embryo. Therefore, to fill this gap in knowledge, desmosomes were imaged by Transmission Electron Microscopy (TEM) as the embryo develops through gastrulation and neural tube formation. Ultrastructurally, the desmosome appeared as an electron-dense cytoplasmic plaque that was present adjacent to the plasma membrane of opposing cells (**Fig. 1.2A**). In a subset of

desmosomes, a midline in the extracellular space between plaques in opposing cells was present. This structure is thought to signify stable trans-interactions between the desmosomal cadherins (**Fig. 1.2B**). These results indicate that in the early embryo of *X. laevis*, desmosomes resembled those observed in *M. musculus*, *D. rerio*, as well as adult amphibians, signifying a conserved ultrastructure (Borysenko and Revel, 1973; Fleming et al., 1991; Garrod and Chidgey, 2008; Goonesinghe et al., 2012).

The number of desmosomes per junction have been reported to increase during human development (Dale et al., 1985; Holbrook and Odland, 1975). Therefore, to determine if *Xenopus* embryos exhibited a similar increase, desmosomes were counted in the outer ectodermal layer in various stages ranging from st. 10 to st. 22. These stages were chosen because they represent a critical period of ectodermal development. During this time, the ectoderm forms, undergoes migratory movements to envelop the whole embryo (Nieuwkoop and Faber, 1967), and begins to express early epidermal differentiation markers (Jonas et al., 1985; Wilson and Hemmati-Brivanlou, 1995). Therefore, desmosomes were counted at st. 10 (9-11 hpf), st. 14 (16-17 hpf), st. 19 (21-22 hpf) and st. 22 (24-25 hpf) (n=2 embryos/ stage). At st. 10 (9-11 hpf), tight junctions and adherens junctions were observed at the apical-most region of all cell-cell junctions (green bar, **Fig. 1.2C**). However, desmosomes were only observed in 28% of these junctions (yellow arrow, **Fig. 1.2C, D**). Further, only one desmosome was observed at each of these junctions (**Table 1.5**). At st. 14 (16-17 hpf), desmosomes were detected at 51% of junctions (yellow arrow, **Fig. 1.2E, F**; **Table 1.5**). At st. 19 (21-22 hpf), desmosomes were detected in 76% of junctions (yellow arrows, **Fig. 1.2G, H**). While 68% of these junctions had one desmosome, two desmosomes were observed in 8% of junctions (**Table 1.5**). At st. 22 (24-25 hpf), desmosomes were observed in 93% of intercellular junctions (yellow arrows, **Fig. 1.2I, J**). At this time, more than half of all junctions

had more than one desmosome. Specifically, 47% of junctions had two desmosomes and 9% of junctions had three or more desmosomes (**Table 1.5**). These results indicate that the number of desmosomes increase during early development of the *X. laevis* embryo, consistent with observations in the developing human embryo.

Thus far, the TEM analysis was only focused on desmosomes in the outer layer of the ectoderm. The *Xenopus* embryonic ectoderm and epidermis are bi-layered (Itoh et al., 1988; Nieuwkoop and Faber, 1967). Therefore, the next step was to determine whether desmosomes could also be detected in the inner epidermal layer. At st. 31 (37-40 hpf), in a subset of images, desmosomes were visible between cells of the inner epidermal layer (red arrow, **Fig. 1.2L**). At st. 44 (92-98 hpf), desmosomes were also present between the outer and inner epidermal layers (green and red arrows, **Fig. 1.2M**). The inner epidermal layer was not examined before st. 31. These results indicate that desmosomes are present between cells of both epidermal layers of the *X. laevis* embryo.

B. COMPARATIVE SEQUENCE ANALYSIS OF *X. LAEVIS* DESMOPLAKIN WITH OTHER VERTEBRATES REVEALED CONSERVED DOMAINS

A comparative sequence analysis of the intracellular desmosomal protein, desmoplakin (Dsp), has not been performed between *X. laevis* and mammalian homologs. Such an analysis provides a measure of sequence identity and similarity between homologs in different species and can be used to predict whether its function is shared. Therefore, a bioinformatics analysis was performed to 1) determine overall gene and protein sequence similarity with homologs of other vertebrate species, 2) identify the key functional domains of *X. laevis* Dsp, and 3) determine sequence similarity between *X. laevis* Dsp.L and Dsp.S homologs.

B.1. OVERALL SEQUENCE COMPARISON REVEALED CONSERVED GENE AND PROTEIN SEQUENCE BETWEEN X. LAEVIS AND MAMMALIAN SPECIES

The first step was to determine the homology of *X. laevis* Dsp to homologs in mammalian species, *H. sapiens* and *M. musculus*. Bioinformatic analysis revealed that the *H. sapiens* coding region shared 65.7% identity with the *X. laevis dsp.L* homolog. *M. musculus* coding region shared 64.4% identity with *X. laevis dsp.L*. The *H. sapiens* and *M. musculus* desmoplakin proteins each shared 66% identity with *X. laevis* Dsp.L (**Table 1.6**). Together, these results indicate that the *X. laevis* Dsp.L shares a high degree of similarity with mammalian homologs, suggesting conserved function.

B.2. COMPARISON OF DESMOPLAKIN FUNCTIONAL DOMAINS REVEALED CONSERVATION BETWEEN *X. LAEVIS* AND MAMMALIAN SPECIES

A multiple sequence alignment of all three homologs revealed stretches of conserved amino acid sequences (**Appendix A.1**). The next step was to determine the similarities of individual domains in the *X. laevis* desmoplakin protein with those in mammalian Dsp homologs. First, a comparative analysis of the plakin domain was performed. Comparative analysis revealed that the plakin domains of both *Homo sapiens* and *Mus musculus* homologs shared 64% identity and 80% similarity respectively with the same domain of *X. laevis* Dsp.L. (**Fig. 1.3, Part I**). A bioinformatics analysis of the plakin subdomains also revealed similarity in sequences between *X. laevis* and mammalian desmoplakin homologs (**Appendix A.3**). Next, the rod domain was compared across species. Comparative analysis revealed that the rod domain of *H. sapiens* and *M. musculus* homologs shared 61% identity and 82% similarity with the corresponding domain in *X. laevis* Dsp.L. (**Fig. 1.3, Part I**). Finally, the similarities of the A, B, and C subdomains in the C-

terminal domain were analyzed. The A, B, and C subdomains in both *H. sapiens* and *M. musculus* shared 87%, 91%, and 93% similarity, respectively, with the corresponding regions in *X. laevis* Dsp.L. (**Table 1.7**; **Fig. 1.3, Part I**). Together, these results indicate that the functional domains of *X. laevis* Dsp.L share a high degree of similarity with those in the mammalian homologs, suggesting that its overall function could also be shared.

B.3. COMPARING *X. LAEVIS* L AND S SUBGENOME HOMOLOGS REVEALED SIZE DIFFERENCES

The desmoplakin allele is present in both the L (Long) and S (Short) subgenomes in *X. laevis*. The S subgenome has experienced more deletions, thus it might be predicted that L and S homologs differ in coding sequence length. Therefore, to determine whether there were differences, pairwise alignments were performed between the gene coding DNA sequence and protein sequences of these homologs. Results revealed that the *X. laevis dsp.S* gene coding DNA sequence shared 91% identity with *dsp.L* (**Table 1.6**). At the protein level, Dsp.S had a length of 2767 a.a., which was 96.5% of the length of Dsp.L, and shared 93% similarity.

Next, the similarity of the functional domains between the homologs was analyzed. The plakin domain of the Dsp.S homolog shared 86% similarity with the same domain in Dsp.L. Analysis of the coding DNA sequence alignment revealed a gap in the S homolog which corresponded to exons 11 and 12 in the L homolog (**Appendix A.2**). This encodes part of the SR56 plakin subdomain which only shared 60% similarity between the homologs (**Table 1.7**). The rod domain of the Dsp.S homolog shared a 96% similarity with the corresponding domain in Dsp.L. The C-terminal domain in the Dsp.S homolog was predicted to contain A, B, and C subdomains and shared 98%, 97% and 99% similarity, respectively, with the same subdomains in Dsp.L (**Fig.**

1.3, Part II). Together, these results suggest that Dsp.S shares a high degree of similarity with Dsp.L but has deletions within the plakin domain, which might result in functional differences.

C. IMMUNOFLUORESCENCE REVEALED DIFFERENCE IN PATTERNS BETWEEN EARLY AND LATE STAGES

C.1. IMMUNOFLUORESCENCE REVEALED VARIABLE LEVELS OF DESMOPLAKIN WITHIN EPIDERMAL TISSUES AT EARLY STAGES

As mentioned above, the ubiquitous presence of desmoplakin in all desmosomes makes it suitable to study the role of desmosomes during development. While the results above revealed that desmosomes are detected in the *X. laevis* embryonic epidermis, it is unknown if desmoplakin localizes to the membrane during this period. Therefore, the pattern of desmoplakin localization when the epidermis undergoes morphogenesis was determined using Immunofluorescence (IF) at st. 21-23 (23-25 hpf). Desmoplakin appeared to be adjacent to the membrane (marked by β-catenin) throughout the epidermis (n=15, 3 experiments, **Fig. 1.4A-A''**). However, the levels of both β-catenin and desmoplakin were not the same in all cells. At the vertex of 4 to 5 surrounding cells, consistent with where cells are fated to intercalate, there appeared to be lower levels of both β-catenin and desmoplakin (white arrow, **Fig. 1.4A**). Other cells with small apical surfaces, consistent with newly intercalating cells, had enriched levels of desmoplakin but not β-catenin (white arrowhead, **Fig. 1.4A**). In summary, the variable levels of desmoplakin within the epidermis suggest that desmosome assembly might be dynamic during epidermal development.

C.2. IMMUNOFLUORESCENCE REVEALED PRESENCE OF DESMOPLAKIN IN EPIDERMALLY-DERIVED TISSUES AT LATE STAGES

As the *Xenopus* embryo approaches pre-metamorphic stages, many structures are derived from the developing epidermis. These include the outer corneal layer of the eye, and the operculum, which have desmosomes (Hu et al., 2013; Nieuwkoop and Faber, 1967). Therefore, desmoplakin was imaged by IF in these epidermally-derived structures at st. 42-43 (80-92 hpf). Results revealed ubiquitous levels of desmoplakin in the outer corneal layer (**Fig. 1.4B-B''**). Desmoplakin was also present throughout the epidermis including the tail fin (Fig. 1.4C-C') and was detected in the operculum and the external gills, which are derived from the visceral arches (**Fig. 1.4D-D''**). These results indicate that desmoplakin presence in many epidermally-derived tissues might suggest a requirement for proper development or functioning of these structures.

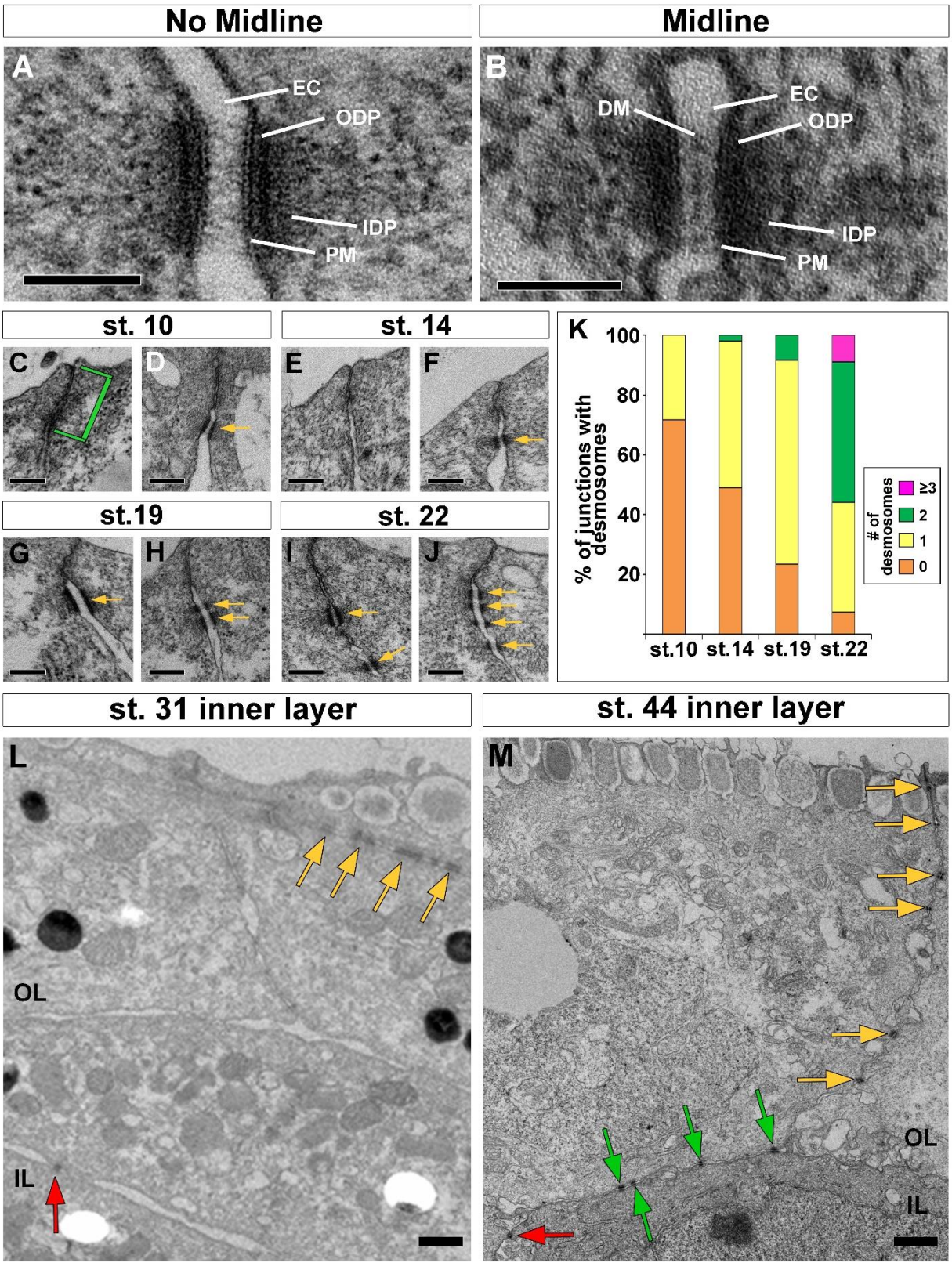
No Midline
Midline
A
EC
ODP
IDP
PM
B
DM
EC
ODP
IDP
PM
st. 10
st. 14
C
D
E
F
st.19
st. 22
G
H
I
J
K
100
80
60
40
20
% of junctions with desmosomes
st.10
st.14
st.19
st.22
# of desmosomes
≥3
2
1
0
st. 31 inner layer
st. 44 inner layer
L
OL
IL
M
OL
IL

Figure 1.2: Transmission Electron Microscopy (TEM) analysis of the *X. laevis* embryonic desmosome during early development.

(A-B) TEM imaging revealing desmosomal ultrastructure in the *Xenopus laevis* embryo without (A) and with (B) midline (white arrow) (Scale bar=100 nm). (C-J) Electron micrographs depicting desmosomes in the X. laevis embryo at various developmental stages (electron-dense plaques, yellow arrows) (Scale bar = 250 nm). Green bracket (C) indicates Tight junction and Adherens junction. (K) Graph depicting the percentage of junctions with desmosomes at various stages. (L) Electron micrograph of st. 31 epidermis revealing desmosomes in the inner epidermal layer (red arrow) (Scale bar=0.5µm). Yellow arrows denote desmosomes in the outer epidermal layer. (M) Electron micrograph of st. 44 epidermis revealing desmosomes in the inner epidermal layer (red arrow) (Scale bar=1µm). Yellow arrows denote desmosomes in the outer epidermal layer and green arrow denote desmosomes between outer and inner epidermal layer. EC=Extracellular space; PM=Plasma membrane; ODP=Outer dense plaque; IDP=Inner dense plaque; DM=Dense midline; OL=Outer Layer; IL=Inner Layer.

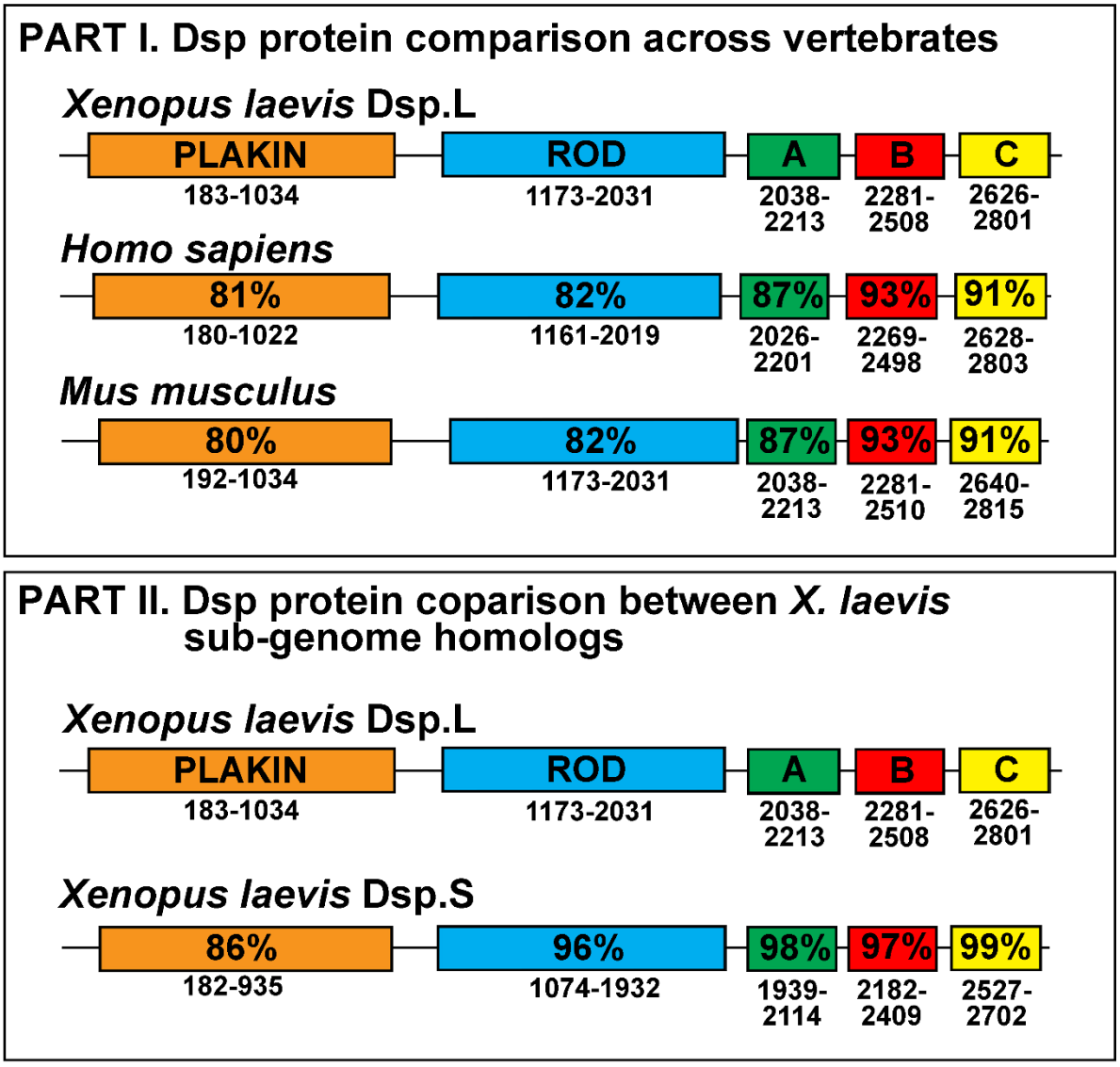

Figure 1.3: Comparative bioinformatics analysis of the desmoplakin protein.
Part I. Comparative analysis of functional domains in desmoplakin protein between vertebrate species and the *X. laevis* Dsp.L homolog. Part II. Comparative analysis of functional domains in desmoplakin protein between the *X. laevis* Dsp.L and Dsp.S subgenome homologs. Percent Similarity with *X. laevis* Dsp.L is denoted for each domain within boxes. Numbers below boxes depict amino acid coordinates for each domain. A,B,C=C-terminal homologous plakin repeat domains.

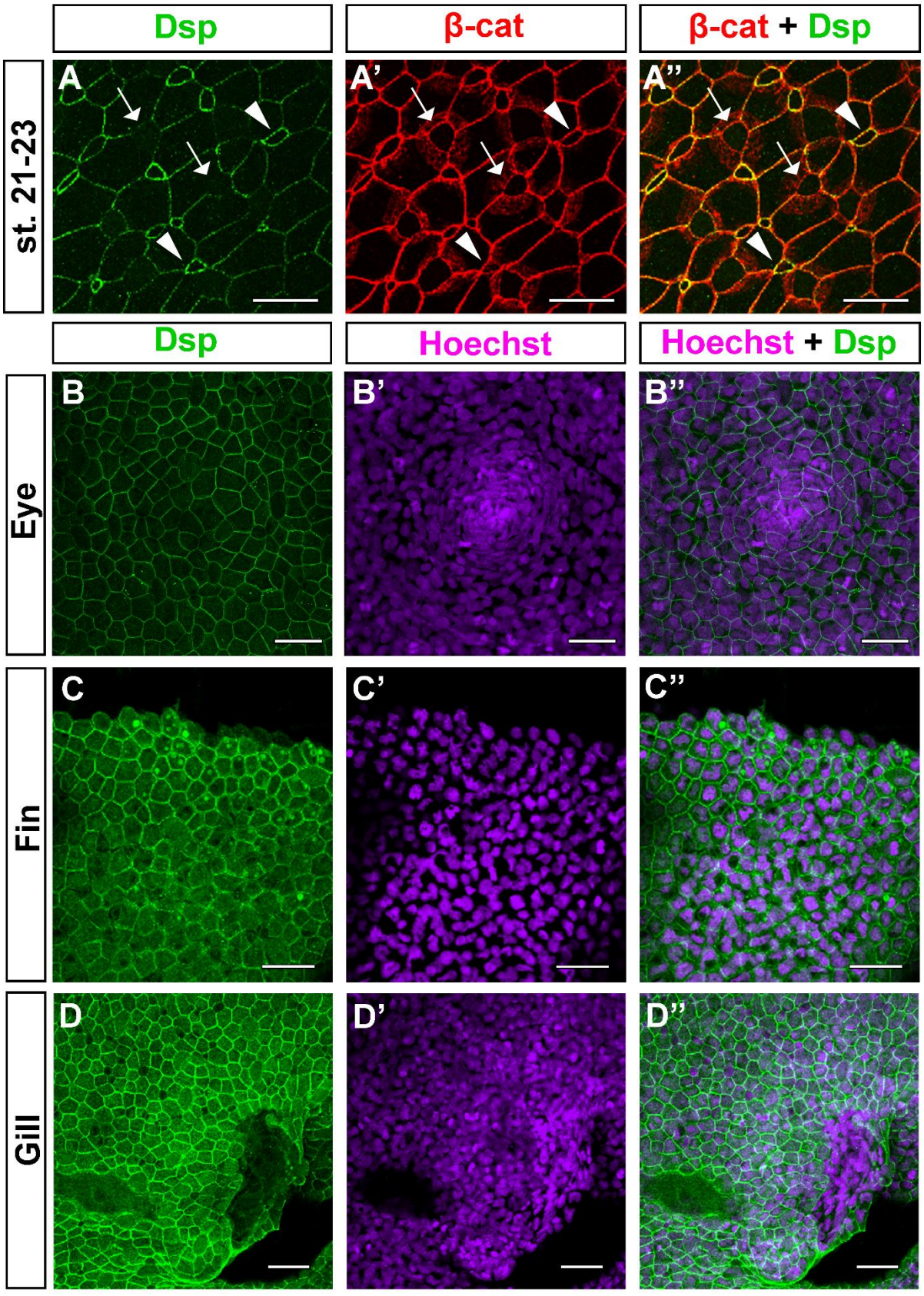
Dsp
β-cat
β-cat + Dsp
st. 21-23
A
A'
A''
Dsp
Hoechst
Hoechst + Dsp
Eye
B
B'
B''
Fin
C
C'
C''
Gill
D
D'
D''

Figure 1.4: Desmoplakin expression in the developing embryo.
(A-A'') Immunofluorescence of desmoplakin (green) and β-catenin (red) at st. 22. Some cells have relatively high desmoplakin intensity (white arrowheads) and other cells have lower levels (white arrow) (Scale bar=25μm). (C-E'') Immunofluorescence of desmoplakin (green) and nuclei (purple) in Eye (B-B''), Fin (C-C'') and Gill (D-D'') epidermis at st. 43 (Scale bar=50μm).

Table 1.5: Percentage of junctions with desmosomes in various developmental stages in the *X. laevis* embryo.

Stage	Embryo	No. of junctions analyzed	Percentage of junctions			
			0 desmosomes/ junction	**1 desmosome/ junction**	**2 desmosomes/ junction**	**N≥3 desmosomes/ junction**
st. 10	1	12	66.67 (n=8)	33.33 (n=4)	0 (n=0)	0 (n=0)
	2	27	74.07 (n=20)	25.93 (n=7)	0 (n=0)	0 (n=0)
st. 14	1	12	41.67 (n=5)	58.33 (n=7)	0 (n=0)	0 (n=0)
	2	39	51.28 (n=20)	46.15 (n=18)	2.56 (n=1)	0 (n=0)
st. 19	1	16	25 (n=4)	62.5 (n=10)	12.5 (n=2)	0 (n=0)
	2	44	22.73 (n=10)	70.45 (n=31)	6.82 (n=3)	0 (n=0)
st. 22	1	17	0 (n=0)	41.18 (n=7)	52.94 (n=9)	5.88 (n=1)
	2	51	9.8 (n=5)	35.29 (n=18)	45.1 (n=23)	9.8 (n=5)

Table 1.6: Desmoplakin gene and protein comparative analysis against *X. laevis* Dsp.L.

Organism	Accession number or Database	Whole Protein (%Identity/ Similarity)	Length (amino acid)	Coding DNA sequence (%Identity)
***X. laevis* (Dsp.L)**	Xenbase Genome build 9.1	100	2866	100
H. sapiens	NP_004406	66.0/ 82.2	2871	65.7
M. musculus	NP_076331	65.6/ 82.1	2883	64.4
***X. laevis* (Dsp.S)**	Xenbase Genome build 9.1	90.1/ 93.4	2767	90.7

Table 1.7: Desmoplakin protein domains comparative analysis against *X. laevis* Dsp.L.

Organism	PLAKIN (%Identity/ Similarity)	ROD (%Identity/ Similarity)	A (%Identity/ Similarity)	B (%Identity/ Similarity)	C (%Identity/ Similarity)
***X. laevis* (Dsp.L)**	100	100	100	100	100
H. sapiens	64.6/ 80.5	61.1/ 81.8	72.6/ 86.9	84.6/ 93.0	76.0/ 91.4
M. musculus	64.3/ 80.0	60.8/ 81.9	71.4/ 87.4	84.6/ 93.4	75.4/ 91.4
***X. laevis* (Dsp.S)**	82.7/ 85.9	92.7/ 95.7	93.7/ 98.3	96.0/ 97.4	94.3/ 98.9

SECTION 2: EMBRYOS WITH REDUCED OR IMPAIRED DESMOPLAKIN FUNCTION HAVE EPIDERMAL DEFECTS, REDUCED MECHANICAL RESISTANCE, AND IMPAIRED RADIAL INTERCALATION

Although the role and regulation of desmoplakin has been studied extensively in cell culture, there are only a handful of studies examining its role in the developing embryo (Gallicano et al., 2001; Gallicano et al., 1998). Therefore, the goal of this section is to determine the function of desmoplakin in the early embryo by performing loss-of-function experiments using various molecular techniques.

PART I

A. KNOCKDOWN WITH MORPHOLINOS RESULTS IN REDUCED DESMOPLAKIN

To understand the role of a protein during development it is necessary to decrease or deplete that protein and assess the effects on the embryo. To do this, first, antisense morpholinos were used to knock down desmoplakin in embryos. Morpholino concentrations can be optimized to examine the effects of decreasing the dosage of Dsp in the embryo. This is especially useful when a complete knockout might be lethal (Gallicano et al., 1998). While morpholinos are an effective method to test the role of gene function in *Xenopus*, effects due to toxicity, nonspecific effects, or the creation of neomorphs can lead to misleading results (Blum et al., 2015; Eisen and

Smith, 2008; Heasman, 2002). Thus, two splice-blocking morpholinos targeting different regions of the *dsp.L* homolog were used in this study.

Two splice-blocking morpholinos against desmoplakin were designed to target either the exon 4-intron 4 splice junction (DspMO1) (**Fig. 1.5A**) or the exon 14-intron 14 splice junction, (DspMO2) (**Fig. 1.5B**) of Dsp.L mRNA. Additionally, DspMO2, but not DspMO1 is predicted to bind efficiently to Dsp.S mRNA (**Table 1.1**). To assess their efficacy, fertilized eggs were injected with DspMO1, DspMO2, control (CMO) or no morpholino (pools of n=10, 2 experiments each). First, the efficacy of DspMO1 was assessed against RNA from tailbud stages (st. 30-31). RT-PCR of the DspMO1 target region revealed a single 422 bp band in DspMO2-, CMO-injected and wild-type embryos (**Fig. 1.5C**). However, in DspMO1-injected embryos, an extra 253 bp band, consistent with exon 4 splicing, was observed (**Fig. 1.5C**). These results indicate that the DspMO1 morpholino produced splicing defects within the target region and a reduction in normal Dsp mRNA. The next step was to determine the efficacy of the DspMO2 morpholino. RT-PCR of the DspMO2 target region revealed a single 388 bp band in CMO-injected and wild-type embryos (**Fig. 1.5D**). However, an extra ~500 bp band, consistent with intron retention, was observed (**Fig. 1.5D**). These results indicate that the DspMO2 morpholino produced splicing defects within the target region and a reduction in normal Dsp mRNA.

To determine whether the splicing defects resulting from the DspMO1 were effective in reducing protein levels, embryos were imaged using immunofluorescence to detect desmoplakin levels. Results revealed that CMO-injected embryos had a normal intensity and pattern of Dsp as described above (**Section 1C**) (**Fig. 1.5E**). However, in both DspMO1- and DspMO2-injected embryos, there was a reduction in desmoplakin (**Fig. 1.5F,G**). These results indicate that the morpholinos effectively lead to reduction in desmoplakin in the epidermis.

B. CRISPR/ CAS9-MEDIATED MUTAGENESIS OF DESMOPLAKIN HOMOLOGS IN F0 MUTANTS RESULTS IN REDUCTION OF DESMOPLAKIN

While the results above confirm that morpholinos effectively target Dsp, using different approaches to study gene and protein function ensures the validity of phenotypes (Blum et al., 2015; Kok et al., 2015). Additionally, morpholino efficacy starts to decrease after a few days (Eisen and Smith, 2008). Therefore, the CRISPR/Cas9 (clustered regularly interspaced short palindromic repeats/CRISPR-associated) system was utilized for targeted mutagenesis of the *dsp* gene (Bhattacharya et al., 2015; Nakayama et al., 2013; Wang et al., 2015). This method creates double stranded breaks in the genome which frequently lead to indels due to the error-prone non-homologous end joining repair mechanism. To generate F0 *dsp* CRISPR mutants, gRNAs were designed to target both the L and S homologs. To ensure that the technique was effective, a positive control was performed by targeting the tyrosinase (*tyra* + *tyrb*) genes as previously described (**Chapter 2**) (Wang et al., 2015). Two CRISPR gRNAs were designed to target sites in the eighth (DspCRISPR1) and nineteenth (DspCRISPR2) exons of the *dsp.L* homolog (corresponding to the eighth and seventeenth exons on the *dsp.S* homolog, respectively) (**Fig. 1.6A**). To determine whether the gRNAs were effective, injected embryos were analyzed for mutations using a T7 endonuclease assay. If mutations are present, the target region is cleaved. First, the efficacy of DspCRISPR1 was determined using DNA from tailbud stages (st. 30-31). Results revealed a 237 bp (*dsp.L*) and 380 bp (*dsp.S*) band in 100% of wild-type embryos (n=12, 3 experiments). However, in 80% of DspCRISPR1-injected embryos, multiple bands, including the 237 bp and 380 bp bands, were detected in both *dsp.L* and *dsp.S* homologs (n=15, 3 experiments) (**Fig. 1.6B**).

The sizes of these extra bands are consistent with mutations in the gRNA target region (**Table 1.4**). This indicates that the gRNA was effective and that the embryos were mosaic.

Next, the efficacy of DspCRISPR2 was assessed using DNA from tailbud stages (st. 30-31). Results revealed a 382 bp (*dsp.L*) and 325 bp (*dsp.S*) band in 100% of wild-type embryos (n=12, 3 experiments). However, in 100% of DspCRISPR2-injected embryos, multiple bands, including the 382 bp and 325 bp bands, were detected in both *dsp.L* and *dsp.S* homologs (n=16, 3 experiments) (**Fig. 1.6B**). The sizes of these extra bands are consistent with mutations in the gRNA target region (**Table 1.4**). This indicates that the gRNA was effective and that DspCRISPR2-injected embryos were also mosaic, similar to DspCRISPR1-injected embryos.

The next goal was to determine whether the mutations in the target region led to a reduction in desmoplakin protein. To do this, embryos were imaged by immunofluorescence to detect desmoplakin presence in F0 mutants. Results revealed that control embryos had a normal pattern of Dsp labeling as described above (**Section 1C**) (**Fig. 1.6C**). However, in both DspCRISPR1 and DspCRISPR2 F0 mutants, there was a reduction in desmoplakin. There was some variability in the amount of desmoplakin loss between individual CRISPR-injected embryos. For example, in a subset of embryos there were low levels of desmoplakin across a wide region of epidermis (**Fig. 1.6D,F**). On the other hand, other embryos displayed a reduction in desmoplakin in smaller patches of epidermis (**Fig. 1.6E,G**). This suggests that the degree of mosaicism is different between injected embryos (Wang et al., 2015). These results indicate that CRISPR-mediated mutagenesis of desmoplakin L and S homologs is effective at reducing desmoplakin protein.

PART II

A. DSP MORPHANTS AND F0 MUTANTS HAVE REDUCED SIZE

Morpholinos successfully resulted in reduction of desmoplakin protein in embryos. The next step was to observe the effects on the morphology of embryos injected with morpholino and CRISPR gRNA. First, DspMO1 morphants were assessed for defects. Embryos appeared normal at cleavage, blastula, and gastrula stages (until 13 hpf). However, at stage 25-30, a large percentage of DspMO1 morphants were shorter. DspMO1 morphants (n=98, 4 experiments) were, on average, 1.45-fold shorter than control morphants (n=77, 4 experiments) (t-test, $p<0.0001$) (**Fig. 1.7A**). Next, DspMO2 morphants were observed to determine if the phenotypes mimicked those of the DspMO1 morphants. Embryos were able to progress through cleavage, blastula, and gastrula stages (until 13 hpf) normally. However, like DspMO1 morphants at stage 25-30, a large percentage of DspMO2 morphants were also shorter. DspMO2 morphants (n=67, 3 experiments) were, on average, 1.35-fold shorter than control morphants (n=76, 3 experiments) (t-test, $p<0.0001$) (**Fig. 1.7B**).

To ensure the specificity of morphant phenotypes, CRISPR/ Cas9 mutants were examined to determine whether they mimicked morphants. Embryos were able to progress through cleavage, blastula, and gastrula stages (until 13 hpf) normally. F0 mutant embryos that were sequenced and found to have mutations in both *dsp* homologs were imaged prior to genotyping. Like the Dsp morphants at stage 25-30, these mutants were also shorter. D'Agostino & Pearson omnibus normality testing revealed that the distribution of length measurements was not normal

(DspCRISPR1=p<0.0001; DspCRISPR2= p<0.001). Non-parametric statistical analysis revealed that DspCRISPR1 (n=109, 2 experiments) and DspCRISPR2 (n=90, 2 experiments) F0 mutants had statistically significant reductions in length (Mann-Whitney test, p<0.0001) relative to wild-type embryos (**Fig. 1.7C,D**).

B. DSPMO1 AND DSPMO2 MORPHANTS EXHIBIT DEFECTS IN EPIDERMALLY-DERIVED STRUCTURES AND THE HEART

B.1. DSPMO1 AND DSPMO2 MORPHANTS HAVE EPIDERMAL DEFECTS AT EARLY STAGES

At early stages (st. 25-30), embryos also displayed epidermal tears, hyperpigmentation, ventral abdominal blistering and neural tube defects in DspMO1 and DspMO2 morphants. Analysis of DspMO1 and DspMO2 morphants were performed separately. While 39.8% of DspMO1 morphants had skin defects (n=296, 6 experiments), this was present in only 3.62% of controls (n=276, 6 experiments) (χ^2-test, p= 3.34E-25) (**Fig. 1.8B**). Skin defects occurred in 27.47% of DspMO2 morphants (n=233, 4 experiments) compared to only 3.41% of control morphants (n=205, 4 experiments) (χ^2-test, p= 9.39E-12) (**Fig. 1.8C**). Ventral blisters were present in 29.25% of DspMO1 morphants (n=294, 6 experiments) compared to only 6.16% of controls (n=276, 6 experiments) (χ^2-test, p= 8.03E-13) (**Fig. 1.8D**). Ventral blisters were present in 17.17% of DspMO2 morphants (n=233, 4 experiments) compared to only 2.93% of control morphants (n=205, 4 experiments) (χ^2-test, p= 0.00039) (**Fig. 1.8E**). While 16.33% of DspMO1 morphants had neural tube closure defects (n=294, 6 experiments), none of the control morphants presented

with these defects (n=276, 6 experiments) (χ^2-test, p= 2.31E-12) (**Fig. 1.8F**). Finally, while 15.02% of DspMO2 morphants had neural tube closure defects (n=233, 4 experiments), only 1.46% of the controls presented with these defects (n=205, 4 experiments) (χ^2-test, p= 4.91E-07) (**Fig. 1.8G**). These results suggest that DspMO1 and DspMO2 morpholinos are associated with defects in size, epidermal development, and neural tube closure of embryos (**Fig. 1.8O**). These results also reveal that defects in both morphants mimic each other, suggesting that these phenotypes are specific to desmoplakin loss at early stages.

B.2. DSPMO1 AND DSPMO2 MORPHANTS HAVE EYE, FIN, AND HEART DEFECTS AT LATE STAGES

Results revealed that desmoplakin is present in epidermally-derived structures such as the lens, fin, and external gill buds in late tailbud stage embryos (>50 hpf). Desmoplakin is also known to be expressed in the mammalian heart, which becomes functional during *Xenopus* late tailbud stages (Lohr and Yost, 2000; Warkman and Krieg, 2007). Therefore, the next step was to determine whether Dsp loss disrupted the development of these structures. Analysis of DspMO1 and DspMO2 morphants were performed separately. Several defects were noticeable in DspMO1 and DspMO2 morphants at stage 41-43. The reduction in anterio-posterior axis length is still retained from mid-tailbud stages but this was not quantified. While control morphants appeared unaffected, many DspMO1 and DspMO2 morphants did not develop proper eye structures, and displayed ruffled fins and pericardial or cardiac edemas. Eye defects, including defects in RPE pigmentation occurred in 44.77% of DspMO1 morphants (n=62, 2 experiments) compared to only 5.45% of control morphants (n=55, 2 experiments) (χ^2-test, p= 5.61E-07) (**Fig. 1.8I**). Similar eye defects occurred in 63.16% of DspMO2 morphants (n=76, 2 experiments) compared to only 7.25% of

control morphants (χ^2-test, p= 2.91E-12) (n=69, 2 experiments) (**Fig. 1.8J**). Fin defects were present in 53.23% of DspMO1 morphants (n=62, 2 experiments) compared to only 1.82% of control morphants (n=55, 2 experiments) (χ^2-test, p= 6.79E-120) (**Fig. 1.8K**). While fin defects were present in 38.16% of DspMO2 morphants (n=76, 2 experiments), none of the controls displayed these defects (n=69, 2 experiments) (χ^2-test, p= 9.65E-09) (**Fig. 1.8L**). Cardiac defects were present in 17.74% of DspMO1 morphants (n=62, 2 experiments), while only 1.82% of control morphants exhibited these defects (n=55, 2 experiments) (χ^2-test, p= 8.51E-89) (**Fig. 1.8M**). While 50% of DspMO2 morphants also exhibited cardiac defects (n=76, 2 experiments), only 2.9% of controls displayed these defects (n=69, 2 experiments) (χ^2-test, p= 2.33E-10) (**Fig. 1.8N**). These results suggest that the DspMO1 and DspMO2 morpholinos perturb the development of many epidermally-derived structures as well as other desmosome-containing tissues such as the heart (**Fig. 1.8O; Table 1.8**). These results also indicate that both morpholinos mimic each other at late stages, suggesting that these defects are specific to Dsp knockdown.

C. DSP CRISPR MUTANTS MIMIC MORPHANT PHENOTYPES AT EARLY AND LATE STAGES

C.1. DSP MUTANTS HAVE REDUCED SIZE AND EPIDERMAL DEFECTS AT EARLY STAGES

At these early stages, defects appeared similar to morphants, including epidermal tears, hyperpigmentation, ventral abdominal blistering and neural tube defects. Skin defects occurred in 7.3% of DspCRISPR1 (n=219, 4 experiments) and 8.18% of DspCRISPR2 F0 mutants (n=232, 4

experiments) compared to only 0.78% of wild-type embryos (n=256, 4 experiments) (χ^2-test, DspCRISPR1, p=0.00021; DspCRISPR2, p=5.64E-05) (**Fig. 1.9A-C**). Ventral blisters were present in 10.95% of DspCRISPR1 (n=219, 4 experiments) and 12.06% of DspCRISPR2 F0 mutants (n=232, 4 experiments) compared to only 1.56% of wild-type embryos (n=256, 4 experiments) (χ^2-test, DspCRISPR1, p=1.46E-05; DspCRISPR2, p=2.83E-06) (**Fig. 1.9D,E**). Finally, while 5.48% of DspCRISPR1 (n=219, 4 experiments) and 5.17% of DspCRISPR2 F0 mutants (n=232, 4 experiments) had neural tube defects, no wild-type embryos presented with these defects (n=256, 4 experiments) (χ^2-test, DspCRISPR1, p=0.00015; DspCRISPR2, p=0.00023) (**Fig. 1.9F,G**).

These results indicate that phenotypes of CRISPR-injected embryos mimic those observed in morphants at early stages, suggesting that these phenotypes are specific to desmoplakin loss. However, the lower prevalence relative to morphants, compounded with variability observed with desmoplakin labeling suggest that these mutants are mosaic.

C.2. DSP MUTANTS HAVE EYE, FIN, AND HEART DEFECTS AT LATE STAGES

Next, CRISPR/ Cas9 F0 mutants were examined to determine whether they mimicked morphants at late stages. The reduction in anterio-posterior axis length is still retained from mid-tailbud stages but this was not quantified. While wild-type controls appeared unaffected, many DspCRISPR1 and DspCRISPR2 F0 mutants did not develop proper eye structures including RPE and displayed ruffled fins and cardiac edemas. Eye defects, including defects in RPE pigmentation and colobomas occurred in 13.33% of DspCRISPR1 (n=165, 3 experiments) and 8.05% of DspCRISPR2 F0 mutants (n=174, 3 experiments) compared to only 1.41% of wild-type embryos (n=213, 3 experiments) (χ^2-test, DspCRISPR1, p=1.62E-08; DspCRISPR2, p=0.0015) (**Fig. 1.9H-**

J). Fin defects were present in 9.09% of DspCRISPR1 (n=165, 3 experiments) and 8.05% of DspCRISPR2 F0 mutants (n=174, 3 experiments) while only 0.47% of wild-type embryos displayed fin defects (n=213, 3 experiments) (χ^2-test, DspCRISPR1, p=7.61E-09; DspCRISPR2, p=0.00012) (**Fig. 1.9K,L**). Finally, cardiac defects, including cardiac edemas were quantified in morphants were present in 10.91% of DspCRISPR1 (n=165, 3 experiments) and 8.05% of DspCRISPR2 F0 mutants (n=174, 3 experiments) while only 0.47% of wild-type embryos displayed cardiac defects (n=213, 3 experiments) (χ^2-test, DspCRISPR1, p=4.08E-06; DspCRISPR2, p=0.00012) (**Fig. 1.9M,N**). These results indicate that phenotypes of CRISPR-injected embryos mimic those observed in morphants at late stages also, suggesting that these phenotypes are specific to Dsp loss. However, the lower prevalence relative to morphants, compounded with variability observed in Dsp labeling, suggest that these mutants are mosaic (**Fig. 1.9O; Table 1.9**).

PART III

A. THE EPIDERMIS OF DSP MORPHANTS IS SUSCEPTIBLE TO DAMAGE BY MECHANICAL STRESS

Epidermal tearing was observed in Dsp morphants and CRISPR F0 mutants. Patients with mutations in desmoplakin and plakophilin 1 also have skin that is prone to tearing when exposed to mechanical agitation (McGrath et al., 1997; Whittock et al., 2002). Therefore, the next step was to determine whether a reduction of desmoplakin in *Xenopus* embryos also results in a reduced resistance to mechanical stresses.

A.1. THE EPIDERMIS OF DSP MORPHANTS IS SUSCEPTIBLE TO DAMAGE BY SHEAR AND IMPACT FORCES

First, an "Impact Assay" was used where in st. 26 embryos were picked up using a pipette and released from a height of 15 cm into a dish lined with 2% agarose (**Fig. 1.10A**). This assay was predicted to cause shear and impact stresses. Results revealed that more DspMO1 morphants (85%) exhibited damage to the epidermis compared to controls (15%) (n=20, 2 experiments) (χ^2-test, p=9.54E-06) (**Fig. 1.10B-D'**). These results indicate that the epidermis of DspMO1 morphants exhibits quantitatively decreased resistance to shear and impact forces.

A.2. THE EPIDERMIS OF DSP MORPHANTS IS SUSCEPTIBLE TO DAMAGE BY ROTATIONAL FORCES

Next, a "Rotation Assay" was used where in st. 26 embryos were placed in a buffer-containing 50 ml conical tube that underwent rotations at 55rpm (t=30s) in a vertical rotating mixer (**Fig. 1.10E**). The embryos were subject to various mechanical stresses as they contacted the surface tension of the media as well as the side of the tube. Results revealed that significantly more DspMO1 morphants (80%) exhibited damage to the epidermis compared to controls (25%) (n=20, 2 experiments) (χ^2-test, p=0.00048) (**Fig. 1.10F-H'**). These results indicate that the epidermis of DspMO1 morphants exhibit reduced resistance to tension and shear forces.

Together, these mechanical assays demonstrate that the epidermis of DspMO1 morphants have quantitatively decreased resistance to mechanical stress such as impact, shear and tensional forces. This suggests that reduction in desmoplakin may contribute to decreased mechanical resistance of the epidermis.

B. DSP MORPHANTS EXHIBIT A LOSS OF JUNCTIONAL DESMOSOMES AND WIDENED INTERCELLULAR GAP

Next, the desmosome structure was examined in Dsp morphants to determine whether Dsp is required for desmosome formation or maintenance. Desmosomes were imaged by TEM to observe and quantify the desmosomal junctions in the embryonic epidermis at st. 30-31 (72-76 hpf). There was an increase in the intercellular gap in DspMO1 morphants relative to controls. This intercellular gap was increased basal to tight and adherens junctions (not quantified, arrows, **Fig. 1.11A-D**). Results also revealed that 57% of junctions in DspMO1 morphants had desmosomes compared to 97% of junctions in controls (n=44 (CMO) and n=56 (DspMO1) in 2

embryos, 2 experiments) (**Fig. 1.11E**). Additionally, while only 2% of junctions in DspMO1 morphants had three or more desmosomes, 27% of junctions in controls had three or more desmosomes (**Table 1.10**). These results suggest that desmoplakin may be required for proper formation or maintenance of the desmosome and maintaining intercellular adhesion.

C. DSP MORPHANTS HAVE DEFECTS IN THE FORMATION OF SPECIALIZED EPIDERMAL CELL TYPES

The *Xenopus* embryonic epidermis has multiple specialized cell types. Since the epidermis of Dsp morphants appeared abnormal, the development of these cells might also be affected in Dsp morphants. Therefore, the α-tubulin of multiciliated cells (MCCs) was imaged by immunofluorescence (**Fig. 1.12A**). At st. 31, cilia appeared shorter and fewer in number per cell in DspMO1 morphants compared to controls (**Fig. 1.12B**). The number of cilia-positive cells relative to the total number of cells was 2.77-fold less in the DspMO1 morphants (0.064; n=9) relative to controls (0.178; n=9, 2 experiments) (t-test, $p<0.00001$) (**Fig. 1.12B-D**).

To determine whether the reduction in multiciliated cells in DspMO1 morphants was due to desmoplakin loss, MCCs were also counted in DspMO2 morphants injected at the 1-cell stage. At st. 31, cilia appeared shorter and fewer in number per cell in DspMO2 morphants compared to controls, similar to DspMO1 morphants (**Fig. 1.12E**). The number of cilia-positive cells relative to the total number of cells was 2.09-fold less in the DspMO2 morphants (0.087; n=8) relative to controls (0.181; n=9, 2 experiments) (t-test, $p<0.00001$) (**Fig. 1.12E-G**). Together, these results indicate that Dsp morphants display impaired development of multiciliated cells.

Next, the Lectin Peanut Agglutinin (Lectin PNA) was labeled to determine whether the development of small secretory cells (SSCs) was affected in Dsp morphants (**Fig. 1.13A**). At st.

34, the number of PNA-positive cells relative to the total number of cells was 5.79-fold less in the DspMO1 morphants (0.023; n=11) relative to controls (0.139; n=10, 2 experiments) (t-test, $p<0.00001$) (**Fig. 1.13B-D**).

To determine whether the reduction in small secretory cells in DspMO1 morphants was due to desmoplakin loss, SSCs were also counted in DspMO2 morphants injected at the 1-cell stage. At st. 34, the number of PNA-positive cells relative to the total number of cells was 3.74-fold less in the DspMO2 morphants (0.031; n=10) relative to controls (0.115; n=10, 2 experiments) (t-test, $p<0.00001$) (**Fig. 1.13E-G**). Together, these results indicate that Dsp morphants have impaired development of small secretory cells.

In summary, these results suggest that a reduction in Dsp may reduce the prevalence and perturb the development of specialized cell types that radially intercalate into the outer epidermis.

D. DSP MORPHANTS HAVE DEFECTS IN RADIAL INTERCALATION

Dsp morphants were demonstrated to have fewer and defective specialized cell types that radially intercalate into the outer epidermal layer. More precisely, there is a reduction in cilia-positive multiciliated cells and Lectin PNA-positive small secretory cells in Dsp morphants. Therefore, the next step was to determine whether the reduction in the number of these cell types was a result of reduced radial intercalation. To track radial intercalation, the epidermis of control and DspMO1 morphants were pulse labeled with biotin from st.19 (46 hpf) until st. 20 (47 hpf) (**Fig. 1.14A**). Embryos fixed and labeled immediately after this treatment demonstrated complete and relatively uniform labeling of the epidermis (not shown). Biotin incubation was followed by a 4-hour washout to allow unlabeled cells to emerge into the outer layer (**Fig. 1.14A**).

Controls fixed after this washout had many biotin-negative regions that were consistently interspersed among biotin positive cells (**Fig. 1.14B-B''**). These unlabeled regions represented the cells that radially intercalated during the washout period. Results revealed a significant, albeit slight reduction in the average number of unlabeled cells in DspMO1 morphants (t-test, p=0.0475) (n= 11, 3 experiments) (**Fig. 1.14C-C''**). There was a large amount of variability, where a subset of DspMO1 morphant embryos had the same or even more unlabeled cells than a subset of the controls (**Fig. 1.14D,D'',E**). There were also significantly fewer multiciliated cells in the same images of DspMO1 morphants (t-test, p<0.0000001, n= 11, 3 experiments; **Fig. 1.14F**). In some DspMO1 morphants, the size of the apical surfaces of many unlabeled cells appeared smaller (arrows, **Fig. 1.14D**). Therefore, the relative surface area of the biotin-negative cells was quantified in the same images. Results revealed that there was indeed a statistically significant reduction in the average surface area of biotin-negative cells in the DspMO1 morphants (n=822 cells, 11 embryos) relative to controls (n=806 cells, 11 embryos) (Mann-Whitney test, p<0.0001, 3 experiments) (**Fig. 1.14G, H**). A histogram analysis revealed that these apically emerging cells had surface areas that followed a binomial distribution with a substantial proportion of cells in CMO morphants greater than 100μm^2. Together, these results indicate that radial intercalation and formation of the multiciliated cells in the embryonic epidermis may require Dsp.

E. DSP MORPHANTS AND F0 MUTANTS HAVE ABNORMAL ORGANIZATION OF KERATIN INTERMEDIATE FILAMENTS

Radial intercalation is partly orchestrated by the cytoskeleton through actin-generated forces and is also regulated by the rigidity of neighboring cells (Sedzinski et al., 2016). Therefore,

keratin intermediate filaments were imaged to determine whether Dsp morphants have perturbations in intermediate filament organization.

To assess this, control and Dsp morphants at st. 30-31 (72-76 hpf) were fixed and labeled for keratin. Results revealed that keratin filaments appear as a contiguous network in controls (n=21, 4 experiments) (**Fig. 1.15A-B**). In DspMO1 morphants, however, keratin appeared to be retracted from the membrane and appeared to have gaps between networks in neighboring cells (n=12/16, 3 experiments) (**Fig. 1.15C-D**). The same results were observed in DspMO2 morphants (n=8/12, 2 experiments) (**Fig.15E-F**). CRISPR F0 mutants also displayed keratin retraction in a subset of embryos (**Fig. 1.15, Part II**). These results indicate that a reduction in Dsp disrupts the organization of keratin intermediate filaments, which may contribute to defects in morphogenesis.

F. DISRUPTION OF DESMOPLAKIN-KERATIN LINK REPRODUCES SOME MORPHANT AND MUTANT PHENOTYPES

Dsp morphants and CRISPR F0 mutants displayed retraction of keratin filaments. Therefore, the next step was to determine whether disrupting the link between desmoplakin and keratin while maintaining desmosome adhesion produced similar phenotypes. To test this, the established dominant-negative DP-NTP (Desmoplakin – N-terminal peptide) construct was injected into embryos (Huen et al., 2002) (**Fig. 1.16A**). This construct has a truncated human desmoplakin which is demonstrated to uncouple intermediate filaments from the desmosome. Membrane-GFP and wild-type embryos were used as controls.

First, endogenous desmoplakin and keratin were imaged by immunofluorescence to determine the effect of DP-NTP on protein localization. Results revealed low endogenous desmoplakin in cells expressing DP-NTP and keratin retraction while appearing normal in controls

(**Fig. 1.16B-E**). These results indicate that DP-NTP replaces endogenous desmoplakin at the membrane and is associated with keratin reorganization.

Next, DP-NTP-injected were examined to determine whether maintaining the desmosomal connection but abolishing the attachment to keratin mimicked the effects of desmoplakin reduction. Results revealed no defects during cleavage, blastula, or gastrula stages. When embryos developed into mid-tailbud stages (st. 30-31), hyperpigmentation was present in DP-NTP expressing regions (**Fig. 1.16G, G'**). The embryos also had a reduction in size, but no embryos displayed epidermal tearing. At late tailbud stages (st. 40-42), embryos displayed cardiac edemas and ruffled fins, although fin ruffling was less severe relative to morphants and mutants (**Fig. 1.16H,I**). These results indicate that the effects of abolishing desmosome-keratin link partially overlap with those observed in Dsp knockdown or knockout techniques. This also suggests that loss of desmosomal adhesion may have relatively severe effects in embryonic development.

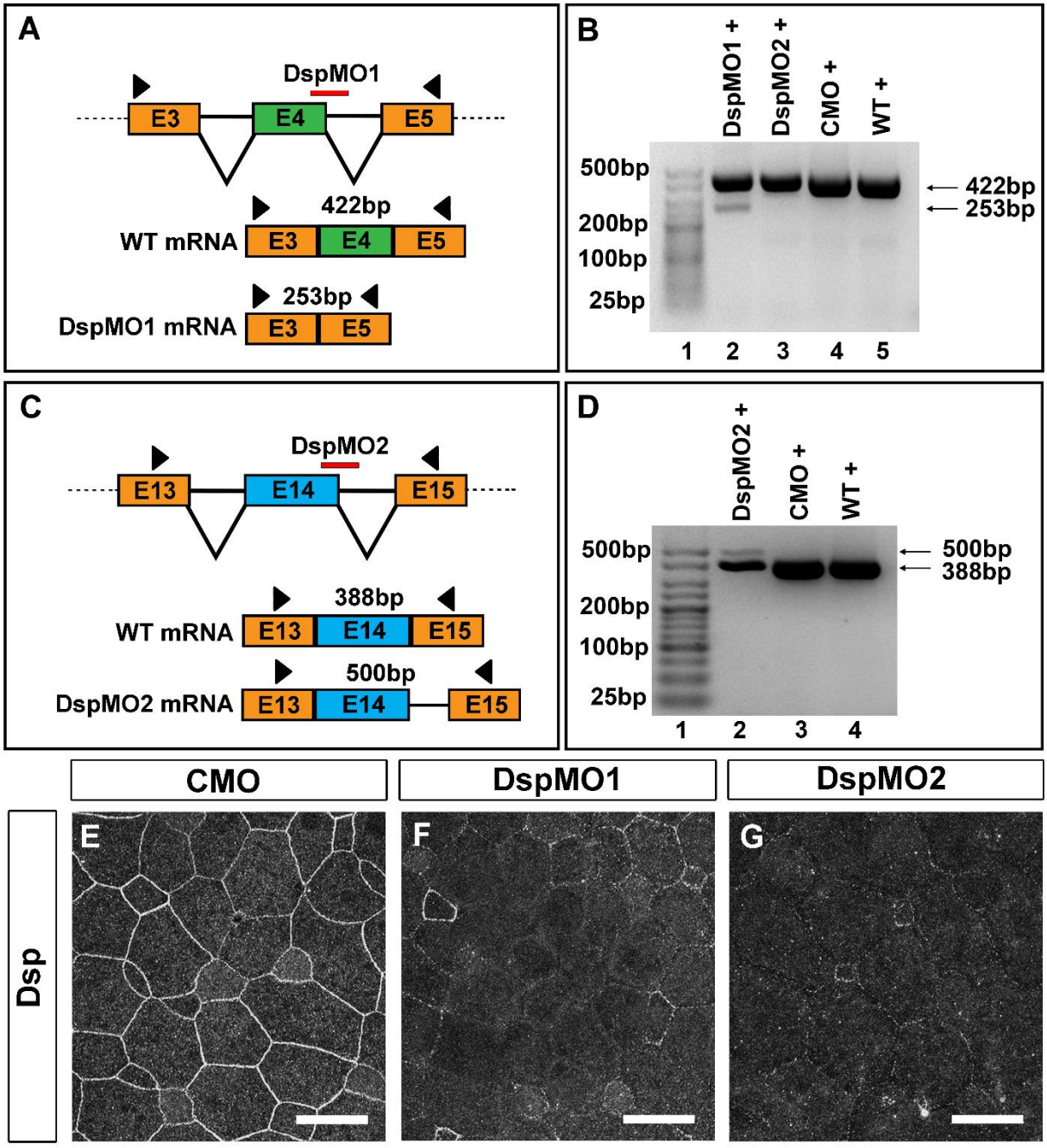

Figure 1.5: Desmoplakin depletion with antisense morpholinos.
(A) Schematic of binding of DspMO1 to exons within *dsp.L* mRNA and resulting splice products. (B) RT-PCR of *dsp.L* reveals alternative splice products in DspMO1 morphants (black arrow) but not in control morphants (CMO) or wild-type (WT). (C) Schematic of binding of DspMO2 to exons within *dsp.L* mRNA and resulting splice products. (D) RT-PCR of *dsp.L* reveals alternative splice products in DspMO2 morphants (black arrow) but not in control morphants (CMO) or wild-type (WT). (E-G) IF of desmoplakin (white) CMO (E), DspMO1 (F), and DspMO2 (G) morphants (Scale bar = 25 μm).

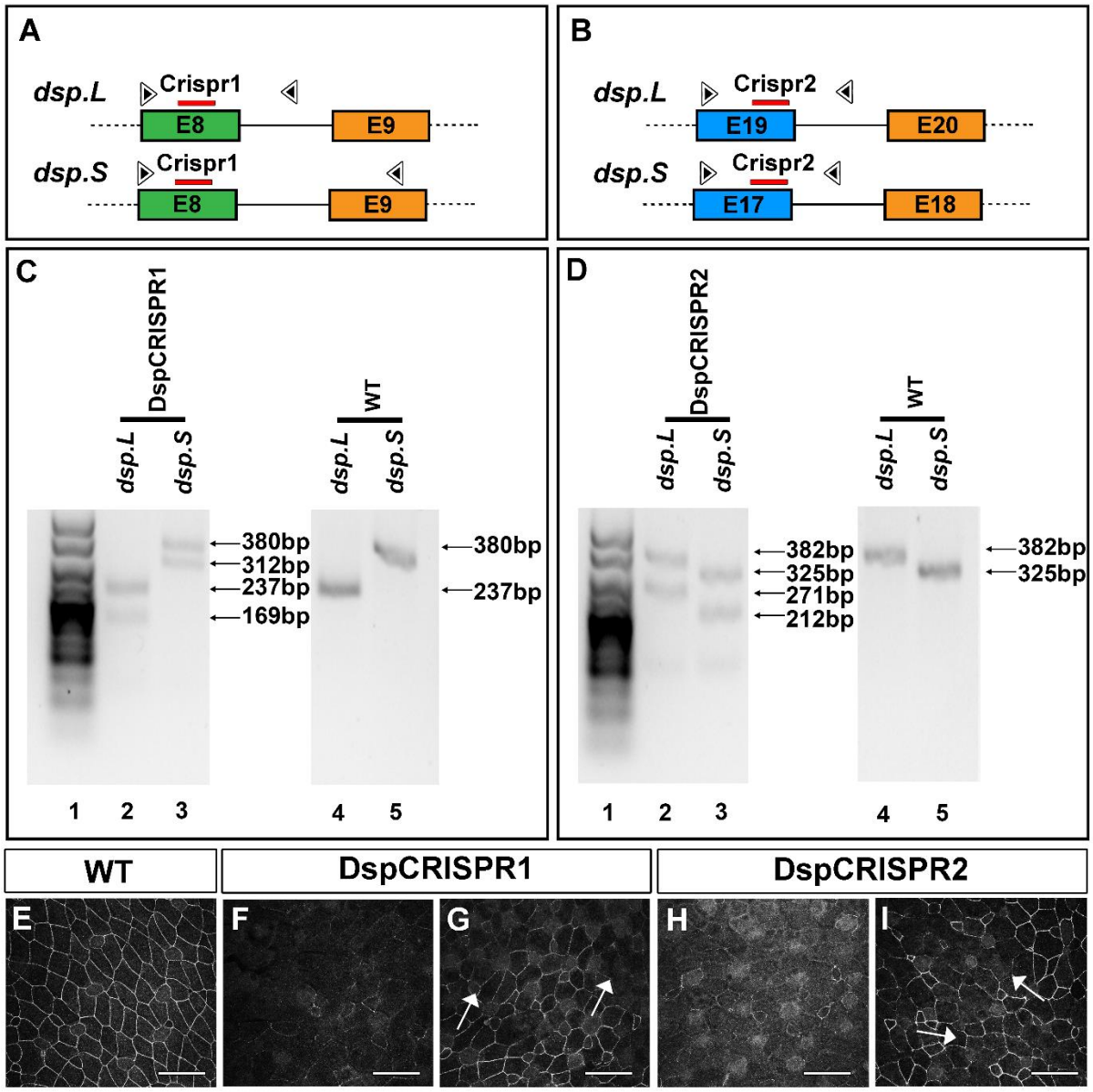

Figure 1.6: Desmoplakin depletion with CRISPR/ Cas9 mutagenesis.
(A,B) Schematic of binding of DspCRISPR1 (A) and DspCRISPR2 (B) gRNA to exons within *dsp.L* and *dsp.S*. Black arrowheads represent primer locations. (C,D) T7 endonuclease I assay revealing mutations in DspCRISPR1 and DspCRISPR2 (Lanes 2,3 in C and D, respectively) F0 mutants but not corresponding wild-type (Lanes 4,5 in C and D). Mutations are identified as presence of more than one band. HyperLadder 25 bp (Bioline) is in Lane 1. (E-I) IF of desmoplakin (white) in wild-type and DspCRISPR F0 mutants. Variability in desmoplakin reduction in DspCRISPR1 (F,G) and DspCRISPR2 (H,I) mutants (Scale bar = 50 µm).

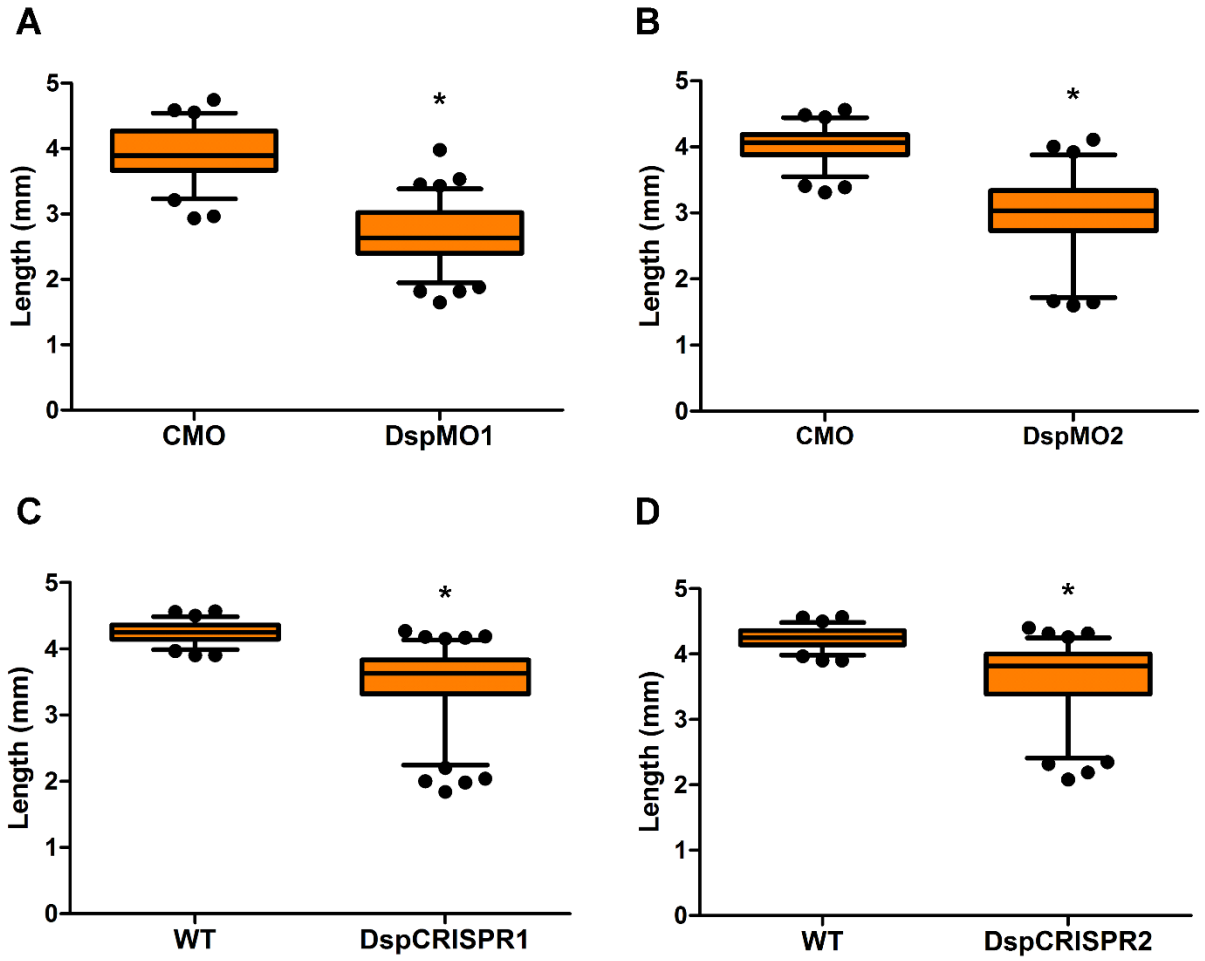

Figure 1.7: Dsp morphants and mutants displayed reduction in size.
(A) Box plot of size ranges between CMO and DspMO1 morphants. (B) Box plot of size ranges between CMO and DspMO2 morphants. (C) Box plot of size ranges between WT embryos and DspCRISPR1 mutants. (D) Box plot of size ranges between WT embryos and DspCRISPR2 mutants. Boxes represent 25th (lower), 50th (median), and 75th (upper) percentiles. Whiskers represent 5th (lower) and 95th (upper) percentiles. Dots above and below whiskers are individual embryos that have sizes outside the 5th and 95th percentile.

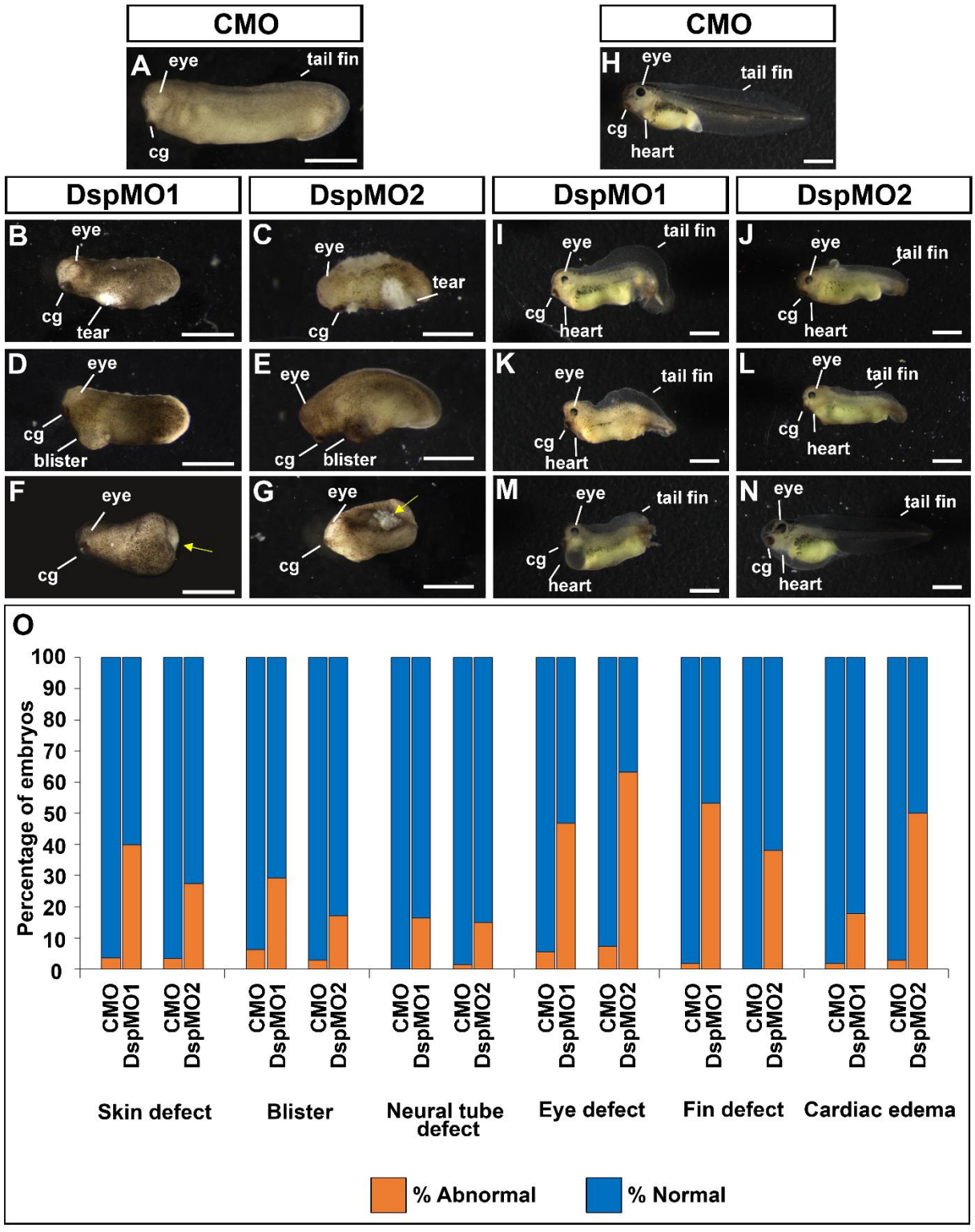
CMO
A
eye
tail fin
cg
CMO
H
eye
tail fin
cg
heart
DspMO1
DspMO2
DspMO1
DspMO2
B
eye
cg
tear
C
eye
tear
cg
I
eye
tail fin
cg
heart
J
eye
tail fin
cg
heart
D
eye
cg
blister
E
eye
cg
blister
K
eye
tail fin
cg
heart
L
eye
tail fin
cg
heart
F
eye
cg
G
eye
cg
M
eye
tail fin
cg
heart
N
eye
tail fin
cg
heart
O
Percentage of embryos
100
90
80
70
60
50
40
30
20
10
0
CMO
DspMO1
CMO
DspMO2
Skin defect
Blister
Neural tube defect
Eye defect
Fin defect
Cardiac edema
% Abnormal
% Normal

Figure 1.8: Desmoplakin knockdown with DspMO1 and DspMO2 results in size reduction, epidermal, and heart defects.
(A-G) Phenotypes observed in CMO (A), DspMO1 (B,D,F), and DspMO2 (C,E,G) morphants at st. 31. (B,C) Epidermal tearing; (D,E) Blister; (F,G) Neural tube defects (yellow arrow). (H-N) Phenotypes observed in CMO (H), DspMO1 (I,K,M), and DspMO2 (J,L,N) morphants at st. 42. (I,J) Eye defects including coloboma; (K,L) Ruffled fin and reduced fin size; (M,N) Cardiac edema. (Scale bar; A-N = 1 mm). (O) Graph of relative prevalence of phenotypes in CMO, DspMO1, and DspMO2 morphants expressed as a percentage.

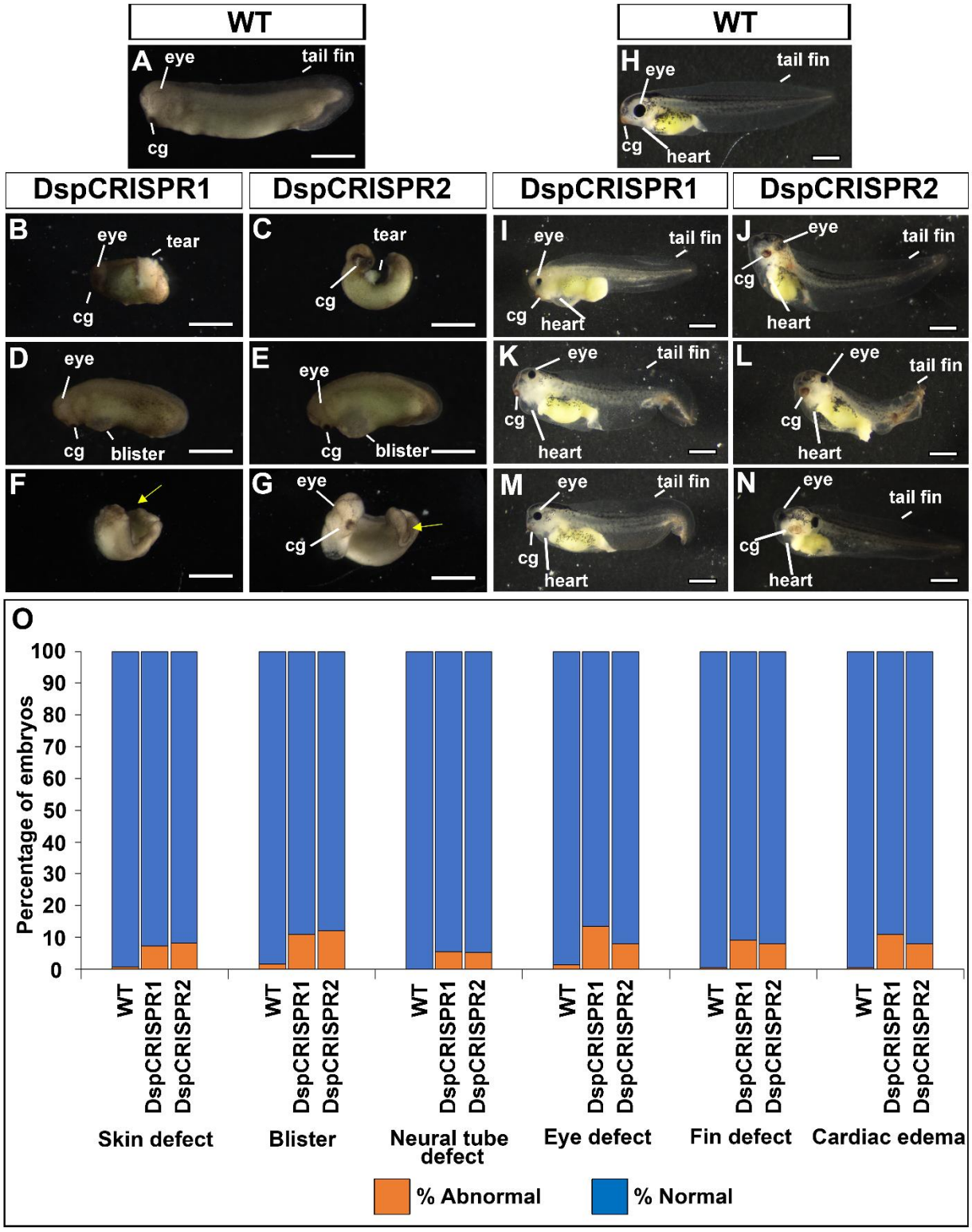
WT
WT
A
eye
tail fin
cg
H
eye
tail fin
cg
heart
DspCRISPR1
DspCRISPR2
DspCRISPR1
DspCRISPR2
B
eye
tear
cg
C
tear
cg
I
eye
tail fin
cg
heart
J
eye
tail fin
cg
heart
D
eye
cg
blister
E
eye
cg
blister
K
eye
tail fin
cg
heart
L
eye
tail fin
cg
heart
F
G
eye
cg
M
eye
tail fin
cg
heart
N
eye
tail fin
cg
heart
O
Percentage of embryos
100
90
80
70
60
50
40
30
20
10
0
WT
DspCRISPR1
DspCRISPR2
Skin defect
Blister
Neural tube defect
Eye defect
Fin defect
Cardiac edema
% Abnormal
% Normal

Figure 1.9: Desmoplakin knockdown with DspCRISPR1 and DspCRISPR2 results in size reduction, epidermal, and heart defects.
(A-G) Phenotypes observed in WT (A), DspCRISPR1 (B,D,F), and DspCRISPR2 (C,E,G) morphants at st. 31. (B,C) Epidermal tearing; (D,E) Blister; (F,G) Neural tube defects (yellow arrow). (H-N) Phenotypes observed in WT (H), DspCRISPR1 (I,K,M), and DspCRISPR2 (J,L,N) morphants at st. 42. (I,J) Eye defects including coloboma; (K,L) Ruffled fin and reduced fin size; (M,N) Cardiac edema. (Scale bar; A-N = 1 mm). (O) Graph of relative prevalence of phenotypes in WT, DspCRISPR1, and DspCRISPR2 morphants expressed as a percentage.

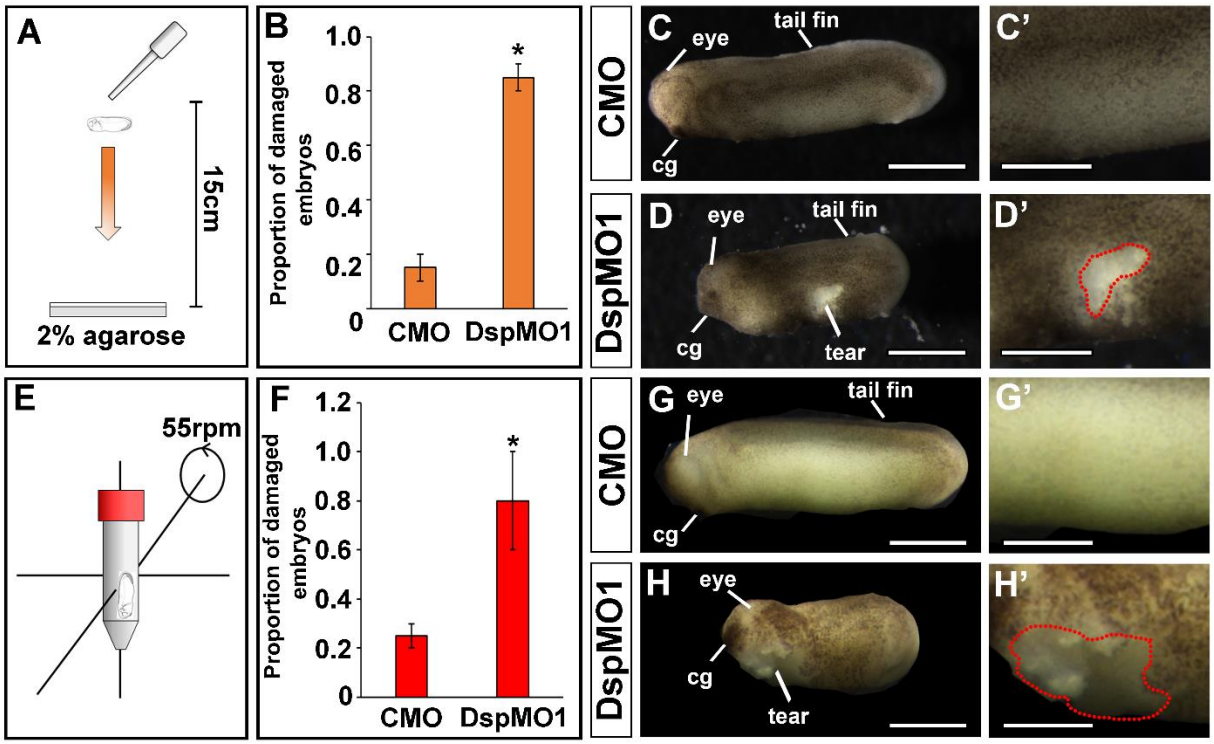

Figure 1.10: Depleting desmoplakin reduces resistance of epidermis to impact and shear stresses.

(A) Schematic of experimental design for the Impact Assay. (B) Bar graphs summarizing quantification of proportion of CMO and DspMO1 morphants with a ruptured epidermis after Impact Assay (mean±s.e.m.). (C-D') Representative images of CMO (C.C') and DspMO1 (D,D') morphants after Impact Assay. (E) Schematic of experimental design for the Rotation Assay. (F) Bar graphs summarizing quantification of proportion of CMO and DspMO1 morphants with a ruptured epidermis after Rotation Assay (mean±s.e.m.). (G-H') Representative images of CMO (G,G') and DspMO1 (H,H') morphants after Rotation Assay.

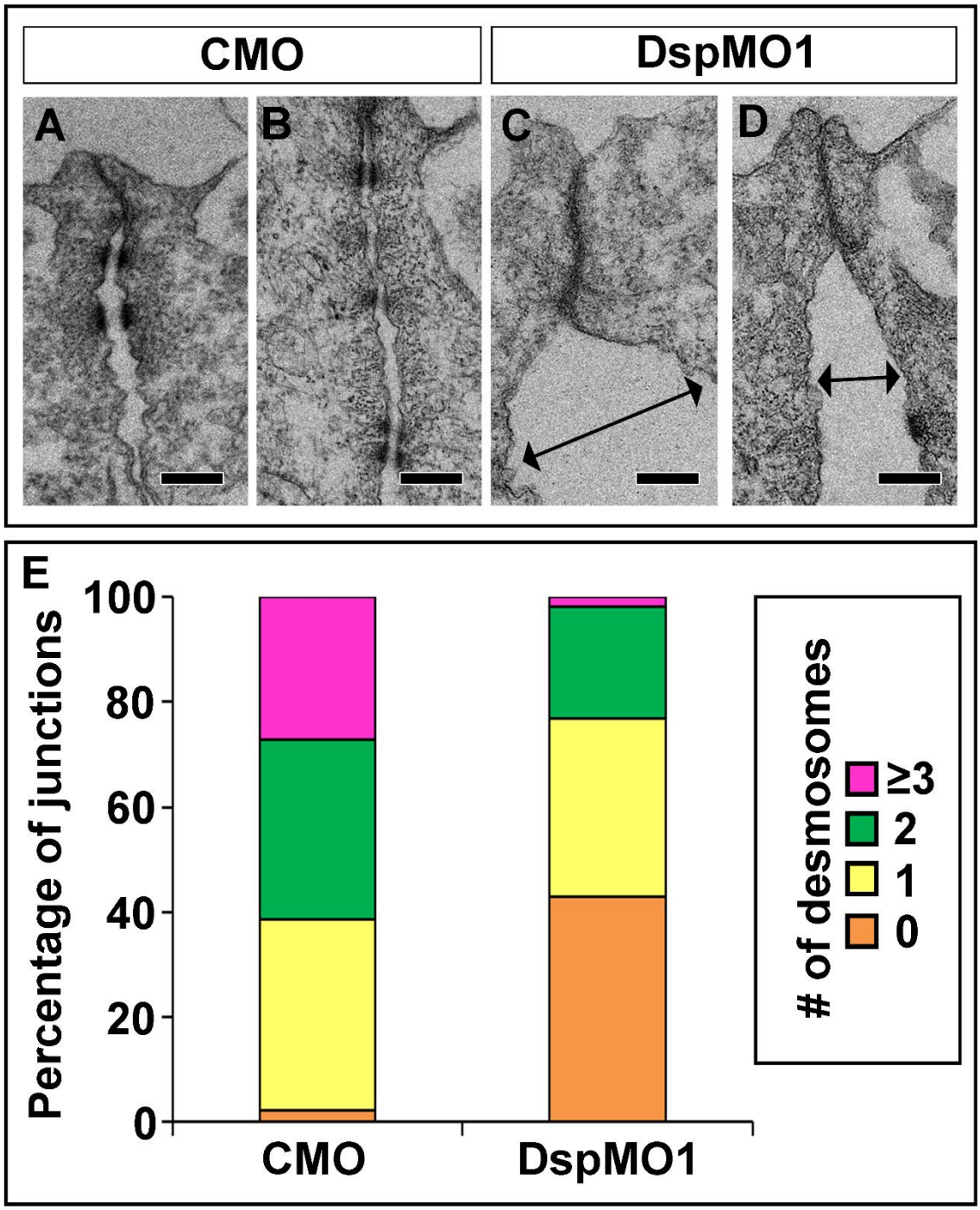

Figure 1.11: Depleting desmoplakin is associated with a loss of junctional desmosomes. (A-D) TEM micrograph of junctions in CMO (A,B) and DspMO1 (C,D) morphants (Scale bars = 250 nm). Intercellular gap in DspMO1 morphants (black arrows in C,D). (E) Graph depicting the percentage of junctions with desmosomes in CMO and DspMO1 morphants.

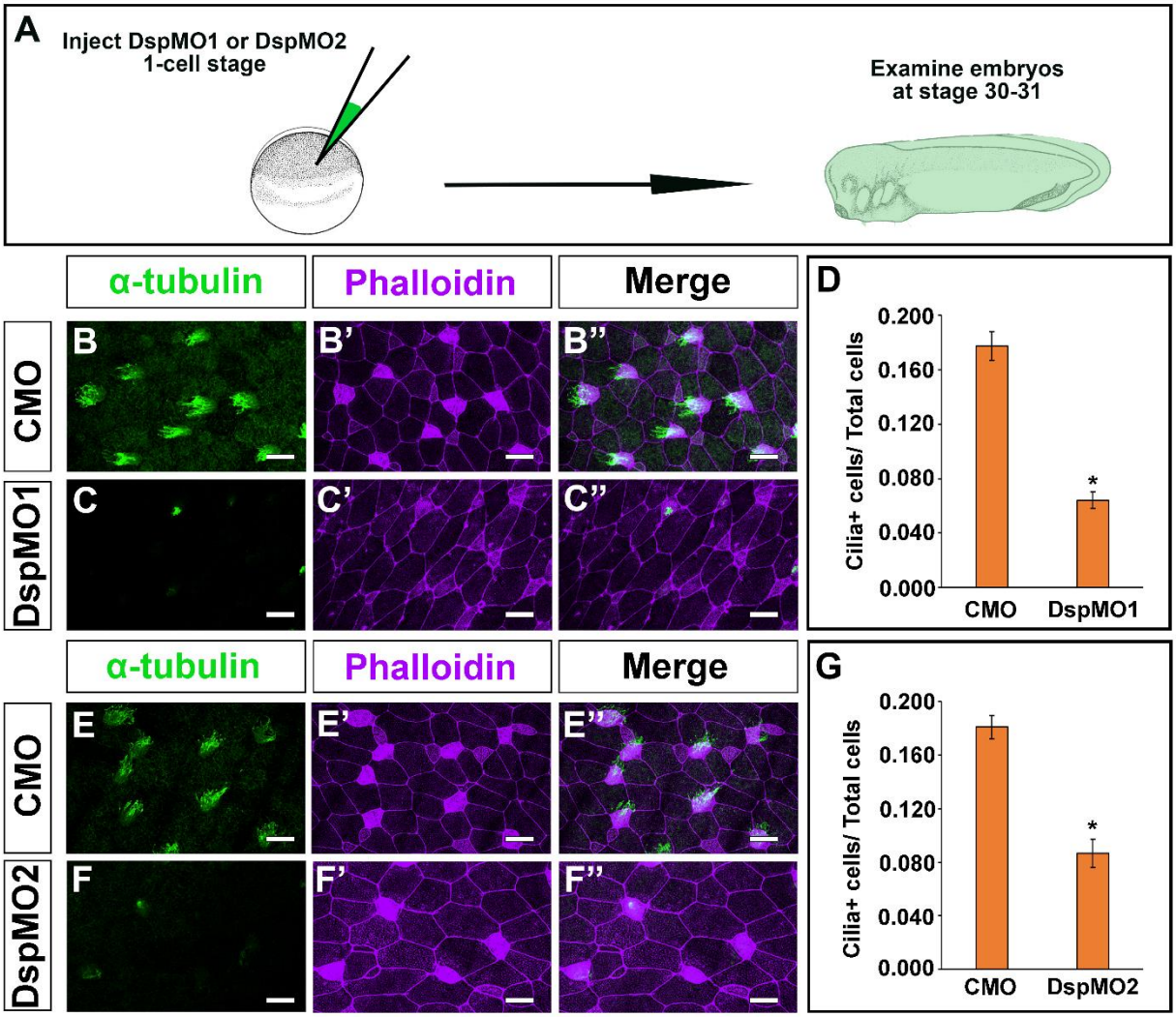

Figure 1.12: Desmoplakin morphants have a reduction in multiciliated cells.
(A) Schematic of morpholino injection and labeling for MCCs. (B-C'') IF of α-tubulin (green) and E-cadherin (purple) in CMO (B-B'') and DspMO1 (C-C'') morphants (Scale bar = 50μm). (D) Graph depicting ratio of cilia+ cells/ Total cells in CMO and DspMO1 morphants. (E-F'') IF of α-tubulin (green) and E-cadherin (purple) in CMO (E-E'') and DspMO2 (F-F'') morphants (Scale bar = 25μm). (G) Graph depicting ratio of cilia+ cells/ Total cells in CMO and DspMO2 morphants.

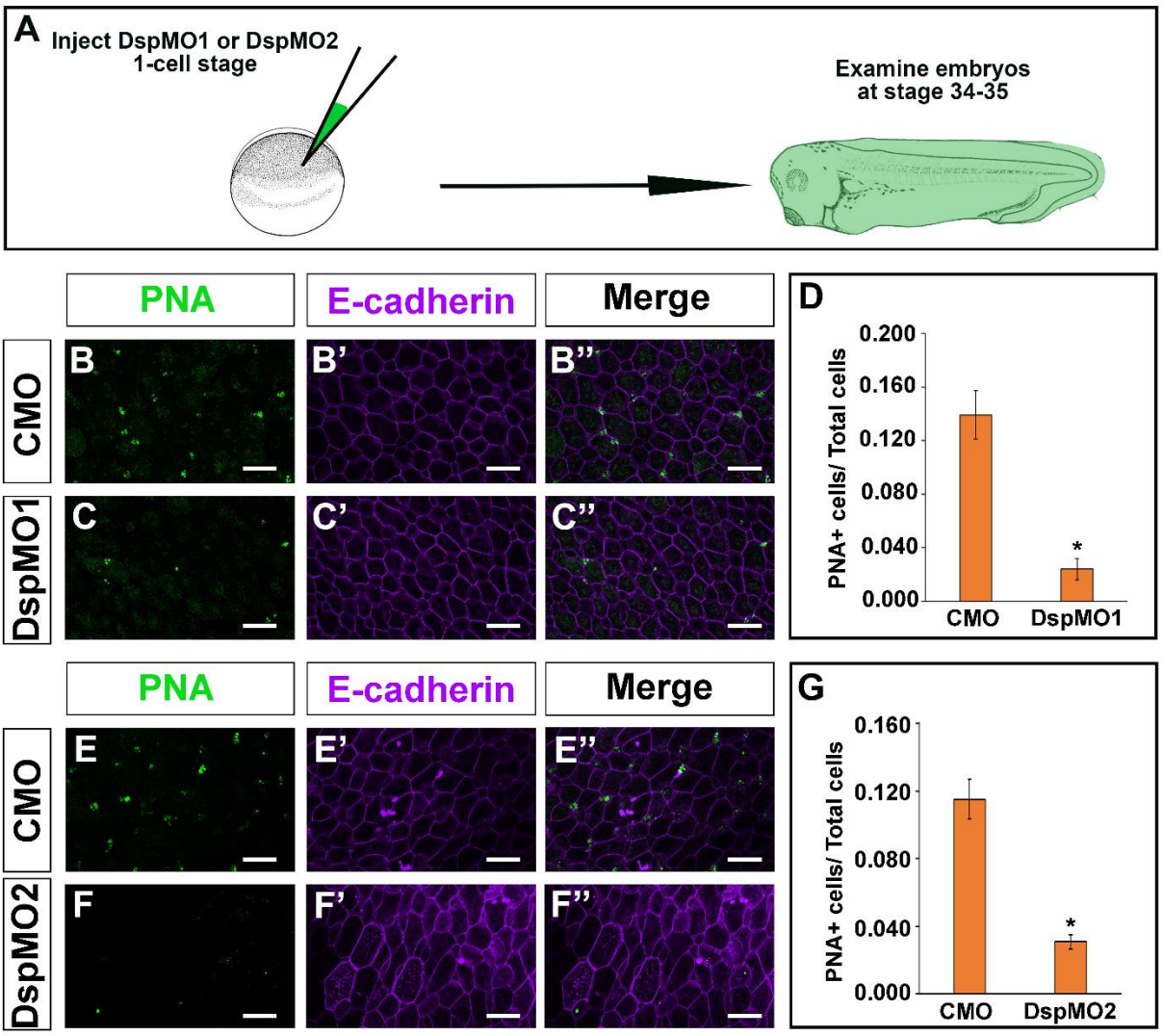

Figure 1.13: Desmoplakin morphants have a reduction in small secretory cells.
(A) Schematic of morpholino injection and labeling for SSCs. (B-C'') IF of Peanut Agglutinin or PNA (green) and E-cadherin (purple) in CMO (B-B'') and DspMO1 (C-C'') morphants (Scale bar = 50µm). (D) Graph depicting ratio of PNA+ cells/ Total cells in CMO and DspMO1 morphants. (E-F'') IF of Peanut Agglutinin or PNA (green) and E-cadherin (purple) in CMO (E-E'') and DspMO2 (F-F'') morphants (Scale bar = 50µm). (G) Graph depicting ratio of PNA+ cells/ Total cells in CMO and DspMO2 morphants.

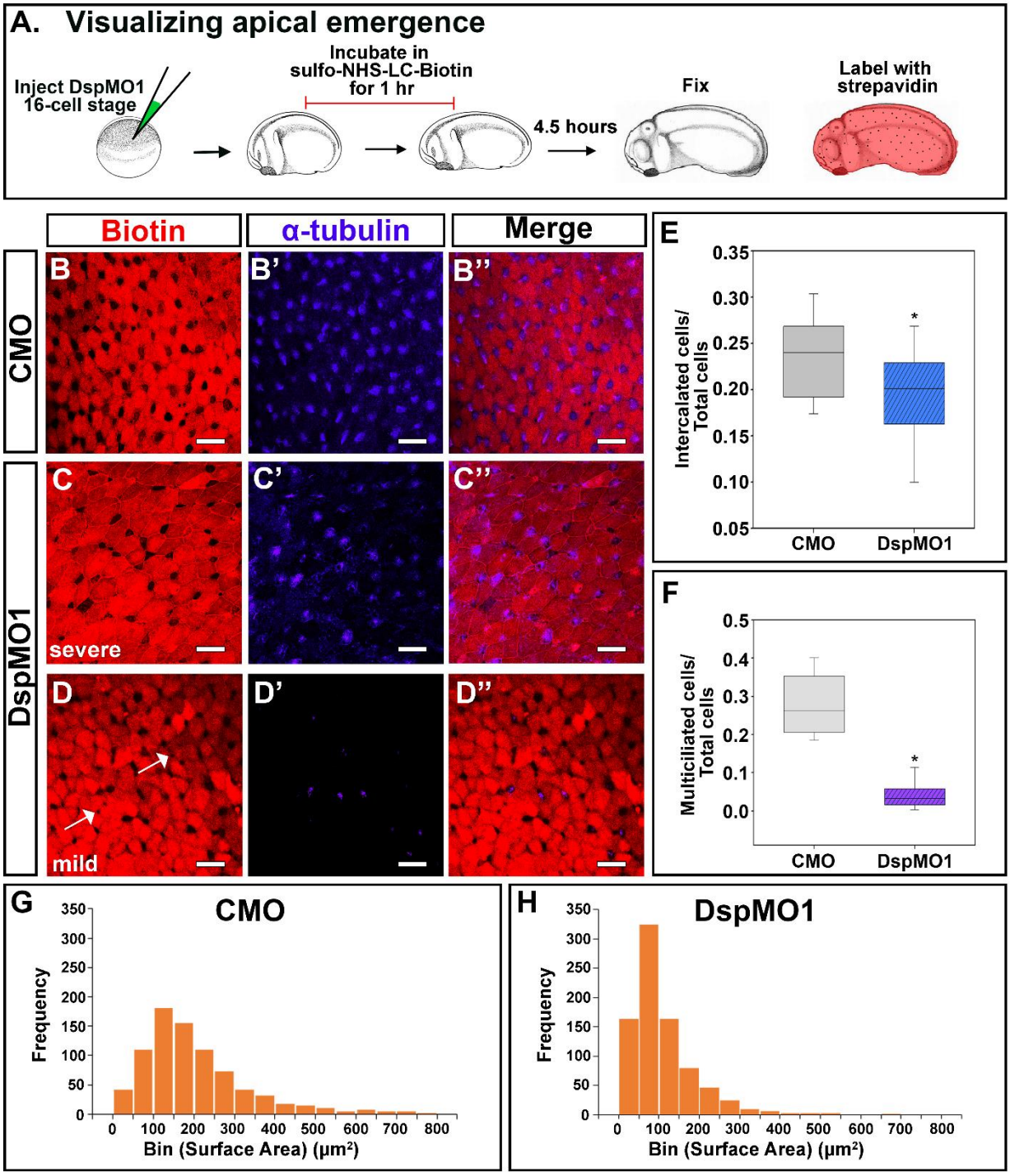
A. Visualizing apical emergence
Inject DspMO1
16-cell stage
Incubate in
sulfo-NHS-LC-Biotin
for 1 hr
4.5 hours
Fix
Label with
strepavidin
Biotin
α-tubulin
Merge
CMO
DspMO1
B
B'
B''
C
C'
C''
severe
D
D'
D''
mild
E
Intercalated cells/
Total cells
0.35
0.30
0.25
0.20
0.15
0.10
0.05
CMO
DspMO1
F
Multiciliated cells/
Total cells
0.5
0.4
0.3
0.2
0.1
0.0
CMO
DspMO1
G
CMO
Frequency
350
300
250
200
150
100
50
0
0 100 200 300 400 500 600 700 800
Bin (Surface Area) (μm²)
H
DspMO1
Frequency
350
300
250
200
150
100
50
0
0 100 200 300 400 500 600 700 800
Bin (Surface Area) (μm²)

Figure 1.14: Desmoplakin morphants have a reduction in radial intercalation and surface area of intercalating cells.
(A) Schematic of morpholino injection and biotin labeling to visualize apical emergence. (B-D'') IF of Biotin label (red) and Multiciliated cells (purple) in CMO (B-B'') and DspMO1 (C-D'') morphants (Scale bar = 50μm). Some intercalated cells in DspMO1 morphants have small apical surface (white arrows, D). (E) Box and whisker plot depicting ratio of Intercalated cells/ Total cells in CMO and DspMO1 morphants. (F) Box and whisker plot depicting ratio of Multiciliated cells/ Total cells in CMO and DspMO1 morphants. (G, H) Histograms depicting frequency and cumulative percentage of Surface Area of intercalated cells in a range of bin sizes in CMO (G) and DspMO1 (H) morphants.

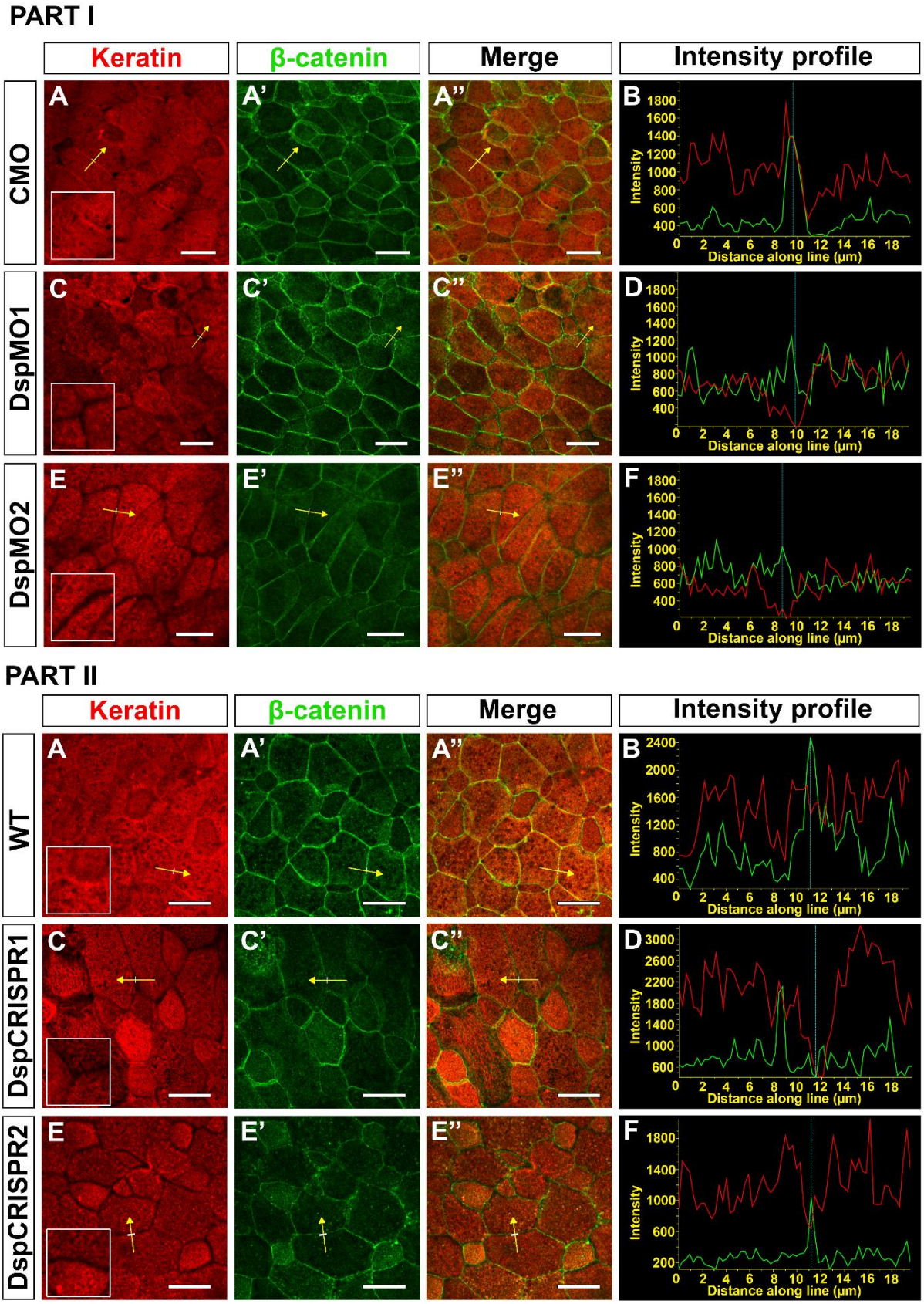
PART I
Keratin
β-catenin
Merge
Intensity profile
CMO
DspMO1
DspMO2
A
A'
A''
B
C
C'
C''
D
E
E'
E''
F
Intensity
Distance along line (μm)
PART II
WT
DspCRISPR1
DspCRISPR2

Figure 1.15: Desmoplakin morphants (Part I) and F0 mutants (Part II) display abnormal organization of keratin intermediate filaments.
(A-A'') Immunofluorescence of keratin Type II (red) and membrane marked by β-catenin (green) in control embryos. (C-C'') Immunofluorescence of keratin Type II with retraction from membrane in DspMO1 (Part I) and DspCRISPR1 (Part II) embryos. (E-E'') Immunofluorescence of keratin Type II with retraction from membrane in DspMO2 (Part I) and DspCRISPR2 (Part II) embryos. Scale bar = 25μm. Inset: Magnified view of cell-cell junction. (B, D, F) Intensity profile for red and green channels along yellow arrow for control (B), DspMO1 and DspCRISPR1 (D), and DspMO2 and DspCRISPR2 (F) embryos. Arrow points to right side of the graph. Vertical blue line represents position of white marker on arrow.

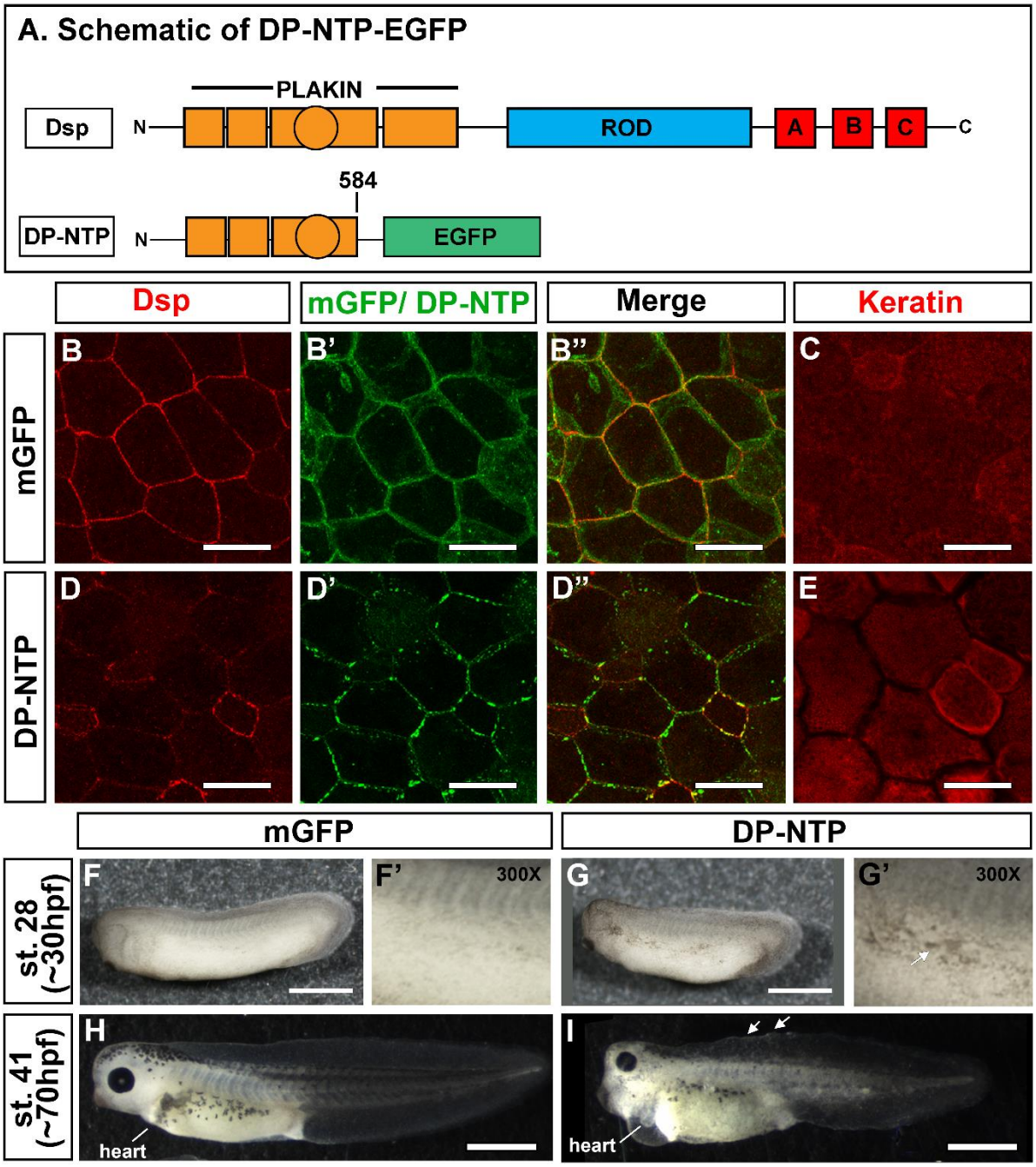

Figure 1.16: Dominant-negative desmoplakin disrupts keratin linkage and is associated with hyperpigmentation, reduced size, and cardiac defects.
(A) Schematic of wild-type Dsp (top) and a C-terminal deletion construct of Dsp, DP-NTP, tagged with EGFP (bottom). (B-B'') IF of desmoplakin in mGFP-injected embryos. (C) IF of Keratin in mGFP-injected embryos. (D-D'') IF of desmoplakin in DP-NTP-EGFP-injected embryos. (E) IF of Keratin in DP-NTP-EGFP-injected embryos. (Scale bar = 20 μm). (F-G') mGFP-injected (F) and DP-NTP-injected (G) embryos at st. 30-31 with an enlarged view of the epidermis (F', G') (Scale bar = 1 mm). (H) mGFP-injected at st. 40-41. (I) DP-NTP-injected embryos at st. 40-41 with cardiac defects and mild fin ruffling (white arrows) (Scale bar = 1 mm).

Table 1.8: Prevalence of phenotypes in Dsp morphants with p-values.

Phenotype	Control morphant (%)	Dsp Morphant (%)	p-value
Skin defect	3.62	39.8 (DspMO1)	3.34E-25
	3.41	27.47 (DspMO2)	9.39E-12
Blister	6.16	29.25 (DspMO1)	8.03E-13
	2.93	17.17 (DspMO2)	0.00039
Neural tube defect	0	16.33 (DspMO1)	2.31E-12
	1.46	15.02 (DspMO2)	4.91E-07
Eye defect	5.45	44.77 (DspMO1)	5.61E-07
	7.25	63.16 (DspMO2)	2.91E-12
Fin defect	1.82	53.23 (DspMO1)	6.79E-120
	0	38.16 (DspMO2)	9.65E-09
Cardiac edema	1.82	17.74 (DspMO1)	8.51E-89
	2.9	50 (DspMO2)	2.33E-10

Table 1.9: Prevalence of phenotypes in Dsp mutants with p-values.

Phenotype	Wild-type (%)	Dsp Mutant (%)	p-value
Skin defect	0.78	7.3 (DspCRISPR1)	0.00021
		8.18 (DspCRISPR2)	5.64E-05
Blister	1.56	10.95 (DspCRISPR1)	1.46E-05
		12.06 (DspCRISPR2)	2.83E-06
Neural tube defect	0	5.48 (DspCRISPR1)	0.00015
		5.17 (DspCRISPR2)	0.00023
Eye defect	1.41	13.33 (DspCRISPR1)	1.62E-08
		8.05 (DspCRISPR2)	0.0015
Fin defect	0.47	9.09 (DspCRISPR1)	7.61E-09
		8.05 (DspCRISPR2)	0.00012
Cardiac edema	0.47	10.91 (DspCRISPR1)	4.08E-06
		8.05 (DspCRISPR2)	0.00012

Table 1.10: Percentage of junctions with desmosomes in CMO and DspMO1 morphants.

Stage	Embryo	No. of junctions analyzed	Percentage of junctions			
			0 desmosomes/ junction	**1 desmosome/ junction**	**2 desmosomes/ junction**	**N≥3 desmosomes/ junction**
CMO	1	26	3.85 (n=1)	26.92 (n=7)	34.62 (n=9)	34.62 (n=9)
	2	18	0 (n=0)	50 (n=9)	33.33 (n=6)	16.67 (n=3)
DspMO1	1	24	33.33 (n=8)	20.83 (n=5)	45.83 (n=11)	0 (n=0)
	2	32	50 (n=16)	43.75 (n=14)	3.13 (n=1)	3.13 (n=1)

SECTION 3: REGULATION OF CELL JUNCTION LOCALIZATION BY C-JUN N-TERMINAL KINASE

Previous studies have demonstrated that JNK signals regulate adherens junction assembly in cultured intestinal epithelial cells (Naydenov et al., 2009). JNK inhibition also protects against E-cadherin internalization by EGTA-mediated calcium depletion in *Xenopus* epidermis (Houssin et al., 2017). Therefore, the next step was to determine whether JNK also regulated desmosomal junctions.

A. INCREASED JNK ACTIVITY IS ASSOCIATED WITH LOSS OF DESMOPLAKIN

First, the previously established constitutively-active JNK1 construct was injected into embryos to determine whether JNK signals regulate junctional disassembly in the *Xenopus* epidermis (**Fig. 1.17A**). This construct consists of a *Mus musculus* Map2k7β2 upstream of human JNK1α1. Map2k7 (MKK7) activates JNK1 in a constitutive manner (Lei et al., 2002; Liao et al., 2006). Wild-type embryos at st. 30-31 (35-38 hpf) were used as controls. Results revealed that while controls had Dsp expression at the cell membrane, CA-JNK-expressing embryos had decreased desmoplakin at the cell edges (70%, n=17, 3 experiments, **Fig. 1.17B,C**). Furthermore, desmoplakin appeared to be present in cytoplasmically-localized globules in a subset of cells in these embryos (**Fig. 1.17C**, arrows). These results suggest the possibility that increased JNK activity reduces desmoplakin levels.

B. DECREASED JNK ACTIVITY DURING GASTRULA STAGES IS ASSOCIATED WITH INCREASED DESMOPLAKIN AT THE MEMBRANE

Increased JNK activity was associated with reduced desmoplakin. Therefore, a plausible hypothesis is that decreased JNK activity would have the opposite effect, i.e., an increase in junctional desmoplakin.

To test this, embryos were treated with a JNK inhibitor, SP600125, at a concentration of 100µM from st. 14 (26 hpf) until st. 19 (31 hpf) (**Fig. 1.17D**). Normally at st. 19, desmoplakin is punctate at the membrane. Results revealed that desmoplakin was increased in 72% of embryos treated with SP600125 relative to controls (n=25, 3 experiments) (**Fig. 1.17E, F**). These results suggest that decreased JNK activity might increase desmoplakin at the membrane.

C. DECREASED JNK FUNCTION IS ASSOCIATED WITH RESISTANCE TO EGTA-MEDIATED DISPLACEMENT OF JUNCTIONAL PROTEINS

JNK inhibition was associated with increased desmoplakin at the junction. Also, inhibiting JNK in cell culture and *Xenopus* embryos alleviated ethylene glycol-bis(β-aminoethyl ether)-N,N,N',N'-tetraacetic acid (EGTA)-mediated internalization of E-cadherin (Houssin et al., 2017; Naydenov et al., 2009). EGTA chelates available calcium in the medium causing internalization of calcium-dependent junctions (Kartenbeck et al., 1991; Wallis et al., 2000). Therefore, the next step was to determine whether JNK inhibition could also alter EGTA-mediated displacement of desmoplakin in the *Xenopus* larval epidermis.

To test this hypothesis, st. 32 embryos were treated with a JNK inhibitor (SP600125) until st.41 followed by a short EGTA (4mM) treatment (**Fig. 1.18A**). Results revealed that the epidermis of control embryos (treated with EGTA) began to dissociate from the rest of the body after an

average of 27 min. (**Fig. 1.18D**). On the other hand, embryos exposed to both the JNK inhibitor and EGTA took on average 63 min longer to begin to dissociate (n=16, 2 experiments; **Fig. 1.18E**; average time to begin dissociation=90 min.).

Next, desmoplakin was imaged by immunofluorescence in treated embryos to determine whether there were changes in localization. Results revealed that in embryos treated with DMSO or SP600125 alone, desmoplakin was maintained at the membrane (**Fig. 1.18F,G**). In the embryos that only received EGTA, the desmoplakin appeared to be re-localized to the cytoplasm (n=16, 2 experiments; **Fig. 1.18H**). However, in embryos treated with both the JNK inhibitor and EGTA, the desmoplakin was maintained at the membrane similar to controls that were treated with DMSO or treated with SP600125 alone (n=16, 2 experiments; **Fig. 1.18I**). These results indicate that JNK inhibition can protect the cells from the anti-adhesive effects of EGTA. Furthermore, JNK inhibition appears to protect against the EGTA-mediated loss of adherens junction and desmosome components from the membrane.

D. JNK INHIBITION ENHANCES THE MECHANICAL RESISTANCE OF DESMOPLAKIN MORPHANTS

JNK inhibition prevented EGTA-induced displacement of desmoplakin and E-cadherin. Additionally, overexpression of E-cadherin can compensate for Pemphigus vulgaris IgG-mediated loss of desmosomal adhesion in cells (Rotzer et al., 2015), suggesting a role for E-cadherin in mechanical resistance. Therefore, the next step was to determine whether JNK inhibition of Dsp morphants improves the mechanical stress response. To test this, DspMO1 and control morphants were treated with the JNK inhibitor (100µM SP600125) or control (DMSO) for 5 hours (st. 22-26). The mechanical resistance of the SP600125- and DMSO-treated DspMO1 and control

morphants was evaluated using the "Impact Assay" (as described in section 2, Part III, A.1) (**Fig. 1.19A**). Results revealed that 77% of the DMSO-treated DspMO1 morphants had epidermal tears (n=24, 3 experiments) (**Fig. 1.19D,F**). On the other hand, only 33% of JNK inhibitor treated DspMO1 morphants had epidermal tears or disruptions (n= 21, 3 replicates, t-test, p= 0.005; **Fig. 1.19E,F**). These results present the possibility that blocking JNK function can increase mechanical resistance in the epidermis of desmoplakin-deficient embryos.

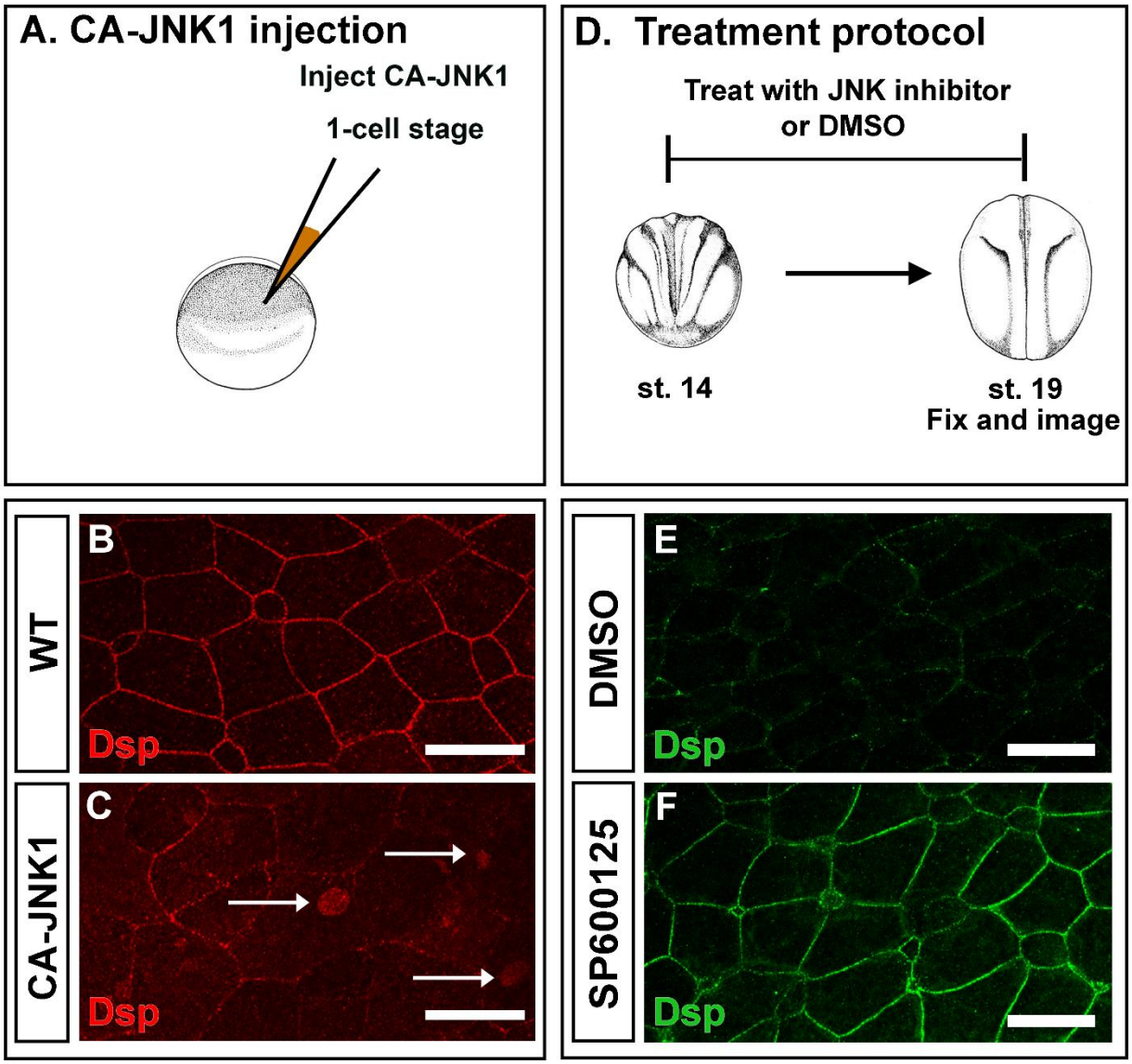

Figure 1.17: Differences in JNK activity is associated with changes in desmoplakin pattern at cell membranes.

(A) Schematic of experimental design for injection of constitutively-active JNK1 (CA-JNK). (B-C) IF of Dsp (red) in WT (B) and CA-JNK-injected embryos (C). Apparent cytoplasmically-localized globules of Dsp in (C) (white arrows) (Scale bar = 25μm). (D) Schematic of experimental design for treatment of embryos with JNK inhibitor SP600125. DMSO is used as control treatment. (E-F) IF of Dsp (green) in DMSO- (E) and SP600125-treated embryos (F) (Scale bar = 25μm).

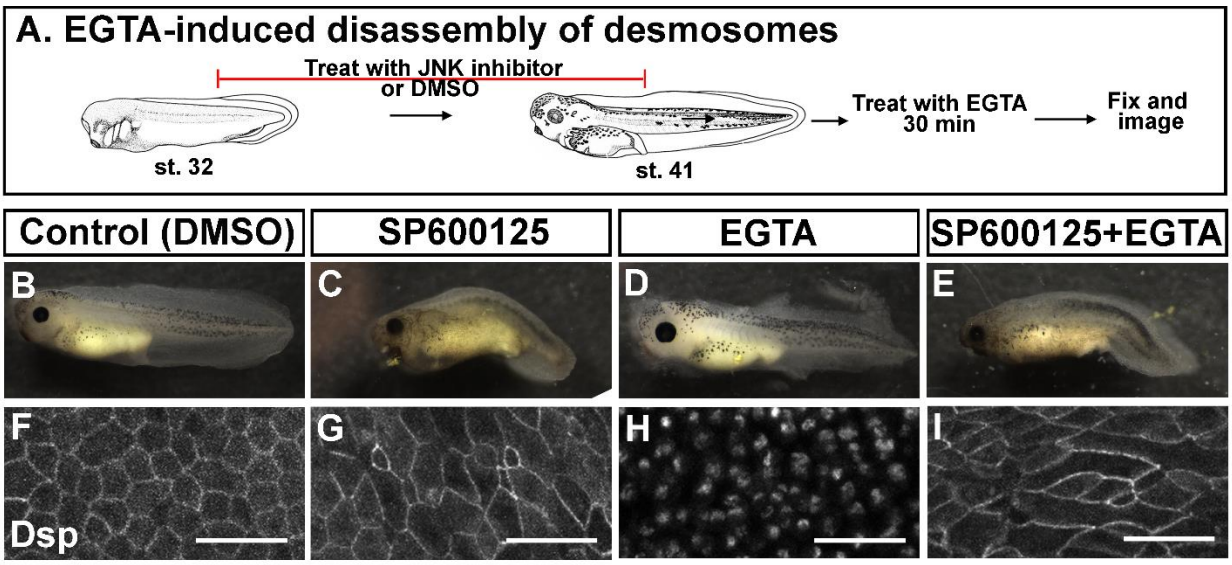

Figure 1.18: Decreased JNK activity is associated with resistance to EGTA-mediated internalization of junctional proteins.
(A) Schematic of experimental design for treatment of embryos with JNK inhibitor SP600125 and EGTA. (B-E) Images of embryos after treatment with DMSO (B), SP600125 (C), DMSO+EGTA (D), and SP600125+EGTA (E). (F-I) IF of desmoplakin after treatment with DMSO (F), SP600125 (H'), DMSO+EGTA (H), and SP600125+EGTA (I) (Scale bar = 50μm).

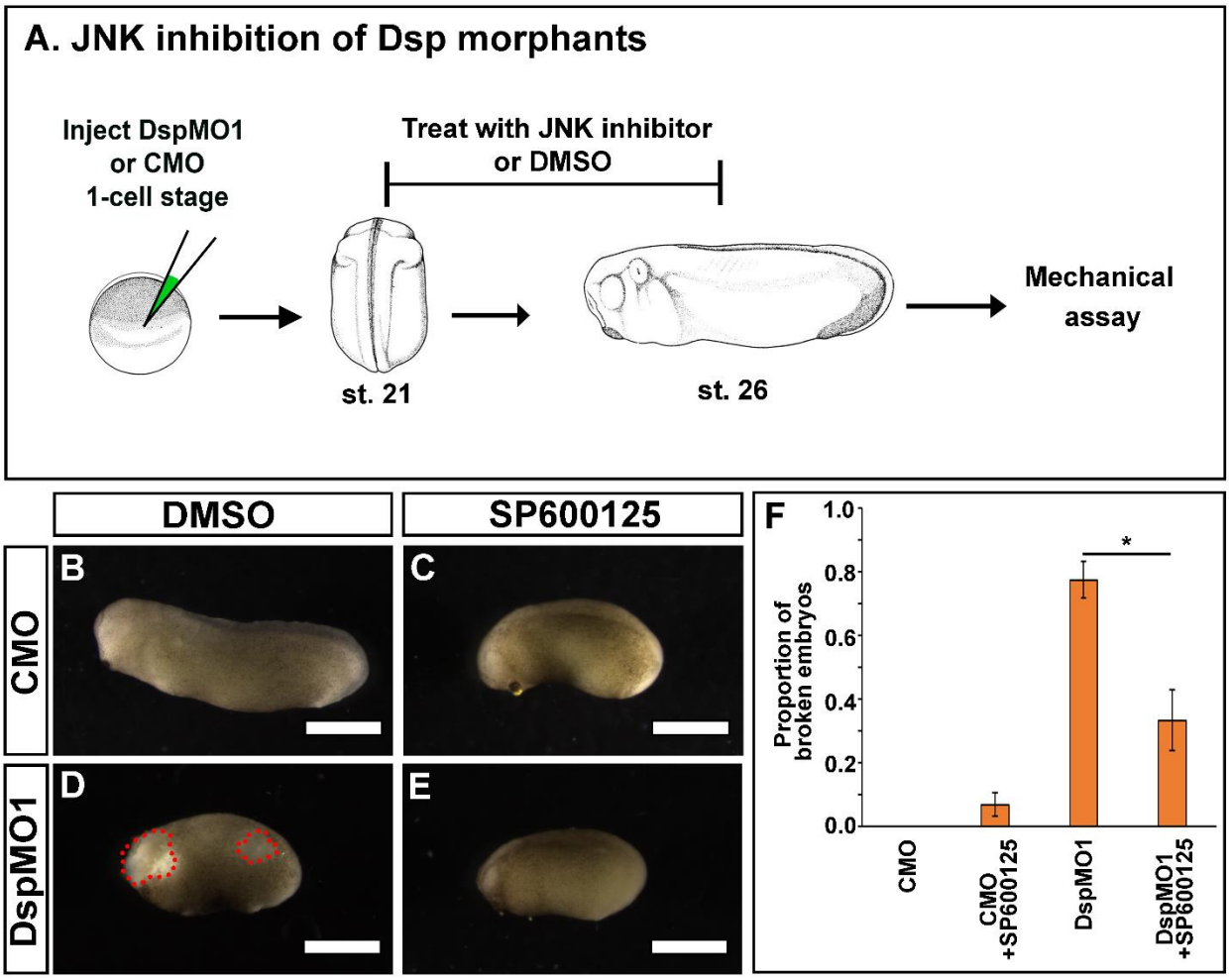

Figure 1.19: JNK inhibition enhances the mechanical resistance of desmoplakin morphants. (A) Schematic of treatment of embryos with JNK inhibitor SP600125 followed by mechanical assay. (B-E) Images of embryos after mechanical assay of CMO+DMSO (B) CMO+SP600125 (C), DspMO1+DMSO (D), and DspMO1+SP600125 (E) (Scale bar = 1 mm). (F) Graph depicting proportion of embryos with damaged epidermis after mechanical assay.

DISCUSSION

Diseases of the desmosome often result in abnormalities in the skin, heart, and hair follicle. This causes increased susceptibility to skin infections and cardiac disorders, the latter of which can be fatal during teenage years. One way to help affected individuals is by targeting signaling pathways that contribute to the pathophysiology of the disease. Hence, creating animal models of desmosomal disease can facilitate the study and development of therapeutic strategies. This study here uses antisense morpholinos and the CRISPR/ Cas9 system to reduce the levels of the desmosomal protein, desmoplakin, in *Xenopus* embryos. Abnormalities are present in the epidermis and desmosome ultrastructure already described in previous literature (Gallicano et al., 2001). Furthermore, there are anomalies in the development of other embryonic structures such as the orofacial region. Perturbations in morphogenesis, including radial intercalation of distinct cell types into the outer layer of the developing epidermis also occur. Additionally, this study demonstrates a potential role for c-Jun N-terminal kinase (JNK) in regulating desmosome assembly *in vivo*.

Desmosome structure and development is highly similar in the frog embryonic epidermis

The desmosome structure in the *Xenopus* embryo is similar to other vertebrates. Ultrastructurally, the desmosome appears as a distinct electron-dense cytoplasmic plaque adjacent to the plasma membrane (Berika and Garrod, 2014; Farquhar and Palade, 1963, 1965). This structure is similar to desmosomes observed in the adult skin and tadpole of *X. laevis*

(Borysenko and Revel, 1973). Importantly, it also resembles those observed in humans, mice and zebrafish (Fleming et al., 1991; Garrod and Chidgey, 2008; Goonesinghe et al., 2012; Holbrook and Odland, 1975). Desmosomes in *Xenopus* embryos were infrequently observed to possess a "midline". Midline-containing desmosomes are also observed as early as blastocyst stages in the mouse (Fleming et al., 1991). Such a midline is thought to indicate a mature desmosome. Evidence in mouse epidermis and tissue culture also suggests that such desmosomes might also be "hyperadhesive" (Garrod and Kimura, 2008; Garrod et al., 2005; Hobbs and Green, 2012). Hyperadhesive desmosomes are insensitive to calcium depletion, which is normally required for desmosomal cadherin dimerization. Tissue remodeling, which occurs frequently in a developing embryo, would require that some desmosomes be more dynamic and therefore, not hyperadhesive. This is indeed the case in the early mouse embryo which initially has calcium-dependent desmosomes that lack a midline. Desmosomes then develop a midline and become hyperadhesive between E12-E14. Hyperadhesive desmosomes can also revert to calcium-dependence in the mouse trophectoderm, which might be required to facilitate cell migration (Kimura et al., 2012). Thus, the presence of a hyperadhesive or mature desmosome in an early embryo might indicate the need for tissue stability at certain times during development.

Consistent with the structural observations of *Xenopus* embryonic desmosomes, molecular studies indicate the presence of desmosomal cadherins in the epidermis of the *X. laevis* adult (Ohga et al., 2004). RNAseq analysis of the *X. laevis* transcriptome also reveals the expression of Desmoglein 2, Desmocollin 3, and Desmoplakin, in the embryo beginning in cleavage stages (Session et al., 2016).

Not only does the *Xenopus* desmosome share structural similarities, it may also increase in numbers as the embryo develops across vertebrates. There was a quantitative increase in the

number of epidermal desmosomes per junction in the outer epidermal layers in the *Xenopus* embryo between gastrulation and neurulation. Similarly, in the mouse embryo, desmosome numbers per junction increase between the cleavage and blastocyst stages (Fleming et al., 1991). In the developing human epidermis, desmosome numbers increase between the 9th and 20th weeks of gestation (Dale et al., 1985; Holbrook and Odland, 1975). Although the observations in *Xenopus*, mouse, and human are recorded at different timepoints, this data indicates that there is an increase in desmosomal numbers per junction as the vertebrate embryo develops. This trend coincides with epidermal development in the *Xenopus* embryo. During this time, the ectoderm undergoes migratory movements such as convergent extension and radial intercalation and begins to express epidermal differentiation markers (Jonas et al., 1985; Nieuwkoop and Faber, 1967; Wilson and Hemmati-Brivanlou, 1995). Maintaining an adhesive outer layer while these dynamic processes occur is crucial. The vitelline membrane, which normally protects the embryo from external forces, is also gradually lost after neurulation as the embryo becomes increasingly motile. Thus, the increase in desmosomes might facilitate stronger intercellular binding to form an epidermis that has greater adhesion and protective capabilities.

At later stages in the *Xenopus* embryo, desmosome numbers continued to increase and began to appear between inner and outer cell layers. During tadpole stages, desmosomes are present between cells within the inner layer. Similarly, such findings are reported in the developing human fetal epidermis (Dale et al., 1985; Holbrook and Odland, 1975). Specifically, desmosomes are observed between the periderm and basal layers of the developing epidermis. As the human epidermis undergoes stratification beginning at the 9th gestational week, desmosomes begin to appear between the new layers as well (Dale et al., 1985). Thus, the appearance of these desmosomes may serve to further strengthen the epidermal tissue.

Together, the similarity in desmosome structure and development between *Xenopus* and mammalian models indicate that the frog is a practical model for the study of desmosomes in the embryo.

The *Xenopus* desmoplakin gene and protein are highly similar to mammalian homologs

Our analysis revealed that desmoplakin, a component that is unique to and present in all desmosomes, is highly similar between *Xenopus* and mammalian homologs. The *Xenopus dsp.L* coding region contains 24 exons similar to the human and mouse homologs (Green et al., 1999). The *Xenopus* Dsp.L protein also shares a high degree of similarity with mouse and human homologs. Furthermore, the three functional domains of Dsp, the plakin, rod, and C-terminal were predicted to be present and shared a high degree of similarity with the corresponding domains in mammalian Dsp. Thus, the high degree of similarity between *Xenopus* and mammalian desmoplakin at the whole protein and domain level suggests that function might also be conserved across species. This further validates the frog model as an ideal model for the study of desmoplakin.

The *Xenopus* desmoplakin L and S homologs are highly similar except in the plakin domain

Genome annotation in *X. laevis* reveals the presence of Dsp on each subgenome, Dsp.L and Dsp.S. Comparative analysis revealed a high degree of similarity between the domains of Dsp.L and Dsp.S homologs. However, while the *dsp.L* and *dsp.S* gene coding regions share 91% identity, the coding region of *dsp.S* only contains 22 exons, where the missing exons correspond to exons 11 and 12 in *dsp.L*. Closer inspection of the individual domains revealed differences in the SR56/ SH3 plakin subdomains. This region corresponds to the missing exons in *dsp.S*. Further,

RNAseq data reveals that both homologs are differentially expressed in the embryonic stages as well as adult tissues (Session et al., 2016). Dsp.S has relatively higher expression until the gastrula stages (st. 10) and this pattern reverses at neurulation stages (st. 15). In adult tissues, both homologs are expressed in the skin, eye and heart tissues, although at differing levels. The high degree of similarity between the homologs suggests that the differential expression patterns might only persist as an ancestral mechanism that was not subject to selection. However, the expression of both Dsp homologs simultaneously suggests an overall higher gene dosage requirement. Investigating the mechanism of transcriptional regulation of each homolog might provide insight into differences in expression. Although not analyzed in this study, only one of the two Dsp morpholinos was predicted to target both the Dsp.L and Dsp.S mRNA, while the other is predicted to target only Dsp.L. This is based on the number of mismatches between the morpholino and the homolog. Therefore, it might be expected that targeting both homologs might have a more detrimental effect than if only one homolog was targeted. Both Dsp morphants present with the same phenotypes with similar severities, suggesting that 1) Dsp.L is the major homolog expressed with minimal contribution from Dsp.S or 2) both homologs are targeted by the morpholino even though one is not predicted to be targeted. One way to confirm this is to perform a qRT-PCR of the Dsp.S mRNA in both morphants. Alternatively, designing morpholinos that are can bind to homolog-specific regions can tease apart the relative importance of each homolog.

Deficient desmoplakin in *X. laevis* results in defects in epidermis and the heart

The desmoplakin morphant and F0 mutant *Xenopus* embryos were able to progress through gastrulation without any apparent defects, similar to the Dsp knockout mouse (Gallicano et al., 2001). Also comparable to mouse embryos lacking desmoplakin, defects became apparent after

this stage. This coincides with the increase in desmosome number, suggesting that desmoplakin and desmosomes might have a more significant role post-gastrulation.

The most distinct phenotype in *Xenopus* Dsp morphants and mutants was the smaller size of the embryos. Mouse embryos lacking Dsp are also smaller (Gallicano et al., 2001). There are several possibilities to explain the small size observed here. Preliminary data reveals a reduction in cell division in the *Xenopus* Dsp morphants. A similar reduction in cell proliferation is reported in the Dsp knockout mouse embryos (Gallicano et al., 2001). Smaller size could also be caused by an increase in cell death in the embryo. However, while it was not determined whether *Xenopus* embryos deficient in Dsp have increased cell death, no significant increase in apoptotic cells is observed in the Dsp knockout mouse (Gallicano et al., 2001). Epidermal cell surface areas in *Xenopus* Dsp morphants were smaller which could also account for a smaller size of the embryo. Convergent extension, which facilitates expansion of the surface area in the developing embryo and elongation along the anterio-posterior axis is partially regulated by cell adhesion (Shimizu et al., 2005; Solnica-Krezel et al., 1996; Walck-Shannon and Hardin, 2014). For example, when desmosomal cadherins Desmocollin 1 and Desmoglein 2 are decreased in zebrafish, convergent extension movements are defective, resulting in reduced anterio-posterior axis length (Goonesinghe et al., 2012). Therefore, perturbations in this process may also occur as a result of reduced desmoplakin. Finally, a failure of all the above processes in combination might culminate in smaller embryo size in Dsp morphants.

Xenopus Dsp morphants and mutants also exhibited epidermal blistering. Such blistering is also documented in plakoglobin- and epidermis-specific Desmocollin 3-knockout mouse models as well as patients with desmosomal diseases such as pemphigus (Bierkamp et al., 1996; Chen et al., 2008; Mahoney et al., 1999; Payne et al., 2004). Blistering can occur as a result of loss of

keratinocyte adhesion or acantholysis. Therefore, reduction of Dsp in *Xenopus* embryos exhibit blisters probably due to impaired adhesion between cell layers.

The skin of *Xenopus* embryos lacking Dsp was more fragile to mechanical perturbations such as impact and shear forces. Such fragility is also present in human patients with desmosomal diseases such as ectodermal dysplasia and skin fragility syndrome, which is caused by Plakophilin-1 mutations (Jonkman et al., 2005; McGrath et al., 1997; Whittock et al., 2002). Additionally, mouse knockout models of plakoglobin, desmoglein 3, and desmocollin 1 exhibit epidermal fragility (Allen et al., 1996; Bierkamp et al., 1996; Chidgey et al., 2001). Also, loss of desmoplakin in mice can result in intercellular separation of epidermal layers and fragility to handling (Gallicano et al., 2001; Vasioukhin et al., 2001). Therefore, this suggests that the sensitivity of the *Xenopus* epidermis to mechanical forces might be a result of impaired desmosomal function which also mimics mammalian models.

Cardiac defects were also present in *Xenopus* Dsp morphants and mutants. Such defects are a prominent clinical feature of disorders of desmosomal proteins, including desmoplakin, plakoglobin, plakophilin 2, desmoglein 2, and desmocollin 2 (Awad et al., 2006; Beffagna et al., 2007; Gerull et al., 2004; McKoy et al., 2000; Norgett et al., 2000; Pilichou et al., 2006; van Tintelen et al., 2006; Yu et al., 2008). The Dsp knockout mouse also has a collapsed heart with a relatively low heart rate (Gallicano et al., 2001). Overall, the similarities in defects further validates the applicability of the frog model for studies of the desmosome.

Besides the common phenotypes associated with desmosome disruption, such as epidermal blistering or tearing and cardiac defects, other less common defects including hyperpigmentation, neural tube and eye defects also occur in *Xenopus* Dsp morphants and mutants.

Xenopus Dsp morphants and F0 mutants exhibited darkened patches of epidermis or hyperpigmentation. In animal models, melanin-containing melanosomes which influence epidermal pigmentation are known to be translocated by actin cytoskeleton and intermediate filaments (Mayerson and Brumbaugh, 1981; Wasmeier et al., 2008; Wu et al., 1998). Actin and microtubules are also involved in melanosome movement in *Xenopus* melanophores (Rogers and Gelfand, 1998; Tuma et al., 1998). Here, keratin filaments appeared to be disrupted in *Xenopus* Dsp morphants. A similar disruption of these filaments is observed in patients with epidermolysis bullosa simplex with mottled hyperpigmentation caused by mutations in Keratin 5 (KRT5) (OMIM:131960) (Bruckner-Tuderman et al., 1989; Uttam et al., 1996). Ultrastructural analysis of hyperpigmented tissue in these patients reveals a perinuclear aggregation of melanosomes (Irvine et al., 2001). While it was not determined whether melanosome aggregation occurs in Dsp morphants, this suggests the possibility that disruption of the desmosome-keratin attachment or changes in actin organization indirectly might affect distribution of melanosomes within cells.

Neural tube defects were observed in *Xenopus* Dsp morphants and mutants. In mice lacking Dsp, neural tube defects were also reported (Gallicano et al., 2001). Notably, no human cases of neural tube closure defects have been associated with defective desmosomes, although this might be because of embryonic lethality.

Eye defects including abnormal RPE pigmentation were also present in *Xenopus* Dsp morphants and mutants. Dsp was detected in the *Xenopus* larval outer corneal epithelium. Similarly, in the bovine, Dsp is detected in the corneal epithelium (Messent et al., 2000). Further, desmosomes persist at the corneal wound edge *in vitro* in rabbits (Kuwabara et al., 1976). Pemphigus vulgaris patients with anti-Dsg3 antibodies also have severe blistering of eyelid

conjunctiva (Lifshitz et al., 2004). Together these results suggest that desmosomes are required in the eye and that Dsp may play a role in the proper development of eye structures.

Xenopus Dsp morphants have reduction in desmosomes and changes in tissue architecture

A reduction in desmosomes per junction was observed in *Xenopus* embryos with deficient Dsp. Further, 43% of junctions had no desmosomes. A similar reduction in size and number of desmosomes is also reported in Dsp knockout mice (Gallicano et al., 1998). The intercellular gap between cells in *Xenopus* Dsp morphants was also increased at junctions with few or no desmosomes. In Dsp knockout mice also, there is a loss of adherence between cells (Gallicano et al., 2001). Similarly, zebrafish Desmocollin 1 and Desmoglein 2 morphants have an increase in intercellular gap when desmosomes are defective or absent (Goonesinghe et al., 2012). Therefore, these results suggest that desmoplakin might be essential for desmosome assembly or stability. However, an epidermis-specific Dsp knockout mouse displays no significant reduction in desmosome number in suprabasal layers, although keratin filament attachment is still perturbed (Vasioukhin et al., 2001). This might warrant further study to determine if desmoplakin acts as a desmosome reinforcer further in development.

Xenopus embryos with deficient Dsp have defects in specialized cell types

Cell types such as multiciliated cells, small secretory cells, and ionocytes are specified and intercalate into the outer epidermal layer in *Xenopus* larvae beginning sometime after gastrulation (Dubaissi et al., 2014). These cells are thought to contribute to the protection of the larva against bacterial infections (Stubbs et al., 2006). *Xenopus* embryos with deficient Dsp exhibited a decrease in the number of cilia-positive multiciliated cells and PNA-positive small secretory cells. When

cilia were present, they were shorter and fewer in number. The defective structures in these cell types indicate that differentiation might be perturbed when Dsp is reduced. The development of these cell types is controlled by many proteins. Forkhead transcription factors, Foxa1 and Foxj1 are involved in the differentiation of small secretory cells and multiciliated cells, respectively (Dubaissi et al., 2014; Stubbs et al., 2008). Other transcriptional regulators such as multicilin and its upstream regulator Gmnc are necessary for expression of ciliogenesis genes such as α-tubulin (Stubbs et al., 2012; Zhou et al., 2015). Further, the planar cell polarity protein, Dishevelled, can regulate the docking of basal bodies which is required prior to extension of cilia (Park et al., 2008). However, there is no reported role for Dsp or desmosomes in multiciliated cell differentiation. Instead, Dsp may indirectly regulate basal body docking and ciliogenesis. For instance, loss of the basal body protein ninein results in impaired primary cilia formation in U2OS human osteosarcoma cells (Graser et al., 2007). Microtubule organization through ninein can, in turn, be regulated by Dsp in epidermal keratinocytes (Lechler and Fuchs, 2007). Thus, although basal body generation differs between monociliated cells (such as primary cilia) and multiciliated cells (Brooks and Wallingford, 2014), Dsp may influence ciliogenesis in these cell types indirectly. Together, these results suggest that Dsp may play a role in differentiation of these cell types by regulating the development of specialized structures.

Desmosomes may play a novel role in radial intercalation

Here, multiciliated cells and small secretory cells were identified based on the expression of a single marker for each cell type. Since a second marker was not used to confirm these results, two main possibilities might explain these findings: 1) cells emerge but differentiation of these cell types is perturbed, and 2) the emergence of cells from the inner layer is disrupted. The

emergence of specialized cell types occurs through the process of radial intercalation (Deblandre et al., 1999; Dubaissi and Papalopulu, 2011; Dubaissi et al., 2014). Therefore, a plausible hypothesis is that radial intercalation is perturbed in embryos with deficient Dsp. Biotin labeling assays confirmed that radial intercalation was slightly but significantly reduced in *Xenopus* Dsp morphants.

Regulation of cell-cell and cell-extracellular matrix interactions can influence radial intercalation (Walck-Shannon and Hardin, 2014). For example, cell-ECM interactions through dystroglycan are required for radial intercalation to occur in the *X. laevis* epidermis (Sirour et al., 2011). Inhibition of the Epidermal Growth Factor pathway leads to defects in E-cadherin turnover and is correlated with reduced intercalation in the zebrafish blastoderm during epiboly (Morita and Heisenberg, 2013; Song et al., 2013). There is also some evidence for proteins that regulate planar cell polarity in this process. For instance, Par3 and Par6 are required for apical positioning of CLAMP in intercalating cells of *X. laevis* epidermis. In turn, CLAMP promotes microtubule stabilization, which is thought to be required for intercalation (Werner et al., 2014). Loss of function of another PCP protein, the Rab11 GTPase, results in defects in establishment of the apical domain of multiciliated cells and, in turn, intercalation in *X. laevis* epidermis (Kim et al., 2012). The results of this study suggest a possible role for desmoplakin in facilitating radial intercalation.

Radial intercalation culminates when emerging cells "dock" in the outer layer. This is followed by expansion of the apical surfaces of these cells. *Xenopus* embryos deficient in Dsp have a significant reduction in apical surface area of intercalating cells. Occasionally, cilia-positive and PNA-positive cells were detected in *Xenopus* Dsp morphants. However, these cells were situated below the apical surface, appearing to be "stuck" between the two layers (data not shown).

Together, these results suggest a problem with both apical emergence and expansion. The resulting defective apical expansion could explain why cells have fewer cilia (in MCCs) or vesicles (in SSCs). The decrease in apical surface area might prevent basal body or vesicle docking at the apical membrane resulting in defective development of these structures.

Two of the three major cytoskeletal filaments, actin and microtubules, are implicated as drivers of emergence and apical expansion in the *Xenopus* epidermis. These processes are partly governed by cell-autonomous RhoA- and formin1-mediated actomyosin tractive forces through E-cadherin (Sedzinski et al., 2016, 2017). Further, CLAMP-mediated stabilization of microtubules at the apical region of intercalating cells is required for radial intercalation (Werner et al., 2014). The current study reveals that keratin filaments are disorganized in *Xenopus* embryos with deficient Dsp. Therefore, it is possible that intermediate filaments, which constitute the third major cytoskeletal protein might also be involved in emergence and apical expansion of intercalating cells. However, further experiments will have to be performed to determine whether this is the case.

In summary, there are two possible mechanisms through which radial intercalation is regulated by the desmosomal complex. First, desmosomal adhesion might be necessary for traction forces, which are found to be important for this process. Therefore, the loss of desmosomal complex from cell contacts when desmoplakin is reduced possibly abrogates this tractive force required for radial intercalation and expansion. Second, tractive forces through the keratin filaments might also be crucial. Therefore, the disorganization of keratin filaments observed in desmoplakin morphants might result in a reduction in transmission of these forces within the intercalating cell (**Fig. 1.20**).

C-Jun N-terminal Kinase (JNK) is a potential regulator of desmoplakin localization and stability

Altering JNK signaling was correlated with changes in desmoplakin localization in *Xenopus* embryos. JNK (c-jun N-terminal kinase), a MAPK protein, is activated by exposure of cells to stressors including osmotic stress and radiation (Ip and Davis, 1998; Rosette and Karin, 1996). It regulates a wide variety of cellular processes including apoptosis, migration, and cell division (Davis, 2000; Dong et al., 2001; Karin and Gallagher, 2005). JNK can also regulate morphogenesis in the embryo, such as convergent extension movements (Kuhl, 2002); (Yamanaka et al., 2002). JNK is also known to regulate cell junction proteins. Constitutively-active JNK1 disrupts E-cadherin organization at cell contacts in *Xenopus* embryos (Houssin et al., 2017). Cytoplasmic puncta of E-cadherin are also observed in these embryos in conjunction with membrane-localized clathrin, suggesting endocytosis in response to JNK activity. Additionally, increased JNK activity is associated with disruption of adherens and tight junction proteins in different epithelial cell types (Naydenov et al., 2009; Samak et al., 2011; You et al., 2013).

In the current study, several experiments reveal a correlation between JNK activity and desmoplakin localization and adhesion. First, increased JNK activity was found to be correlated with reduced membrane desmoplakin in *Xenopus* embryonic epidermis. Cytosolic clusters of desmoplakin were also present in these embryos. Conversely, inhibiting JNK in the neurulating *Xenopus* embryo was associated with increased desmoplakin at cell contracts relative to controls.

Second, inhibition of JNK protected against cytosolic displacement of desmoplakin in the presence of EGTA, a calcium chelator. The EGTA-induced desmoplakin dissociation assay is used to demonstrate the occurrence of hyperadhesion or calcium-independent adhesion (Garrod et al., 2005; Mattey and Garrod, 1986; Wallis et al., 2000). Following JNK inhibition, there is resistance

to EGTA-mediated internalization of E-cadherin in *Xenopus* embryonic epidermis (Houssin et al., 2017). Naydenov and colleagues (2009) also demonstrate an increase in phospho-JNK (active JNK) following calcium depletion, further suggesting this increase in active JNK as a mechanism for EGTA-mediated loss of desmosome adhesion. Post-translational modification of desmosomal proteins might influence stability or adhesion. For instance, phosphorylation of Dsp at specific serine residues is associated with desmosome disassembly or loss of hyperadhesion (Dehner et al., 2014; Kroger et al., 2013). This phenomenon is found to occur in a Protein Kinase C alpha (PKCα)-dependent manner, although a direct interaction is yet to be demonstrated (Bass-Zubek et al., 2008; Godsel et al., 2005; Hobbs and Green, 2012; Kroger et al., 2013; Sheu et al., 1989). Furthermore, PKCα is an established regulator of desmosomal hyperadhesion in confluent cell culture and wound edge epidermis (Garrod and Chidgey, 2008; Garrod et al., 2005; Wallis et al., 2000). Similarly, JNK can also regulate cell adhesion and migration by phosphorylating cell junction proteins including β-catenin and focal adhesion protein paxillin, respectively (Huang et al., 2003; Lee et al., 2009). Therefore, JNK might regulate desmosomal hyperadhesion directly or indirectly through phosphorylation of desmosomal proteins.

Third, the epidermis of *Xenopus* Dsp morphants displays increased resistance to mechanical stress following JNK inhibition. Previous data reveals maintenance of adhesion against EGTA-mediated calcium depletion in *Xenopus* embryos following treatment with a JNK inhibitor (Houssin et al., 2017). E-cadherin is also not internalized in these embryos. Since the JNK pathway is known to be involved in mechanotransduction, it is possible that JNK signaling might affect the mechanical response of *Xenopus* Dsp morphants. For example, mechanical stretching can activate JNK in multiple cell types *in vitro* (Ingram et al., 2000; Katsumi et al., 2005; Pereira et al., 2011). Mechanically-activated JNK can further lead to cellular and morphological effects such as actin

remodeling in endothelial cells and enhanced migration in human mesenchymal stem cells (Mengistu et al., 2011; Yuan et al., 2012). Activation of JNK through mechanotransductive signals can also induce osteoblast apoptosis (Matsui et al., 2014). However, the response of JNK to mechanotransduction in these instances occurs over minutes or hours. The mechanical assays performed here are virtually instantaneous, making it implausible that JNK-mediated increase in adhesion is due to rapid modifications of desmosomal proteins. Instead, the inhibition of JNK during the treatment phase might modify desmosomal adhesion. Dsp morphants still form some desmosomes at cell-cell junctions. Preliminary data also reveals that E-cadherin is present at the membrane in Dsp morphants but may be reduced. Therefore, JNK inhibition in Dsp morphants might increase resistance to mechanical forces by strengthening adhesive contacts at existing desmosomes and adherens junctions.

There are a number of plausible mechanisms through which JNK might be regulating desmosome assembly or stability. First, JNK may directly interact with and phosphorylate desmosomal or desmosome-associated proteins, leading to conformational changes and disassembly. JNK phosphorylates the armadillo protein β-catenin leading to disruption of the adherens junction (Lee et al., 2009; You et al., 2013). The adherens junctions and desmosomes are analogous to each other since both junctions contain members of the cadherin and armadillo protein families. For example, desmosomes contain plakoglobin, a member of the armadillo family most closely related to β-catenin (Peifer et al., 1992). Further, plakoglobin has overlapping functions with β-catenin, being able to interact with the same molecules (Zhurinsky et al., 2000). Plakoglobin is also able to interact with Tcf/ Lef proteins, a β-catenin target in the canonical Wnt signaling pathway (Kolly et al., 2007; Williamson et al., 2006). Therefore, plakoglobin might be a hypothetical target for JNK phosphorylation in the desmosome. JNK phosphorylates β-catenin

at the Ser37 and Thr41 residues (Lee et al., 2009; You et al., 2013). Both residues appear to be conserved in plakoglobin as well, further suggesting that plakoglobin is a putative JNK target. JNK also associates with the underlying intermediate filaments. JNK can phosphorylate keratin 8 leading to intermediate filament reorganization (He et al., 2002; Park et al., 2011). Thus, a plausible hypothesis is that JNK phosphorylates plakoglobin or keratin (or both) leading to desmosome disruption.

Second, JNK might regulate desmosome assembly through a transcriptional mechanism. In the current study, the JNK inhibition and activation paradigms were performed over many hours or days. Therefore, it is possible that changes in desmoplakin localization observed are due to JNK-mediated transcription. Inhibition of JNK in human epidermal keratinocytes over 48h leads to over 2-fold transcriptional induction of desmosomal genes of suprabasal cells including Desmoglein 1 and Desmocollin 1 (Gazel et al., 2006). Also, JNK inhibition in HaCaT keratinocytes alters expression of basal epidermal markers Keratin 5, Keratin 17, and Desmoglein 3 (Kitagawa et al., 2014). However, while changes to desmoplakin expression were not investigated here, a microarray of JNK-inhibited *Xenopus* embryos did not reveal deregulation of expression of any desmosomal genes. This suggests that JNK might differentially regulate transcriptional control of desmosomal genes in different stages of development or different models.

Third, JNK activity might also regulate desmosome assembly indirectly through the adherens junction. As mentioned above, inhibiting JNK activity leads to adherens junction formation in many epithelial cell types (Naydenov et al., 2009; Samak et al., 2011; You et al., 2013). There is also evidence to suggest that adherens junctions formation is a prerequisite to desmosome formation. For instance, disruption of adherens junctions and classical cadherins delay

desmosome assembly in keratinocytes and other epithelial cell types, although a detailed mechanism is yet to be determined (Amagai et al., 1995a; Gumbiner et al., 1988). Therefore, JNK activity might regulate desmosome formation indirectly through its effects on adherens junction formation.

Fourth, JNK might regulate desmosome assembly though an endocytic mechanism. Upon injection of constitutively-active JNK1 in *Xenopus* embryos, there is an increase in membrane-localized clathrin (Houssin et al., 2017). JNK might also remodel actin filaments near the membrane through activation of the ezrin-radixin-moesin complex, which associates with epithelial junctions (Ivanov et al., 2004b; Naydenov et al., 2009). Actin filament remodeling into contractile F-actin rings is known to be required for endocytosis of epithelial junctions (Ivanov et al., 2004a). While there are no direct JNK targets reported in this process, other MAPK proteins have been shown to be involved in junction endocytosis. For instance, p38MAPK inhibition prevents Pemphigus vulgaris IgG-mediated endocytosis of Dsg3 in keratinocytes (Jolly et al., 2010). Moreover, this endocytosis is thought to occur through a caveolin-1-dependent mechanism (Delva et al., 2008). Therefore, JNK might regulate desmosome assembly dynamics through control of the endocytic pathway.

In summary, there are many direct and indirect mechanisms through which JNK activity might regulate desmosome assembly. Based on what is known about JNK-mediated assembly of the tight and adherens junctions as well as interaction with keratin filaments, it is likely that the JNK-mediated phosphorylation of desmosomal proteins, for example, plakoglobin, regulates desmosome assembly (**Fig. 1.21**). On the other hand, JNK activity might also regulate desmosomal gene expression based on evidence of this pathway occurring in mammalian tissues (**Fig. 1.22**).

CONCLUSIONS AND FUTURE DIRECTIONS

The current study reveals roles for the desmosomal protein, desmoplakin, in the embryonic epidermis using the *Xenopus laevis* model. In addition to phenotypes commonly observed with desmosomal disruption, there are defects in neural tube closure and improper development of eye structures. There is evidence for the presence of junctional desmosomes in these tissues. This suggests that desmosomes are important for the morphogenesis of these tissues in the developing embryo. Knowledge of fate maps in the *Xenopus* embryo makes it a convenient model to alter the expression of desmoplakin (or other desmosomal proteins) in a tissue-specific manner. This method is one way to determine the function of desmoplakin in specific tissues. Such experiments can verify whether some of the phenotypes observed in this study are a consequence of 1) loss of desmoplakin function in the developing tissue itself or, 2) a non-specific effect due to disruption of an earlier developmental process.

The results of the present study also reveal a relationship between desmosomes and radial intercalation in the epidermis. Specifically, there are perturbations in both radial intercalation and apical expansion when desmoplakin is reduced. Loss of desmosome from the cell contacts might 1) enhance the ability of cells to intercalate due to less resistance, or 2) hinder the process due to less traction. The defective apical expansion might disrupt the final stages of differentiation and development of specialized structures. Assembly of actin and microtubule cytoskeletal filaments are thought to partially regulate radial intercalation, implying that keratin filaments might also play

a role (Sedzinski et al., 2016, 2017; Werner et al., 2014). Together, Dsp localization and Dsp-mediated linkage of keratin might act as mediators of radial intercalation (**Fig. 1.20**).

It is unknown whether Dsp and keratin attachment are required cell-autonomously or in the neighboring cells to facilitate apical expansion. One way to test this is to perform donor transplants of the outer epidermal layer prior to intercalation. This method involves removing the outer epidermal layer of a desmoplakin morphant and replacing the outer epidermal layer of the "host" control embryo or vice-versa. If desmoplakin or the desmoplakin-intermediate filament attachment is required in the outer layer for intercalation, then donor transplants that have reduced desmoplakin would exhibit reduced intercalation. If desmoplakin is required in the intercalating cell, then host embryos that have reduced desmoplakin would exhibit reduced intercalation. Desmoplakin may also be required for proper organization of actin or microtubules which, in turn, are known to be required for radial intercalation. Desmoplakin serves as a microtubule organizing center in differentiated keratinocytes (Lechler and Fuchs, 2007). Desmoplakin loss is also correlated with changes in actin cytoskeleton organization (Sumigray and Lechler, 2012; Vasioukhin et al., 2001). In addition, disruption of the desmosomal complex in Dsp morphants may lead to mislocalization of plakophilin 1, which is involved in actin cytoskeleton dynamics (Hatzfeld et al., 2000). To determine whether actin or microtubule organization is affected, immunofluorescence labelling of either filament can be performed.

Finally, data from this study highlights JNK as a possible regulator of desmosome assembly and adhesion. Phosphorylation and other post-translational modifications of junctional proteins is associated with control of junction assembly and adhesive strength. Alternatively, JNK might regulate desmosome assembly through a transcriptional pathway. Junction remodeling is crucial in tissues undergoing dynamic processes including morphogenesis, wound healing, and

cell division (Garrod et al., 2005; Higashi et al., 2016; Thomason et al., 2012). Indeed, JNK activity is high in the proliferating basal layer and relatively lower in differentiated suprabasal layers of human neonatal foreskin epidermis (You et al., 2013). Collectively, there are at least two plausible mechanisms through which JNK might regulate desmosome assembly and adhesion (**Fig. 1.21, 1.22**).

It is not yet known whether JNK interacts with desmosomal proteins as it does with proteins in the adherens and tight junctions. Performing a Co-IP and mass spectrometry of proteins that associate with JNK might give some insight into interactions. One caveat is the insoluble nature of the desmosomal plaque. This characteristic makes it difficult to separate the desmosomal proteins and therefore, study protein-protein interactions. However, new tools such as the biotin ligase-based BioID can be utilized to screen for possible protein-protein interactions (Roux et al., 2013). For example, a fusion protein of biotin ligase with JNK can be injected into embryos. Performing a capture of biotinylated proteins in these embryos followed by mass spectrometry can reveal if desmosomal proteins interact with JNK. If JNK-mediated phosphorylation of plakoglobin leads to changes in desmosome assembly dynamics, a phospho-deficient mutant of plakoglobin can be used. An expected result would be that overexpression of JNK would not affect desmosome assembly. Alternatively, a JNK *in vitro* kinase assay can be performed with plakoglobin as a substrate, which can then be analyzed for phosphorylation using mass spectrometry.

If JNK exerts direct transcriptional control, a ChIP-Seq can be performed following treatment to determine whether cJun or the AP-1 complex are bound to promoter sequences. If there are changes in the level of binding to desmosomal genes, it would suggest that JNK transcriptionally regulates these loci. Alternatively, a bioinformatics analysis of promoter sequences can be performed to identify consensus binding sites for cJun or the AP-1 complex.

The assay to test for hyperadhesion also suggests that inhibiting JNK improves the adhesiveness of the desmosomal complex. Specifically, inhibiting JNK might lead to conformational changes in the calcium-binding domain of the desmoglein or desmocollins (**Fig. 1.23**). One way to test this hypothesis is to image desmosomes using TEM to determine if there are more desmosomes with a midline, which is thought to represent a hyperadhesive desmosome.

Since altering JNK activity has effects on desmosomal assembly and adhesion, it might influence radial intercalation as well. For instance, one plausible hypothesis is that overexpression of JNK leads to reduced intercalation due to reduction in desmoplakin at cell contacts.

The results of this study have possible applications in treating human desmosomal disease. For example, inhibition p38MAPK alleviates some of the pathogenic effects of Pemphigus Vulgaris IgG in tissue culture, such as endocytosis of Desmoglein 3 (Saito et al., 2012). A plausible hypothesis is that inhibition of JNK might also prevent Desmoglein 3 internalization, similar to the effects observed in *Xenopus* epidermis.

In conclusion, the present study validates the use of the frog as a tractable model for the study of desmosomes. The study also demonstrates potential functions for desmoplakin and desmosomes in regulating epidermal morphogenesis and radial intercalation in the embryo. Finally, JNK is identified as a potential regulator of desmosome assembly and adhesion. This implicates JNK as a new therapeutic target in desmosomal disease treatment. Further investigation into the mechanism of JNK-mediated regulation of the desmosome might reveal its efficacy in treating human disease.

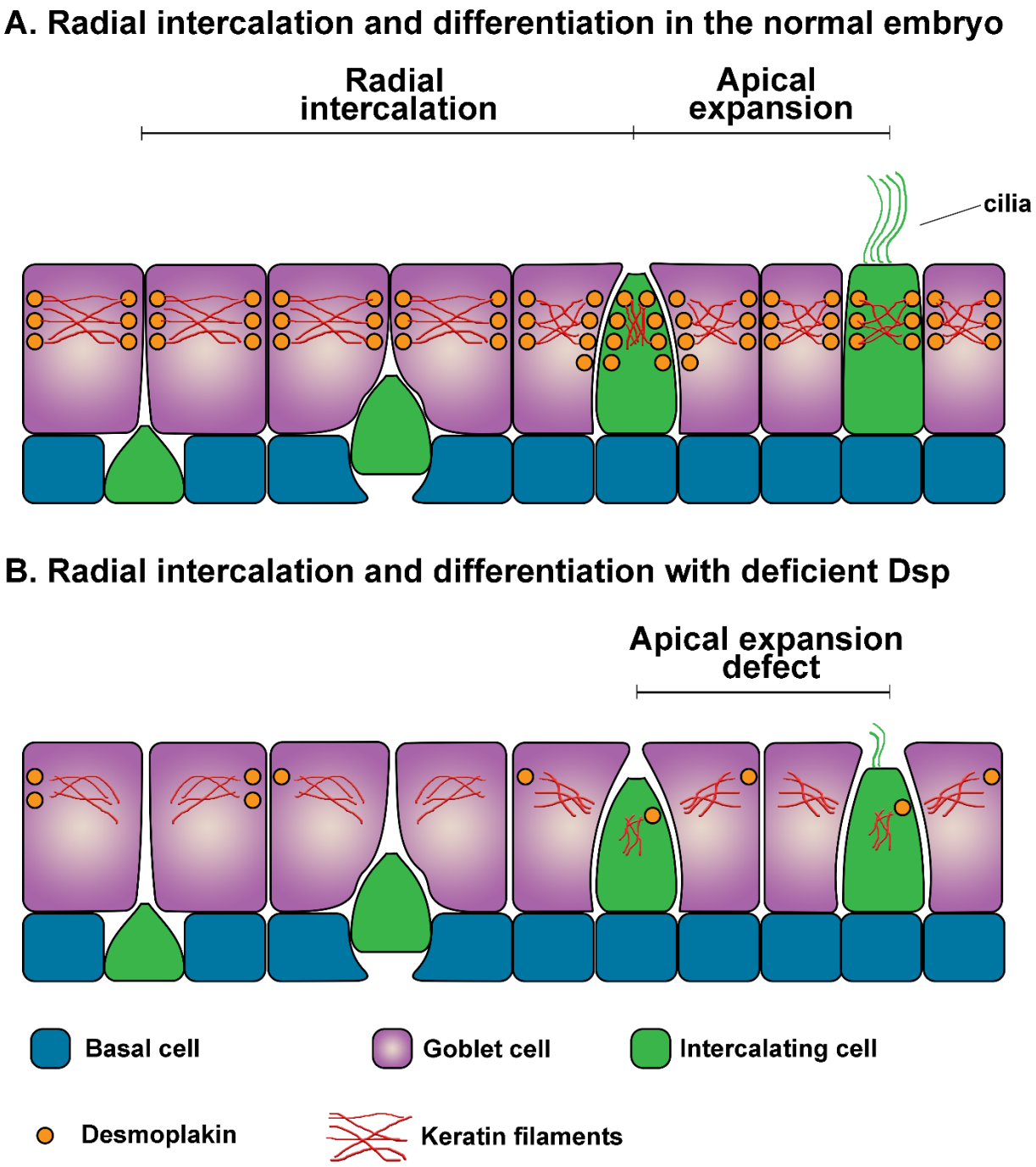

Figure 1.20: Desmoplakin is a potential mediator of radial intercalation.
(A) Radial intercalation in a normal embryo occurs through a step-wise process of apical emergence followed by apical expansion and development of specialized characteristics such as cilia in a multiciliated cell. This probably occurs through enrichment of Dsp. (B) Radial intercalation in embryos with deficient Dsp is faulty, possibly due to defective apical emergence and expansion, leading to smaller apical surface and defective development of specialized structures such as fewer and shorter cilia.

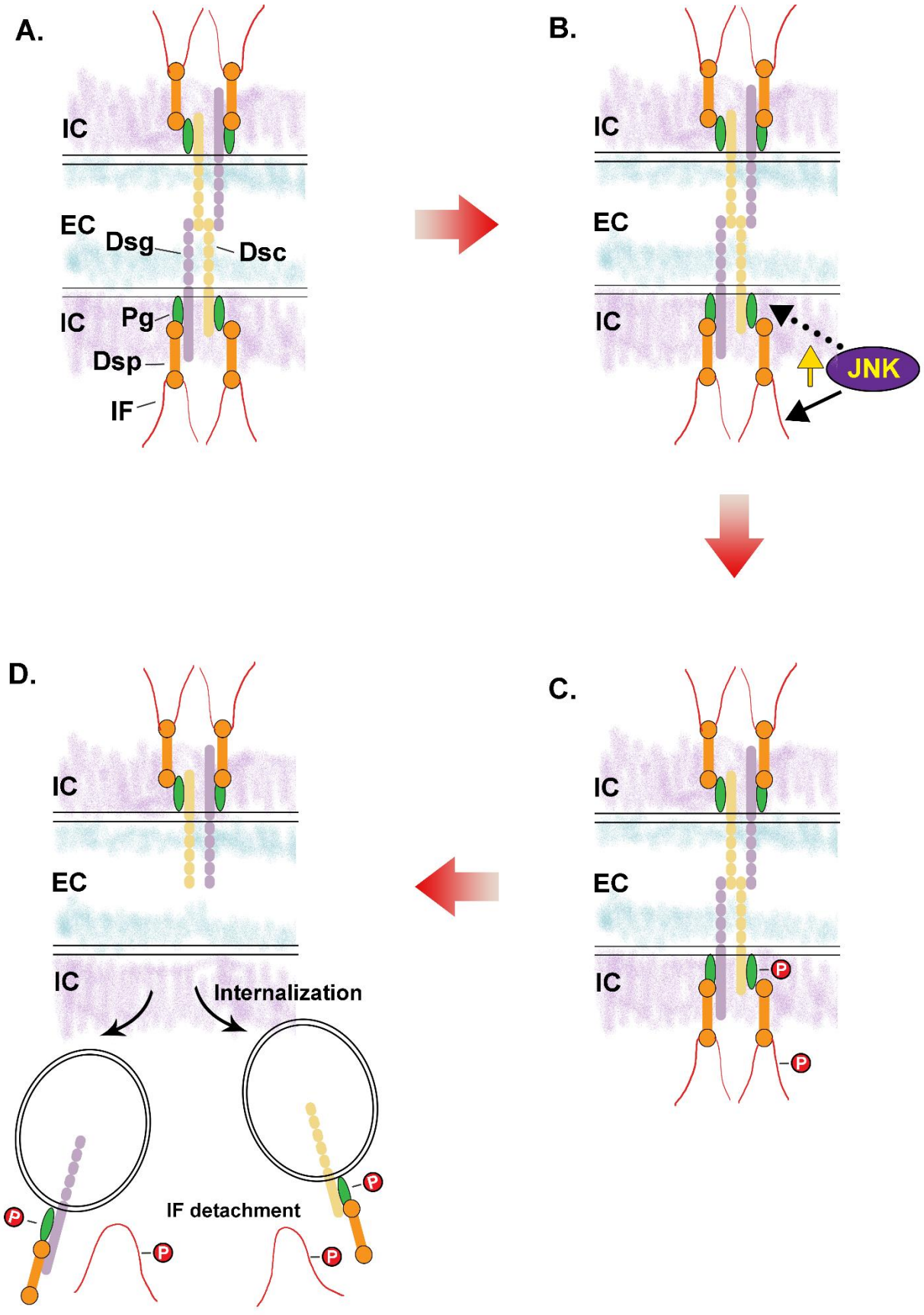
A.
IC
EC
Dsg
Dsc
IC
Pg
Dsp
IF
B.
IC
EC
IC
JNK
C.
IC
EC
IC
P
P
D.
IC
EC
IC
Internalization
IF detachment
P
P
P
P

Figure 1.21: Model for JNK-mediated regulation of desmosome assembly through post-translational modification.
(A) A desmosomal complex at the cell-cell junction. (B, C) Increased JNK activity might lead to direct or indirect phosphorylation of desmosomal proteins such as plakoglobin (Pg) and keratin filaments. (D) Phosphorylation probably leads to keratin detachment and internalization of desmosomal components.

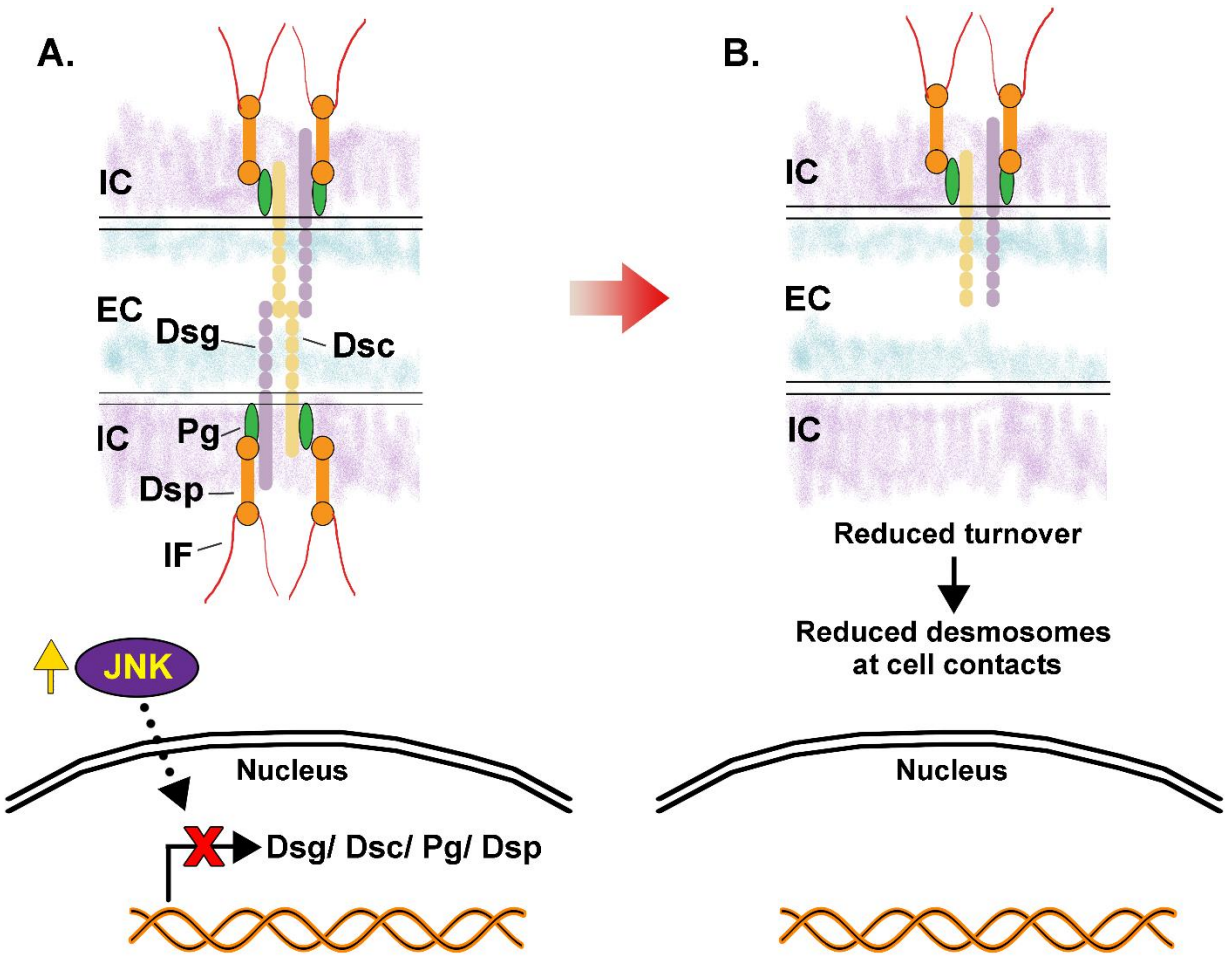

Figure 1.22: Model for JNK-mediated regulation of desmosome assembly through transcriptional changes.
(A) Increased JNK activity might lead to reduced expression of desmosomal genes such as desmoglein (Dsg), desmocollin (Dsc), plakoglobin (Pg), and desmoplakin (Dsp). (B) These changes in expression might reduce the number of desmosomes at cell contacts as the embryo develops.

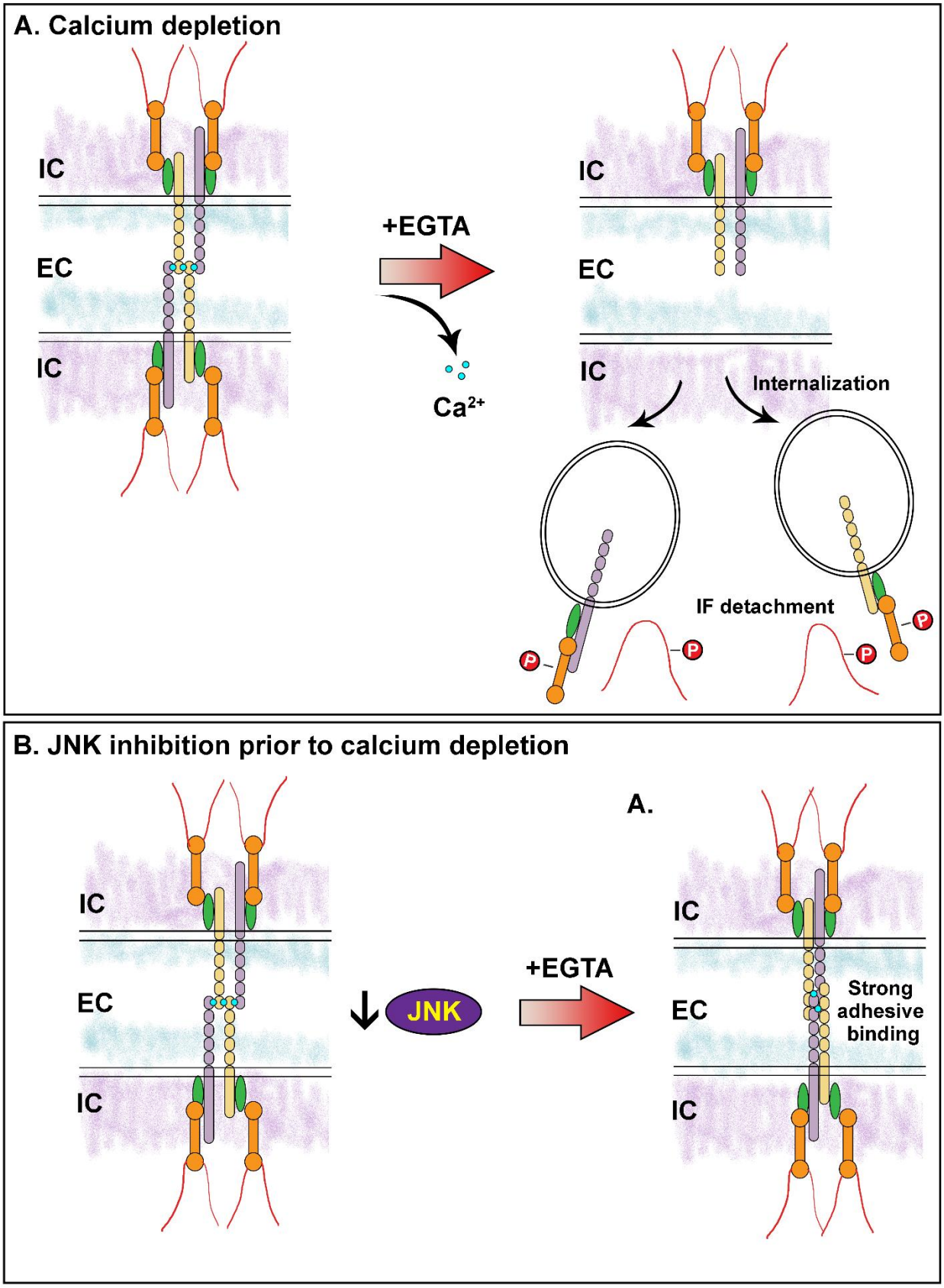
A. Calcium depletion
IC
EC
IC
+EGTA
Ca2+
IC
EC
IC
Internalization
IF detachment
P
P
P
P
B. JNK inhibition prior to calcium depletion
IC
EC
IC
JNK
+EGTA
A.
IC
EC
IC
Strong adhesive binding

Figure 1.23: Model for JNK-mediated regulation of desmosome hyperadhesion.
(A) Exposure to EGTA triggers calcium chelation which results in loss of calcium-dependent binding. (B) Reducing JNK activity prior to EGTA-mediated calcium chelation protects the desmosome from internalization by probably leading to a more organized structure and calcium-independence.

CHAPTER 2: FAST AND EFFICIENT CRISPR/ CAS9 DESIGN FOR GENERATION OF *XENOPUS LAEVIS* DESMOPLAKIN MUTANTS

INTRODUCTION

This protocol presents a method for the generation of desmoplakin (Dsp) mutants in *Xenopus laevis*. First, a gene-specific single guide RNA (sgRNA) was designed and synthesized as a double stranded DNA (dsDNA) template with an RNA polymerase binding site and loop sequence. This template was then transcribed into an oligo containing the sgRNA target site and loop sequence. Then, sgRNA along with Cas9 protein were injected into the embryo at an appropriate developmental stage based on whether whole embryo or tissue-specific targeting is required. DNA was then extracted from F0 mutants and analyzed with the T7 endonuclease I assay to determine if mutations were present. This protocol also describes methods to sequence the sgRNA target site to identify specific mutations.

RELATED INFORMATION

Some methods described here are partially adapted from a protocol used for generating mutants in zebrafish (*Danio rerio*) (Shah et al., 2016). Additional considerations for efficient sgRNA design have been described elsewhere (Doench et al., 2016; Doench et al., 2014; Xu et al., 2015).

MATERIALS

REAGENTS

Agarose gel (3% [w/v] in 1X TAE buffer)

Prepare as 1:1 ratio of regular agarose (1.5% [w/v]) and Super Fine Resolution agarose (1.5% [w/v]). This mix is easier to dissolve and has high resolution.

Alkaline Lysis Buffer (1X)

Prepare fresh from 50X stock (25mM NaOH, 0.2mM Na^{2+}-EDTA).

Cas9 protein

Store at -80°C.

Ethanol (70% [w/v], prepared in nuclease-free water)

Lithium chloride precipitation solution

Store at -20°C.

MEGAscript T7 transcription kit

Store at -20°C.

Modified Barth's Solution (MBS) (0.1X)

Na^{2+}-EDTA (0.25M)

NEBuffer 2 (10X)

Neutralization buffer (1X)

Prepare fresh from 50X stock (40mM Tris-HCl).

Nuclease-free water

PCR product purification kit

Phusion PCR Master Mix

Store at -20°C.

Scaffold Oligo (PAGE purified)

5'-

GATCCGCACCGACTCGGTGCCACTTTTTCAAGTTGATAACGGACTAGCCTTATTTTA

ACTTGCTATTTCTAGCTCTAAAAC-3'

T7 endonuclease I (M0302, NEB) *Store at -20°C.*

This is used to detect heteroduplex DNA resulting from CRISPR/ Cas9-mediated mutagenesis.

Xenopus laevis embryos, stage of interest

Embryo jelly coat must be removed completely prior to microinjection. See ***Dejellying Xenopus laevis Embryos (Sive et al., 2007)*** *for more details.*

EQUIPMENT

Dissecting or stereoscopic microscope

Equipment for injecting *Xenopus* embryos

see **Microinjection of *Xenopus* Embryos (Sive et al., 2010)**.

Forceps

Freezer, -20°C and -80°C

Gloves, powder-free

Incubator, 15-23°C

Microcentrifuge

Micropipettors, 2-, 20-, and 100-µl, with corresponding tips

Microwave oven

PCR tubes, 0.2ml, as needed

Petri dishes, polystyrene

Pipette pump

Alternatively, a transfer pipette can be used.

Spectrophotometer

Thermal cycler, with Ramp function

Tissue grinder or pestle (optional; see Step 22)

Vortex mixer

METHOD

A. DESIGN OF GENE- AND HOMOLOG-SPECIFIC sgRNA TEMPLATE

1. Obtain coding sequence in the *Xenopus laevis* genome on Xenbase (xenbase.org).

2. Determine if Dsp is present on the Long (L) and Short (S) chromosomes.

X. laevis *is an allotetraploid, therefore, there are subgenome homologs of Dsp on both the L and S chromosomes (Graf and Kobel, 1991; Session et al., 2016). This step helps in identifying conserved sequence motifs between both subgenome homologs.*

3. Ensure that exons in the coding region of all homologs are present.

Creating mutations in exons can result in successful loss of function. Exons are also preferable because many X. laevis *genes have incompletely sequenced introns (except when proximal to exon boundaries) making them unreliable targets.*

4. Use individual exons as targets in a prediction software and run the program to obtain the most efficient sgRNA(s) against a target region.

The CHOPCHOP tool was used to predict sgRNA targets in Xenopus laevis *(http://chopchop.cbu.uib.no/).The sgRNA sequence generated was a 23 bp oligonucleotide which includes a 3 bp NGG protospacer-adjacent motif (PAM) at the 3' end. The target region was chosen as close to the N-terminus or within well-characterized functional domains (Shi et al., 2015a). In order of preference, the first two nucleotides of this sequence should be GG>GA=GT>GC for efficient transcription by T7 RNA polymerase (Milligan and Uhlenbeck, 1989; Shah et al., 2015). Multiple sgRNAs each targeting different exonic regions were chosen. This ensures specificity of phenotypes (Shah et al., 2016).*

To target one subgenome homolog:

i. Choose an sgRNA with >3nt mismatches between homologs, preferably within 8-12 base pairs proximal to the PAM site.

Alternatively, choose a region not conserved between subgenome homologs. Greater than 5 mismatches can increase off-target mutagenesis (Fu et al., 2013). Therefore, it is always important to determine off-target site binding (for example, by performing a BLAST search).

To target both subgenome homologs:

ii. Choose an sgRNA with <3nt mismatch between homologs.

IMPORTANT: Mismatches should not lie within the PAM sequence or 8-12 base pairs proximal to the PAM site when targeting both homologs.

Alternatively, choose a perfectly matched sgRNA for each homolog which will be injected together. In some cases, type and position of mismatch may either reduce or have no effect on efficiency (Doench et al., 2016). Here, sgRNAs were designed to target two different exons in X. laevis *Dsp (**Chapter 1**, **Table 1.3**).*

B. SYNTHESIS OF sgRNA

As stated above in Section I, the software generates a 5'-$(N)_{20}$-NGG-3' sequence, where NGG is the PAM sequence. This PAM sequence is required for targeted binding and cleavage by Cas9 (Jinek et al., 2012; Sternberg et al., 2014). However, only the 5'-$(N)_{20}$-3' sequence is incorporated into the guide oligo.

5. To the desired sgRNA sequence (without PAM), add AATTAATACGACTCACTATA to the 5' side and GTTTTAGAGCTAGAAATAGC to the 3' side. This will result in an oligo that is 60 bp long (5'-AATTAATACGACTCACTATA-$(N)_{20}$-GTTTTAGAGCTAGAAATAGC-3').

The 5'-AATTAATACGACTCACTATA-3' oligo on the 5' side contains the T7 RNA polymerase minimal promoter sequence to facilitate transcription. The 5'-GTTTTAGAGCTAGAAATAGC-3' oligo on the 3' side is an overlap with the loop-sequence oligo.

6. Order the 60 bp oligo above and the 80 bp scaffold oligo.

Since both oligos are long, PAGE purification was performed to remove smaller oligos that are a byproduct of synthesis. The scaffold oligo partially overlaps with the 60 bp oligo in Step 5 and contains the loop sequence for Cas9 interaction (Hsu et al., 2014; Jinek et al., 2012).

7. Prepare both oligos as 100µM (stock concentration) and 10µM (working concentration) aliquots in nuclease-free water.

Primers can be stored at -20°C. Stocks can even be stored at -80°C with minimal freeze-thaw cycles for longer shelf life.

8. Synthesize the dsDNA template for transcription using the following Reaction mix and Protocol.

Reaction mix:

Reagents	**Volume**
2X Phusion Master Mix	12.5µl
60 bp oligo (10µM)	5µl
80 bp scaffold oligo (10µM)	5µl
Nuclease-free water	2.5µl
Total	**25µl**

Protocol:

i. 98°C for 30s.

ii. (98°C for 10s, 61°C for 10s, 72°C for 15s) X 45 cycles.

iii. 72°C for 5 min.

iv. 4°C hold.

This reaction yields a 120 bp dsDNA PCR product. Optional: Run 1µl on a gel to ensure the product is synthesized and of appropriate size.

9. Clean the PCR product using DNA concentrator columns, eluting and dissolving in the smallest volume of nuclease-free water.

Measure concentration with a spectrophotometer. Ideally, a concentration of 200-300 ng/µl should be achieved.

10. Use the clean PCR product as the template for the RNA *in vitro* transcription (IVT) kit (MEGAscript T7) using ~100ng of the PCR product per reaction. Set up 2 reactions and pool together before next step.

Follow manufacturer's protocol for IVT.

11. Stop the reaction by adding 1µl DNase and incubating at 37°C for 15 minutes.

12. Add 60µl Lithium chloride and 60µl nuclease-free water and incubate at -20°C overnight.

13. Centrifuge at maximum speed at 4°C for 30 minutes.

14. Remove supernatant.

Pellet should be visible. If not, amount may be insufficient. Scale up IVT reaction as required.

15. Add 1ml of freshly-prepared 70% ethanol and centrifuge at maximum speed at 4°C for 10 minutes.

16. Discard ethanol and spin for 10s at maximum speed to remove residual ethanol.

17. Air dry and elute in 7-10µl nuclease-free water.

Optional: Quantify a diluted sample. Store RNA at -80°C.

C. MICROINJECTION OF *XENOPUS* EMBRYOS

We performed titrations of sgRNA and Cas9 protein to rule out toxicity effects in addition to using multiple sgRNAs. The concentrations of sgRNA mentioned here were found to be appropriate for mutagenesis of Dsp. It is also recommended to first perform positive or negative controls

(preferably both) when determining the function of a gene not tested in Xenopus *before. A positive control targets a gene that is thought to be involved in the same process as the gene of interest and allows setting a threshold for phenotypic screening. A negative control targets a gene not involved in that process and provides a measure of natural variability for that phenotype. It can also give information about toxicity or stress effects of the reagents or the injection itself (Shah et al., 2016).*

18. Prepare 830ng/µl aliquots of sgRNA (in nuclease-free water) and 2µg/µl aliquots of Cas9 protein.

Store sgRNA and Cas9 protein at -80°C, avoiding repeated freeze-thaw cycles.

19. On the day of injection, mix Cas9 and sgRNA(s) to final concentration of 750ng/µl (Cas9) and 500ng/µl (sgRNA).

20. Inject ~2nl per embryo at 1-cell stage (1.5ng Cas9 and 1ng sgRNA/ embryo). Perform microinjections as described in **Microinjection of *Xenopus* Embryos (Sive et al., 2010).**

The amount of sgRNA and Cas9 can depend on factors such as functional redundancy, and whether the protein function is cell-autonomous or can be rescued by wild-type cells. For best results, inject and culture embryos in 15°C 0.1X MBS to delay the first mitotic division.
For mosaic embryos, perform injections at 4-cell stage. Alternatively, since fate maps are well-characterized in X. laevis, *perform injections at 16- to 32-cell stage to target only a specific subset*

of cells or tissues (Dale and Slack, 1987; Moody, 1987; Moody and Kline, 1990). Adjust concentrations and injection volumes accordingly.

D. DNA EXTRACTION FROM F0 MUTANT EMBRYOS

*A quick diagnostic test of successful mutation by CRISPR/ Cas9 is the presence of phenotypic changes. Dsp F0 mutants mimicked phenotypes observed in Dsp morphants but at lower prevalence (**Chapter 1**, **Fig. 1.9-1.10**). The tyrosinase genes,* tyra *and* tyrb, *were also targeted to determine the effect on morphology of F0 mutants (Wang et al., 2015). Embryos injected with sgRNAs targeting both* tyra *and* tyrb *developed normally except for defects in pigmentation patterns (**Fig. 2.1B-D**). Similar to reports in (Wang et al., 2015), there was phenotypic variability in the amount of pigmentation lost.*

However, absence of phenotypes suggests a number of explanations. As mentioned above, these may include low mutagenesis rate coupled with rescue by wild-type cells, and unknown functionally-redundant genes. Alternatively, the gene of interest may not be mutated at all. In most cases, DNA will have to be extracted to determine presence of mutations in the genome.

21. Place one embryo per PCR tube on ice. Remove any medium with a pipette.

Here, we use embryos at stage 30-31 (35-38hpf) but use any stage after stage 20 (22hpf) to obtain sufficient quantities of DNA.

22. Add 35µl 1X Alkaline Lysis Buffer and heat at 95°C for 40 minutes.

Alkaline Lysis Buffer should be freshly prepared from 50X stock. Optional: Macerate embryos with a pestle to increase yield.

23. Cool to 4°C.

24. Add 35µl of 1X Neutralization Buffer.

Neutralization Buffer should be freshly prepared from 50X stock.

25. Vortex lightly and store at -20°C. Spin with centrifuge every time before usage.

E. DETECTING MUTATIONS IN THE TARGET SEQUENCE

To confirm that mutations have occurred in the target region, there are a number of methods such as high resolution melting (HRM) analysis and nuclease digest (Restriction Fragment Length Polymorphism). Here, we provide a modified T7 endonuclease I assay from New England Biolabs, Inc. (NEB) for fast and effective mutation analysis. This method relies on the random nature of different indels and heteroduplex formation (Mashal et al., 1995).

26. Amplify the target region with specific primers using the following reaction mix and protocol.

Reaction mix:

Reagents	**Volume**
2X Phusion Master Mix	15µl
Sample DNA	Variable (100ng)
Primers (10µM)	3µl each
Nuclease-free water	To 30µl
Total	**30µl**

Protocol:

i. 98°C for 30s.

ii. (98°C for 5s, 61°C for 10s, 72°C for 20s) X 35 cycles.

iii. 72°C for 120s.

iv. 4°C hold.

Primers should be designed to create products 200bp-1kb in size. Primers should be designed in such a way that the target site is off-center within the amplicon so that digestion produces easily resolvable DNA fragments.

IMPORTANT: At least one primer in the primer pair should be sufficiently different to be able to distinguish between L and S homologs. Additionally, design primers such that amplicons from L and S homologs are also distinctly different sizes to avoid ambiguity. Primer design for an sgRNA

targeting both desmoplakin homologs is provided in ***Table 1.4****. Primer design for an sgRNA targeting both tyrosinase homologs is provided in* ***Table 2.1****.*

27. Clean the PCR product using DNA concentrator columns, eluting and dissolving in nuclease-free water.

28. Measure the concentration using a spectrophotometer.

29. Analyze the purified PCR product for mutations.

Reaction mix:

Reagents	**Volume**
Purified PCR product	Variable (200ng)
10X NEBuffer 2	2µl
Nuclease-free water	To 19µl
Total	**19µl**

Protocol:

i. 95°C for 5 min.

ii. 95°C-85°C @ -2°C/s.

iii. 85°C-25°C @ -0.1°C/s.

iv. 4°C hold.

30. Add 1µl of T7 endonuclease I and incubate at 37°C for 15 min.

31. Stop reaction by adding 1.5µl of 0.25 Na^{2+}-EDTA.

32. Run samples on an agarose gel to identify if mutations are present.

If mutations are not present, only one band of expected size will be observed. If mutations are present, three bands are observed. The largest band is the expected amplicon size of the original target. The remaining two bands are the products of cleavage of unmatched heteroduplexes. Their combined size roughly equals the original size. An example for mutation analysis in the desmoplakin homologs is shown in ***Fig. 1.6****.*

The T7 endonuclease I method is fast and requires no special equipment but does not provide information about the specific nature of the mutation(s). As an alternative, we have also sequenced the total PCR product to determine if mutations are present in the dsp.L *homolog. However, sequencing a heterogeneous mix of templates results in ambiguous base calling (****Fig. 2.2****). Performing colony sequencing or Next Generation Sequencing of the PCR product mix can*

provide the specific nature of the different mutations. The colony sequencing method still only provides a semi-quantitative measure of the mutation frequency. The NGS method is highly quantitative but is also expensive (Shah et al., 2016).

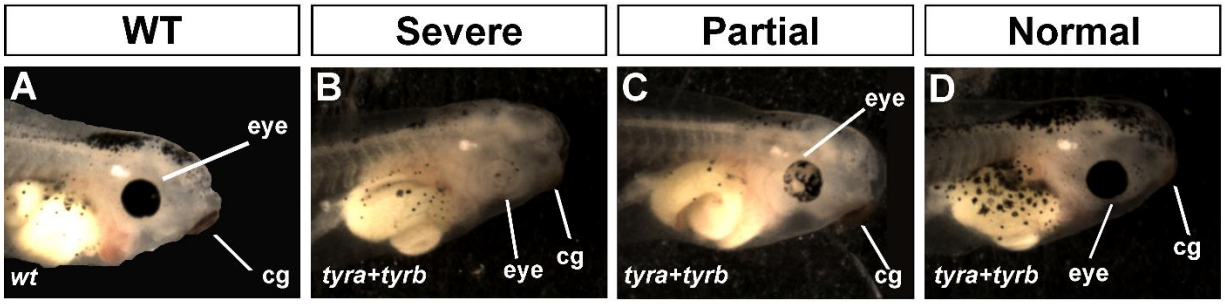

Figure 2.1: CRISPR/ Cas9 targeting of tyrosinase genes resulted in pigmentation defects. (A) Wild-type embryo with normal pigmentation in head and trunk melanocytes and Retinal Pigmented Epithelium of the eye. (B) *tyra+tyrb* CRISPR F0 mutants with severe loss of pigmentation in head and trunk melanocytes and RPE. (C) *tyra+tyrb* CRISPR F0 mutants with partial loss of pigmentation in head and trunk melanocytes and RPE. (D) *tyra+tyrb* CRISPR F0 mutants with relatively normal pigmentation in head and trunk melanocytes and RPE.

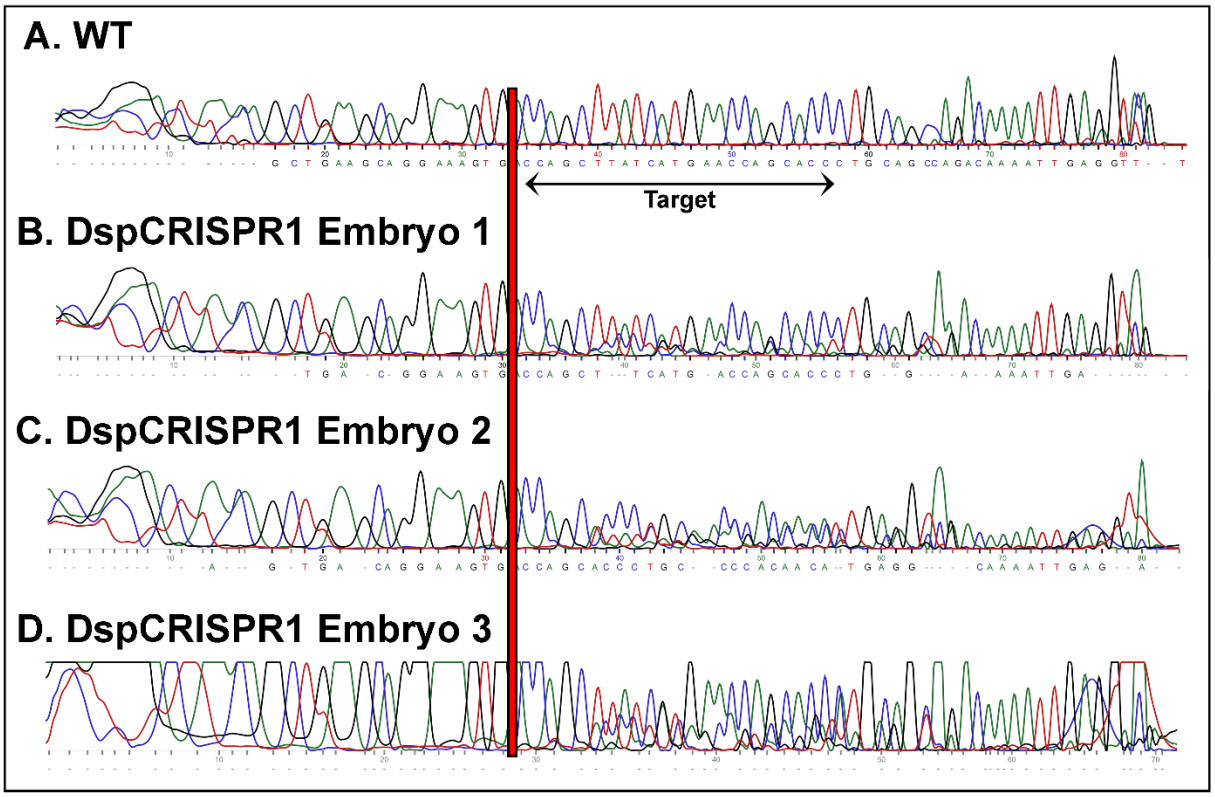

Figure 2.2: CRISPR/ Cas9 induced mutations in target region of desmoplakin gene. (A) Chromatogram of wild-type *dsp.L* homolog within target region of DspCRISPR1 sgRNA. Target sequence is denoted by black double-headed arrow. (B-D) Chromatogram of DspCRISPR1 F0 mutant *dsp.L* homolog within target region of DspCRISPR1 sgRNA in Embryo 1 (B), Embryo 2 (C) and Embryo 3 (D). Red line indicates start position of sgRNA target in all samples. Bases are color-coded as follows: Guanine=Black; Adenine=Green; Cytosine=Blue; Thymine=Red.

Table 2.1: CRISPR gRNA sequences against tyrosinase homologs.

gRNA	**gRNA sequence + PAM** **(5' –> 3')**
Tyra	GGGTCGATGATAGAGAGGAC**TGG**
Tyrb	GGCCCGTAGCAGAGCTGGTG**AGG**

DISCUSSION

Xenopus laevis is an excellent and highly tractable model for the study of developmental processes. Some advantages include large egg size for microinjections, large brood size, and gene conservation. Still, constraints such as allotetraploidy, incompletely annotated genome, and time to reach sexual maturity had presented challenges for the generation of genetic mutants. However, recent developments have helped overcome some of these issues. For instance, open reading frames in the *X. laevis* (and related *X. tropicalis*) genomes are rapidly being annotated on the *Xenopus* genome database, Xenbase. This is tied with the identification of homologs on the Long (L) and Short (S) chromosomes of *X. laevis* in addition to information about expression patterns (Session et al., 2016). These milestones have made it possible to generate mutants and establish mutant lines in *Xenopus* (Shi et al., 2015b).

The CRISPR/ Cas9 genome modification system was developed from an RNA-mediated adaptive defense system naturally present in bacteria and archaea (Jinek et al., 2012; Wiedenheft et al., 2012). Over the last five years, it has been employed for the creation of transgenic tissues and whole organisms (Cong et al., 2013). In comparison to other recent genome-editing techniques such as Zinc-finger nucleases (ZFN) and transcription activator-like effectors nucleases (TALEN), this system has proven to be fast, scalable, and relatively easy to engineer in most laboratories (Christian et al., 2010; Doudna and Charpentier, 2014; Miller et al., 2007; Miller et al., 2011; Porteus and Baltimore, 2003; Wood et al., 2011). It has already been widely used in cells, mice, *Drosophila*, *C. elegans* and zebrafish (Bassett et al., 2014; Friedland et al., 2013; Hisano et al.,

2015; Yang et al., 2014). Until recently, morpholinos and TALENs were utilized for loss-of-function studies and transgenics in zebrafish and *Xenopus* (Christian et al., 2010; Heasman, 2002; Nasevicius and Ekker, 2000). However, the CRISPR/ Cas9 system has been successfully used to generate F0 mutants in *X. tropicalis* and *X. laevis* (Banach et al., 2017; Bhattacharya et al., 2015; Nakayama et al., 2013; Wang et al., 2015). Additionally, other protocols exist for generation of germline mutants in *Xenopus sp*. (Aslan et al., 2017).

In this protocol, we use an established PCR-based system of synthesizing a dsDNA template that is transcribed into the sgRNA with appropriate CRISPR-targeting sequences (Bhattacharya et al., 2015; Shah et al., 2016). This RNA is simply injected along with Cas9 protein into the embryo or oocyte. In comparison to using a plasmid-based delivery system for sgRNA or Cas9 mRNA, this method results in a relatively rapid rate of mutagenesis. Furthermore, the Cas9 protein has reportedly less toxicity than the mRNA (Bhattacharya et al., 2015). Only the 20nt guide RNA will have to be custom-designed for the intended target.

Here, we have targeted the desmosomal structural protein, desmoplakin. A higher concentration of sgRNA was necessary to see phenotypes when targeting *dsp* relative to *tyrosinase*. Similarly, other groups also use lower amounts of sgRNA when targeting *tyrosinase* (Bhattacharya et al., 2015; Wang et al., 2015). This is likely because of the cell-autonomous requirement for *tyrosinase* in melanophores (Cichorek et al., 2013; Iozumi et al., 1993). For instance, there is variability in pigmentation loss in *Xenopus tyrosinase* mutants. Desmoplakin is a structural cell junction protein and therefore desmoplakin loss may be necessary in a large contiguous patch of tissue for phenotypes to be visible. Thus, higher levels of sgRNA could be required due to rescue by neighboring wild-type cells in embryos with low *dsp* mutagenesis efficiency.

We provide a protocol for targeting both subgenome homologs and suggest methods to only target one of the two homologs if desired. Also, steps to design homolog-specific primers for mutation analysis are detailed here. Since the *X. laevis* is allotetraploid, many loci are present as four copies within two ancestral subgenomes (Matsuda et al., 2015; Uno et al., 2013). This may result in lack of phenotypes if both subgenome homologs are not targeted due to potential redundancy. This may not necessarily be the case for genes that have variable expression between subgenomes. An RNAseq transcriptome analysis details this variability between loci (Session et al., 2016). Additionally, some genes exist only as a diploid state on either the 'L' or 'S' chromosome (estimated to be 17-40% of genes) (Hellsten et al., 2007; Session et al., 2016; Uno et al., 2013). Therefore, taking into account these considerations while targeting a specific gene will facilitate efficient mutagenesis.

Xenopus has historically been used extensively as a model to understand vertebrate development. Knowledge about fate maps also makes it suitable for targeted mutagenesis. This protocol can also be potentially used for other CRISPR/ Cas9 applications. For instance, CRISPR/ Cas9 can be used to generate knock-ins in *Xenopus*, which can be used to study the effects of polymorphisms associated with human disease (Aslan et al., 2017). Expressing fusion reporters in *Xenopus* has already been used to study Rho GTPase activity, cell shape changes, and other dynamic processes (Davidson et al., 2008; Stephenson and Miller, 2017). Combining CRISPR/ Cas9 with fusion reporter-knock-in has the potential benefit of stable expression over a longer period of development, although this remains to be tested. Applying transgenic approaches to *Xenopus* can further add to the multitude of advantages already present in this model.

APPENDIX

A.1. MULTIPLE SEQUENCE ALIGNMENT OF DESMOPLAKIN PROTEIN REVEALED HIGHLY SIMILAR FUNCTIONAL DOMAINS

Pairwise alignments of whole desmoplakin protein homologs against *X. laevis* Dsp.L revealed high sequence similarity. Multiple sequence alignments were performed using Clustal Omega against *X. laevis* Dsp.L to visualize the extent of similarity between the homologs (**Fig. A.1**). Overall, the sequences shared large regions of similarity within local stretches. These large motifs correspond to important desmoplakin functional domains. This indicates that the *X. laevis* Dsp.L homolog is largely conserved at the domain level with mammalian counterparts suggesting a shared function.

Desmoplakin multiple sequence alignment across species

Figure A.1: Multiple sequence alignment of desmoplakin protein across species revealed conserved sequence. Multiple sequence alignment of desmoplakin protein sequences in *X. laevis* Dsp.L, human and mouse was performed with Clustal Omega (EMBL-EBI) using the HHalign algorithm. The threshold for shading was set to 50% using the BOXSHADE tool (EMBL-EBI) in the Clustal Omega generated sequence alignment. Start and End amino acid coordinates are marked for all Dsp functional domains, including, Plakin domain, Rod domain, and C-terminal tail domains (A,B,C) using arrowheads. Black shading denotes residues identical to *X. laevis* Dsp.L. Gray shading denotes residues similar to *X. laevis* Dsp.L.

A.2. SEQUENCE ALIGNMENT OF *XENOPUS* DESMOPLAKIN HOMOLOGS REVEALED DIFFERENCES IN EXON NUMBER

While the *X. laevis* S subgenome has experienced more deletions, genes retained on both subgenomes sometimes display differences in gene expression. Such homologous pairs are also predicted to differ in coding sequence length (Session et al., 2016). The *X. laevis* Dsp.S homolog had 96.5% of the length of the Dsp.L homolog. Therefore, alignments of the gene coding regions of *X. laevis* Dsp.L and Dsp.S were performed to determine where the deletions occurred in the coding region. Results revealed that while infrequent mismatches occurred in some regions, a very large gap was present only in Dsp.S (**Fig. A.2**). This gap coincided with exons 11 and 12 of *X. laevis* Dsp.L (**Fig. A.3**). This gap that is observed only in the *X. laevis* S homolog but not the L homolog suggests that ancestral deletions occurred in Dsp.S.

Desmoplakin *X. laevis* homologs mRNA sequence alignment

Figure A.2: Multiple sequence alignment of *Xenopus* desmoplakin protein revealed gap in Dsp.S. Multiple sequence alignment of desmoplakin protein sequences of *X. laevis* Dsp.L and *X. laevis* Dsp.S was performed with Clustal Omega (EMBL-EBI) using the HHalign algorithm. The threshold for shading was set to 50% using the BOXSHADE tool (EMBL-EBI) in the Clustal Omega generated sequence alignment. Black arrowheads denote exon 11 (*X. laevis* Dsp.L). White arrowheads denote exon 12 (*X. laevis* Dsp.L). Black shading denotes residues identical to each other. Gray shading denotes residues similar to each other.

Figure A.3: Multiple sequence alignment of *Xenopus* desmoplakin coding regions revealed gap in Dsp.S. Multiple sequence alignment of desmoplakin coding DNA sequences of *X. laevis* Dsp.L and *X. laevis* Dsp.S was performed with Clustal Omega (EMBL-EBI) using the HHalign algorithm. Black arrowheads denote exon 11 (*X. laevis* Dsp.L). White arrowheads denote exon 12 (*X. laevis* Dsp.L). Asterisk denotes identical residues.

A.3. COMPARATIVE ANALYSIS OF PLAKIN SUBDOMAINS REVEALED SIMILARITY ACROSS SPECIES

The results above revealed a high degree of similarity in plakin, rod and C-terminal domains across species. The plakin domain consists of six spectrin repeats and an Src homology 3 domain (**Fig. A.4**). Therefore, performed pairwise alignments were performed between *X. laevis* Dsp.L and mammalian Dsp homologs to determine the homology of these regions. Results revealed that the SR34 domain of H. *sapiens* and *M. musculus* homologs each shared 88% similarity with the corresponding domain in *X. laevis* Dsp.L (**Table A.1**). The SR56 domain of *H. sapiens* and *M. musculus* homologs each shared 91% similarity with the corresponding domain in *X. laevis* Dsp.L. The SR78 domain of *H. sapiens* and *M. musculus* homologs each shared 70% similarity with the corresponding domain in *X. laevis* Dsp.L. The SR8-CT linker domain of *H. sapiens* and *M. musculus* homologs each shared 77% similarity with the corresponding domain in *X. laevis* Dsp.L. Comparative analysis of plakin subdomains between Dsp.L and Dsp.S also revealed a high level of similarity. An exception was the SR56 subdomain, which only shared 60% similarity. The predicted SH3 domain which lies within was truncated in Dsp.S (**Fig. A.4**).

Together, these results indicate that the plakin subdomains share a high degree of similarity between *X. laevis* Dsp.L and mammalian homologs. The Dsp.L and Dsp.S homologs shared overall high similarity except in one domain. This region is where the deletion in Dsp.S lies and very likely explains the relatively low homology.

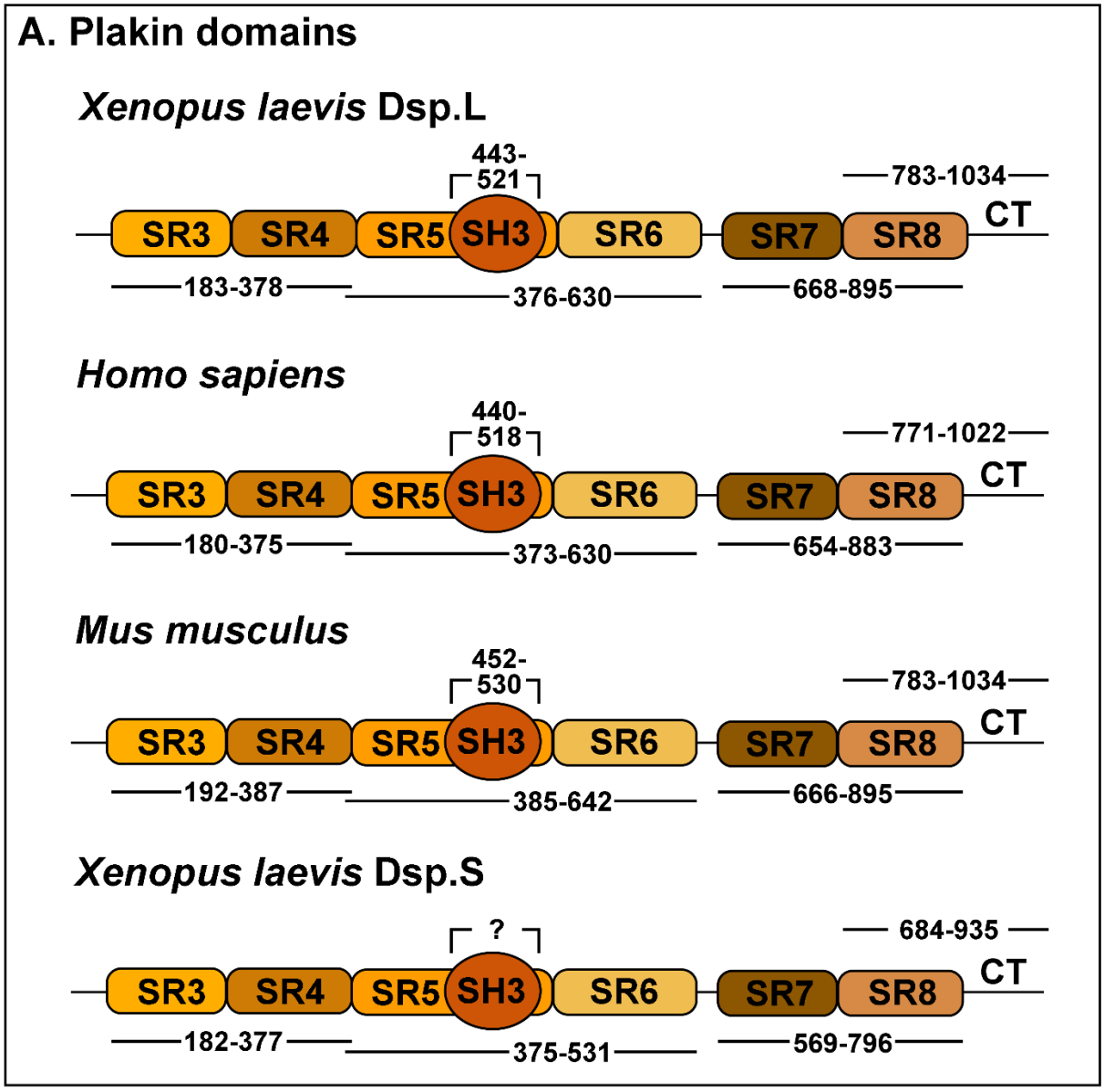

Figure A.4: Comparative bioinformatics analysis of the plakin domain in the desmoplakin protein. (A) Comparative analysis of plakin subdomains in the desmoplakin protein between vertebrate species and the *X. laevis dsp.L* homolog. Numbers below boxes depict amino acid coordinates for each subdomain. SR=Spectrin Repeat; SH3=Src homology 3; CT=C-Terminal region.

Table A.1: Desmoplakin plakin subdomains comparative analysis against *X. laevis* Dsp.L.

Organism	**SR34 %Identity/ Similarity**	**SR56 %Identity/ Similarity**	**SH3 %Identity/ Similarity**	**SR78 %Identity/ Similarity**	**SR8-CT %Identity/ Similarity**
***X. laevis* (Dsp.L)**	100	100	100	100	100
H. sapiens	75.9/88.2	79.1/90.9	79.5/92.3	45.4/70.5	61.8/77.5
M. musculus	75.4/87.7	78.3/90.9	79.5/92.3	45.4/70.0	62.2/77.5
***X. laevis* (Dsp.S)**	94.4/98.5	58.3/59.8	-	94.7/97.8	94.0/96.8

REFERENCES

Adams, M.J., Reichel, M.B., King, I.A., Marsden, M.D., Greenwood, M.D., Thirlwell, H., Arnemann, J., Buxton, R.S., Ali, R.R., 1998. Characterization of the regulatory regions in the human desmoglein genes encoding the pemphigus foliaceous and pemphigus vulgaris antigens. Biochem J 329 (Pt 1), 165-174.

Aebi, U., Häner, M., Troncoso, J., Eichner, R., Engel, A., 1988. Unifying principles in intermediate filament (IF) structure and assembly. Protoplasma 145, 73-81.

Al-Jassar, C., Bernadomicron, P., Chidgey, M., Overduin, M., 2013. Hinged plakin domains provide specialized degrees of articulation in envoplakin, periplakin and desmoplakin. PLoS One 8, e69767.

Al-Jassar, C., Knowles, T., Jeeves, M., Kami, K., Behr, E., Bikker, H., Overduin, M., Chidgey, M., 2011. The nonlinear structure of the desmoplakin plakin domain and the effects of cardiomyopathy-linked mutations. J Mol Biol 411, 1049-1061.

Alberts, B.B., D.; Lewis, J.; Raff, M.; Roberts, K.; Watson, J.D., 1994. Cell junctions, Molecular Biology of the Cell (3rd edn.). Garland Publishing, New York (1994), pp. 950-963.

Allen, E., Yu, Q.C., Fuchs, E., 1996. Mice expressing a mutant desmosomal cadherin exhibit abnormalities in desmosomes, proliferation, and epidermal differentiation. J Cell Biol 133, 1367-1382.

Amagai, M., Fujimori, T., Masunaga, T., Shimizu, H., Nishikawa, T., Shimizu, N., Takeichi, M., Hashimoto, T., 1995a. Delayed assembly of desmosomes in keratinocytes with disrupted classic-cadherin-mediated cell adhesion by a dominant negative mutant. J Invest Dermatol 104, 27-32.

Amagai, M., Ishii, K., Hashimoto, T., Gamou, S., Shimizu, N., Nishikawa, T., 1995b. Conformational epitopes of pemphigus antigens (Dsg1 and Dsg3) are calcium dependent and glycosylation independent. J Invest Dermatol 105, 243-247.

Amagai, M., Klaus-Kovtun, V., Stanley, J.R., 1991. Autoantibodies against a novel epithelial cadherin in pemphigus vulgaris, a disease of cell adhesion. Cell 67, 869-877.

Armstrong, D.K., McKenna, K.E., Purkis, P.E., Green, K.J., Eady, R.A., Leigh, I.M., Hughes, A.E., 1999. Haploinsufficiency of desmoplakin causes a striate subtype of palmoplantar keratoderma. Hum Mol Genet 8, 143-148.

Aslan, Y., Tadjuidje, E., Zorn, A.M., Cha, S.W., 2017. High-efficiency non-mosaic CRISPR-mediated knock-in and indel mutation in F0 Xenopus. Development 144, 2852-2858.

Awad, M.M., Dalal, D., Cho, E., Amat-Alarcon, N., James, C., Tichnell, C., Tucker, A., Russell, S.D., Bluemke, D.A., Dietz, H.C., Calkins, H., Judge, D.P., 2006. DSG2 mutations contribute to arrhythmogenic right ventricular dysplasia/cardiomyopathy. Am J Hum Genet 79, 136-142.

Bagowski, C.P., Xiong, W., Ferrell, J.E., Jr., 2001. c-Jun N-terminal kinase activation in Xenopus laevis eggs and embryos. A possible non-genomic role for the JNK signaling pathway. J Biol Chem 276, 1459-1465.

Banach, M., Edholm, E.S., Robert, J., 2017. Exploring the functions of nonclassical MHC class Ib genes in Xenopus laevis by the CRISPR/Cas9 system. Dev Biol 426, 261-269.

Bass-Zubek, A.E., Hobbs, R.P., Amargo, E.V., Garcia, N.J., Hsieh, S.N., Chen, X., Wahl, J.K., 3rd, Denning, M.F., Green, K.J., 2008. Plakophilin 2: a critical scaffold for PKC alpha that regulates intercellular junction assembly. J Cell Biol 181, 605-613.

Bassett, A.R., Tibbit, C., Ponting, C.P., Liu, J.L., 2014. Mutagenesis and homologous recombination in Drosophila cell lines using CRISPR/Cas9. Biol Open 3, 42-49.

Bazzi, H., Demehri, S., Potter, C.S., Barber, A.G., Awgulewitsch, A., Kopan, R., Christiano, A.M., 2009. Desmoglein 4 is regulated by transcription factors implicated in hair shaft differentiation. Differentiation 78, 292-300.

Beffagna, G., De Bortoli, M., Nava, A., Salamon, M., Lorenzon, A., Zaccolo, M., Mancuso, L., Sigalotti, L., Bauce, B., Occhi, G., Basso, C., Lanfranchi, G., Towbin, J.A., Thiene, G., Danieli, G.A., Rampazzo, A., 2007. Missense mutations in desmocollin-2 N-terminus, associated with arrhythmogenic right ventricular cardiomyopathy, affect intracellular localization of desmocollin-2 in vitro. BMC Med Genet 8, 65.

Bennett, B.L., Sasaki, D.T., Murray, B.W., O'Leary, E.C., Sakata, S.T., Xu, W., Leisten, J.C., Motiwala, A., Pierce, S., Satoh, Y., 2001. SP600125, an anthrapyrazolone inhibitor of Jun N-terminal kinase. Proceedings of the National Academy of Sciences 98, 13681-13686.

Berika, M., Garrod, D., 2014. Desmosomal adhesion in vivo. Cell Commun Adhes 21, 65-75.

Bhattacharya, D., Marfo, C.A., Li, D., Lane, M., Khokha, M.K., 2015. CRISPR/Cas9: An inexpensive, efficient loss of function tool to screen human disease genes in Xenopus. Dev Biol 408, 196-204.

Bierkamp, C., McLaughlin, K.J., Schwarz, H., Huber, O., Kemler, R., 1996. Embryonic heart and skin defects in mice lacking plakoglobin. Dev Biol 180, 780-785.

Billett, F.S., Gould, R.P., 1971. Fine structural changes in the differentiating epidermis of Xenopus laevis embryos. J Anat 108, 465-480.

Blank, J.L., Gerwins, P., Elliott, E.M., Sather, S., Johnson, G.L., 1996. Molecular cloning of mitogen-activated protein/ERK kinase kinases (MEKK) 2 and 3. Regulation of sequential phosphorylation pathways involving mitogen-activated protein kinase and c-Jun kinase. J Biol Chem 271, 5361-5368.

Blum, M., De Robertis, E.M., Wallingford, J.B., Niehrs, C., 2015. Morpholinos: Antisense and Sensibility. Dev Cell 35, 145-149.

Bogoyevitch, M.A., Kobe, B., 2006. Uses for JNK: the many and varied substrates of the c-Jun N-terminal kinases. Microbiol Mol Biol Rev 70, 1061-1095.

Bonne, S., van Hengel, J., Nollet, F., Kools, P., van Roy, F., 1999. Plakophilin-3, a novel armadillo-like protein present in nuclei and desmosomes of epithelial cells. J Cell Sci 112 (Pt 14), 2265-2276.

Bornslaeger, E.A., Corcoran, C.M., Stappenbeck, T.S., Green, K.J., 1996. Breaking the connection: displacement of the desmosomal plaque protein desmoplakin from cell-cell interfaces disrupts anchorage of intermediate filament bundles and alters intercellular junction assembly. J Cell Biol 134, 985-1001.

Borysenko, J.Z., Revel, J.P., 1973. Experimental manipulation of desmosome structure. Am J Anat 137, 403-421.

Bray, S.J., 2006. Notch signalling: a simple pathway becomes complex. Nat Rev Mol Cell Biol 7, 678-689.

Breathnach, A.S., Wyllie, L.M., 1965. Fine structure of cells forming the surface layer of the epidermis in human fetuses at fourteen and twelve weeks. J Invest Dermatol 45, 179-189.

Brooke, M.A., Nitoiu, D., Kelsell, D.P., 2012. Cell-cell connectivity: desmosomes and disease. J Pathol 226, 158-171.

Brooks, E.R., Wallingford, J.B., 2014. Multiciliated cells. Curr Biol 24, R973-982.

Broussard, J.A., Yang, R., Huang, C., Nathamgari, S.S.P., Beese, A.M., Godsel, L.M., Lee, S., Zhou, F., Sniadecki, N.J., Green, K.J., Espinosa, H.D., 2017. The desmoplakin/intermediate filament linkage regulates cell mechanics. Mol Biol Cell.

Bruckner-Tuderman, L., Vogel, A., Ruegger, S., Odermatt, B., Tonz, O., Schnyder, U.W., 1989. Epidermolysis bullosa simplex with mottled pigmentation. J Am Acad Dermatol 21, 425-432.

Butz, S., Stappert, J., Weissig, H., Kemler, R., 1992. Plakoglobin and beta-catenin: distinct but closely related. Science 257, 1142-1144.

Calkins, C.C., Setzer, S.V., Jennings, J.M., Summers, S., Tsunoda, K., Amagai, M., Kowalczyk, A.P., 2006. Desmoglein endocytosis and desmosome disassembly are coordinated responses to pemphigus autoantibodies. J Biol Chem 281, 7623-7634.

Carvajal-Huerta, L., 1998. Epidermolytic palmoplantar keratoderma with woolly hair and dilated cardiomyopathy. J Am Acad Dermatol 39, 418-421.

Celentano, A., Cirillo, N., 2017. Desmosomes in disease: a guide for clinicians. Oral Dis 23, 157-167.

Chain, F.J., Evans, B.J., 2006. Multiple mechanisms promote the retained expression of gene duplicates in the tetraploid frog Xenopus laevis. PLoS Genet 2, e56.

Chalmers, A.D., Strauss, B., Papalopulu, N., 2003. Oriented cell divisions asymmetrically segregate aPKC and generate cell fate diversity in the early Xenopus embryo. Development 130, 2657-2668.

Chan, Y., Anton-Lamprecht, I., Yu, Q.C., Jackel, A., Zabel, B., Ernst, J.P., Fuchs, E., 1994. A human keratin 14 "knockout": the absence of K14 leads to severe epidermolysis bullosa simplex and a function for an intermediate filament protein. Genes Dev 8, 2574-2587.

Chen, J., Den, Z., Koch, P.J., 2008. Loss of desmocollin 3 in mice leads to epidermal blistering. J Cell Sci 121, 2844-2849.

Chen, S.N., Gurha, P., Lombardi, R., Ruggiero, A., Willerson, J.T., Marian, A.J., 2014. The hippo pathway is activated and is a causal mechanism for adipogenesis in arrhythmogenic cardiomyopathy. Circ Res 114, 454-468.

Chen, Z., Yang, A., Xu, C., Xing, Y., Gong, W., Li, J., 2011. c-Jun N-terminal kinase is involved in the regulation of proliferation and apoptosis by integrin-linked kinase in human retinoblastoma cells. Graefes Arch Clin Exp Ophthalmol 249, 1399-1407.

Chidgey, M., Brakebusch, C., Gustafsson, E., Cruchley, A., Hail, C., Kirk, S., Merritt, A., North, A., Tselepis, C., Hewitt, J., Byrne, C., Fassler, R., Garrod, D., 2001. Mice lacking desmocollin 1 show epidermal fragility accompanied by barrier defects and abnormal differentiation. J Cell Biol 155, 821-832.

Chidgey, M., Dawson, C., 2007. Desmosomes: a role in cancer? Br J Cancer 96, 1783-1787.

Chitaev, N.A., Troyanovsky, S.M., 1997. Direct Ca2+-dependent heterophilic interaction between desmosomal cadherins, desmoglein and desmocollin, contributes to cell-cell adhesion. J Cell Biol 138, 193-201.

Choi, H.J., Park-Snyder, S., Pascoe, L.T., Green, K.J., Weis, W.I., 2002. Structures of two intermediate filament-binding fragments of desmoplakin reveal a unique repeat motif structure. Nat Struct Biol 9, 612-620.

Christian, M., Cermak, T., Doyle, E.L., Schmidt, C., Zhang, F., Hummel, A., Bogdanove, A.J., Voytas, D.F., 2010. Targeting DNA double-strand breaks with TAL effector nucleases. Genetics 186, 757-761.

Chun, M.G., Hanahan, D., 2010. Genetic deletion of the desmosomal component desmoplakin promotes tumor microinvasion in a mouse model of pancreatic neuroendocrine carcinogenesis. PLoS Genet 6, e1001120.

Chung, M.I., Kwon, T., Tu, F., Brooks, E.R., Gupta, R., Meyer, M., Baker, J.C., Marcotte, E.M., Wallingford, J.B., 2014. Coordinated genomic control of ciliogenesis and cell movement by RFX2. Elife 3, e01439.

Chung, M.I., Peyrot, S.M., LeBoeuf, S., Park, T.J., McGary, K.L., Marcotte, E.M., Wallingford, J.B., 2012. RFX2 is broadly required for ciliogenesis during vertebrate development. Dev Biol 363, 155-165.

Cibois, M., Scerbo, P., Thomé, V., Pasini, A., Kodjabachian, L., 2014. Induction and differentiation of the Xenopus ciliated embryonic epidermis. Xenopus Development, 112-129.

Cichorek, M., Wachulska, M., Stasiewicz, A., Tyminska, A., 2013. Skin melanocytes: biology and development. Postepy Dermatol Alergol 30, 30-41.

Cirillo, N., Lanza, A., Prime, S.S., 2010. Induction of hyper-adhesion attenuates autoimmune-induced keratinocyte cell-cell detachment and processing of adhesion molecules via mechanisms that involve PKC. Exp Cell Res 316, 580-592.

Clark, I.B., Muha, V., Klingseisen, A., Leptin, M., Muller, H.A., 2011. Fibroblast growth factor signalling controls successive cell behaviours during mesoderm layer formation in Drosophila. Development 138, 2705-2715.

Collins, J.E., Garrod, D., 1994. Molecular biology of desmosomes and hemidesmosomes. RG Landes Company.

Collins, J.E., Legan, P.K., Kenny, T.P., MacGarvie, J., Holton, J.L., Garrod, D.R., 1991. Cloning and sequence analysis of desmosomal glycoproteins 2 and 3 (desmocollins): cadherin-like desmosomal adhesion molecules with heterogeneous cytoplasmic domains. J Cell Biol 113, 381-391.

Conacci-Sorrell, M.E., Ben-Yedidia, T., Shtutman, M., Feinstein, E., Einat, P., Ben-Ze'ev, A., 2002. Nr-CAM is a target gene of the beta-catenin/LEF-1 pathway in melanoma and colon cancer and its expression enhances motility and confers tumorigenesis. Genes Dev 16, 2058-2072.

Cong, L., Ran, F.A., Cox, D., Lin, S., Barretto, R., Habib, N., Hsu, P.D., Wu, X., Jiang, W., Marraffini, L.A., Zhang, F., 2013. Multiplex genome engineering using CRISPR/Cas systems. Science 339, 819-823.

Constant, S.L., Dong, C., Yang, D.D., Wysk, M., Davis, R.J., Flavell, R.A., 2000. JNK1 is required for T cell-mediated immunity against Leishmania major infection. J Immunol 165, 2671-2676.

Conway, J.F., Parry, D.A., 1988. Intermediate filament structure: 3. Analysis of sequence homologies. International Journal of Biological Macromolecules 10, 79-98.

Cowin, P., Kapprell, H.P., Franke, W.W., Tamkun, J., Hynes, R.O., 1986. Plakoglobin: a protein common to different kinds of intercellular adhering junctions. Cell 46, 1063-1073.

Dale, B.A., Holbrook, K.A., Kimball, J.R., Hoff, M., Sun, T.T., 1985. Expression of epidermal keratins and filaggrin during human fetal skin development. J Cell Biol 101, 1257-1269.

Dale, L., Slack, J.M., 1987. Fate map for the 32-cell stage of Xenopus laevis. Development 99, 527-551.

Davidson, L.A., Dzamba, B.D., Keller, R., Desimone, D.W., 2008. Live imaging of cell protrusive activity, and extracellular matrix assembly and remodeling during morphogenesis in the frog, Xenopus laevis. Dev Dyn 237, 2684-2692.

Davis, R.J., 2000. Signal transduction by the JNK group of MAP kinases. Cell 103, 239-252.

Deacon, K., Blank, J.L., 1997. Characterization of the mitogen-activated protein kinase kinase 4 (MKK4)/c-Jun NH2-terminal kinase 1 and MKK3/p38 pathways regulated by MEK kinases 2 and 3. MEK kinase 3 activates MKK3 but does not cause activation of p38 kinase in vivo. J Biol Chem 272, 14489-14496.

Deblandre, G.A., Wettstein, D.A., Koyano-Nakagawa, N., Kintner, C., 1999. A two-step mechanism generates the spacing pattern of the ciliated cells in the skin of Xenopus embryos. Development 126, 4715-4728.

Dehner, C., Rotzer, V., Waschke, J., Spindler, V., 2014. A desmoplakin point mutation with enhanced keratin association ameliorates pemphigus vulgaris autoantibody-mediated loss of cell cohesion. Am J Pathol 184, 2528-2536.

Delgehyr, N., Sillibourne, J., Bornens, M., 2005. Microtubule nucleation and anchoring at the centrosome are independent processes linked by ninein function. J Cell Sci 118, 1565-1575.

Delmar, M., McKenna, W.J., 2010. The cardiac desmosome and arrhythmogenic cardiomyopathies: from gene to disease. Circ Res 107, 700-714.

Delva, E., Jennings, J.M., Calkins, C.C., Kottke, M.D., Faundez, V., Kowalczyk, A.P., 2008. Pemphigus vulgaris IgG-induced desmoglein-3 endocytosis and desmosomal disassembly are mediated by a clathrin- and dynamin-independent mechanism. J Biol Chem 283, 18303-18313.

Delva, E., Tucker, D.K., Kowalczyk, A.P., 2009. The desmosome. Cold Spring Harb Perspect Biol 1, a002543.

DeMarais, A.A., Moon, R.T., 1992. The armadillo homologs beta-catenin and plakoglobin are differentially expressed during early development of Xenopus laevis. Dev Biol 153, 337-346.

Den, Z., Cheng, X., Merched-Sauvage, M., Koch, P.J., 2006. Desmocollin 3 is required for pre-implantation development of the mouse embryo. J Cell Sci 119, 482-489.

Derijard, B., Raingeaud, J., Barrett, T., Wu, I.H., Han, J., Ulevitch, R.J., Davis, R.J., 1995. Independent human MAP-kinase signal transduction pathways defined by MEK and MKK isoforms. Science 267, 682-685.

Dickinson, A.J., 2016. Using frogs faces to dissect the mechanisms underlying human orofacial defects. Semin Cell Dev Biol 51, 54-63.

Dickinson, A.J., Sive, H.L., 2009. The Wnt antagonists Frzb-1 and Crescent locally regulate basement membrane dissolution in the developing primary mouth. Development 136, 1071-1081.

Ding, X., Aoki, V., Mascaro, J.M., Jr., Lopez-Swiderski, A., Diaz, L.A., Fairley, J.A., 1997. Mucosal and mucocutaneous (generalized) pemphigus vulgaris show distinct autoantibody profiles. J Invest Dermatol 109, 592-596.

Doench, J.G., Fusi, N., Sullender, M., Hegde, M., Vaimberg, E.W., Donovan, K.F., Smith, I., Tothova, Z., Wilen, C., Orchard, R., Virgin, H.W., Listgarten, J., Root, D.E., 2016. Optimized sgRNA design to maximize activity and minimize off-target effects of CRISPR-Cas9. Nat Biotechnol 34, 184-191.

Doench, J.G., Hartenian, E., Graham, D.B., Tothova, Z., Hegde, M., Smith, I., Sullender, M., Ebert, B.L., Xavier, R.J., Root, D.E., 2014. Rational design of highly active sgRNAs for CRISPR-Cas9-mediated gene inactivation. Nat Biotechnol 32, 1262-1267.

Dong, C., Davis, R.J., Flavell, R.A., 2001. Signaling by the JNK group of MAP kinases. c-jun N-terminal Kinase. J Clin Immunol 21, 253-257.

Dong, C., Yang, D.D., Tournier, C., Whitmarsh, A.J., Xu, J., Davis, R.J., Flavell, R.A., 2000. JNK is required for effector T-cell function but not for T-cell activation. Nature 405, 91-94.

Dong, C., Yang, D.D., Wysk, M., Whitmarsh, A.J., Davis, R.J., Flavell, R.A., 1998. Defective T cell differentiation in the absence of Jnk1. Science 282, 2092-2095.

Donovan, N., Becker, E.B., Konishi, Y., Bonni, A., 2002. JNK phosphorylation and activation of BAD couples the stress-activated signaling pathway to the cell death machinery. J Biol Chem 277, 40944-40949.

Doudna, J.A., Charpentier, E., 2014. Genome editing. The new frontier of genome engineering with CRISPR-Cas9. Science 346, 1258096.

Dragatsis, I., Efstratiadis, A., Zeitlin, S., 1998. Mouse mutant embryos lacking huntingtin are rescued from lethality by wild-type extraembryonic tissues. Development 125, 1529-1539.

Drysdale, T.A., Elinson, R.P., 1992. Cell Migration and Induction in the Development of the Surface Ectodermal Pattern of the Xenopus laevis Tadpole. Development, Growth & Differentiation 34, 51-59.

Dubaissi, E., Papalopulu, N., 2011. Embryonic frog epidermis: a model for the study of cell-cell interactions in the development of mucociliary disease. Dis Model Mech 4, 179-192.

Dubaissi, E., Rousseau, K., Lea, R., Soto, X., Nardeosingh, S., Schweickert, A., Amaya, E., Thornton, D.J., Papalopulu, N., 2014. A secretory cell type develops alongside multiciliated cells, ionocytes and goblet cells, and provides a protective, anti-infective function in the frog embryonic mucociliary epidermis. Development 141, 1514-1525.

Ducibella, T., Albertini, D.F., Anderson, E., Biggers, J.D., 1975. The preimplantation mammalian embryo: characterization of intercellular junctions and their appearance during development. Dev Biol 45, 231-250.

Duellman, W.E., Trueb, L., 1994. Biology of amphibians. Johns Hopkins University Press, Baltimore.

Eisen, J.S., Smith, J.C., 2008. Controlling morpholino experiments: don't stop making antisense. Development 135, 1735-1743.

Ellinger-Ziegelbauer, H., Brown, K., Kelly, K., Siebenlist, U., 1997. Direct activation of the stress-activated protein kinase (SAPK) and extracellular signal-regulated protein kinase (ERK) pathways by an inducible mitogen-activated protein Kinase/ERK kinase kinase 3 (MEKK) derivative. J Biol Chem 272, 2668-2674.

Eshkind, L., Tian, Q., Schmidt, A., Franke, W.W., Windoffer, R., Leube, R.E., 2002. Loss of desmoglein 2 suggests essential functions for early embryonic development and proliferation of embryonal stem cells. Eur J Cell Biol 81, 592-598.

Evans, B.J., 2008. Genome evolution and speciation genetics of clawed frogs (Xenopus and Silurana). Front Biosci 13, 4687-4706.

Evans, B.J., Kelley, D.B., Tinsley, R.C., Melnick, D.J., Cannatella, D.C., 2004. A mitochondrial DNA phylogeny of African clawed frogs: phylogeography and implications for polyploid evolution. Mol Phylogenet Evol 33, 197-213.

Farquhar, M.G., Palade, G.E., 1963. Junctional complexes in various epithelia. J Cell Biol 17, 375-412.

Farquhar, M.G., Palade, G.E., 1965. Cell junctions in amphibian skin. J Cell Biol 26, 263-291.

Fawcett, S.R., Klymkowsky, M.W., 2004. Embryonic expression of Xenopus laevis SOX7. Gene Expr Patterns 4, 29-33.

Ferreira, D.M., Castro, R.E., Machado, M.V., Evangelista, T., Silvestre, A., Costa, A., Coutinho, J., Carepa, F., Cortez-Pinto, H., Rodrigues, C.M., 2011. Apoptosis and insulin resistance in liver and peripheral tissues of morbidly obese patients is associated with different stages of non-alcoholic fatty liver disease. Diabetologia 54, 1788-1798.

Ferrer, I., Gomez-Isla, T., Puig, B., Freixes, M., Ribe, E., Dalfo, E., Avila, J., 2005. Current advances on different kinases involved in tau phosphorylation, and implications in Alzheimer's disease and tauopathies. Curr Alzheimer Res 2, 3-18.

Fleming, T.P., Garrod, D.R., Elsmore, A.J., 1991. Desmosome biogenesis in the mouse preimplantation embryo. Development 112, 527-539.

Fontao, L., Favre, B., Riou, S., Geerts, D., Jaunin, F., Saurat, J.H., Green, K.J., Sonnenberg, A., Borradori, L., 2003. Interaction of the bullous pemphigoid antigen 1 (BP230) and desmoplakin with intermediate filaments is mediated by distinct sequences within their COOH terminus. Mol Biol Cell 14, 1978-1992.

Fox, H., 1986. Epidermis, Biology of the Integument. Springer, pp. 78-110.

Friedland, A.E., Tzur, Y.B., Esvelt, K.M., Colaiacovo, M.P., Church, G.M., Calarco, J.A., 2013. Heritable genome editing in C. elegans via a CRISPR-Cas9 system. Nat Methods 10, 741-743.

Fu, Y., Foden, J.A., Khayter, C., Maeder, M.L., Reyon, D., Joung, J.K., Sander, J.D., 2013. High-frequency off-target mutagenesis induced by CRISPR-Cas nucleases in human cells. Nat Biotechnol 31, 822-826.

Fuchs, E., Green, H., 1980. Changes in keratin gene expression during terminal differentiation of the keratinocyte. Cell 19, 1033-1042.

Fujita, M., Furukawa, F., Fujii, K., Horiguchi, Y., Takeichi, M., Imamura, S., 1992. Expression of cadherin cell adhesion molecules during human skin development: morphogenesis of epidermis, hair follicles and eccrine sweat ducts. Arch Dermatol Res 284, 159-166.

Furuse, M., Hata, M., Furuse, K., Yoshida, Y., Haratake, A., Sugitani, Y., Noda, T., Kubo, A., Tsukita, S., 2002. Claudin-based tight junctions are crucial for the mammalian epidermal barrier: a lesson from claudin-1-deficient mice. J Cell Biol 156, 1099-1111.

Gallicano, G.I., Bauer, C., Fuchs, E., 2001. Rescuing desmoplakin function in extra-embryonic ectoderm reveals the importance of this protein in embryonic heart, neuroepithelium, skin and vasculature. Development 128, 929-941.

Gallicano, G.I., Kouklis, P., Bauer, C., Yin, M., Vasioukhin, V., Degenstein, L., Fuchs, E., 1998. Desmoplakin is required early in development for assembly of desmosomes and cytoskeletal linkage. J Cell Biol 143, 2009-2022.

Gantress, J., Maniero, G.D., Cohen, N., Robert, J., 2003. Development and characterization of a model system to study amphibian immune responses to iridoviruses. Virology 311, 254-262.

Garriock, R.J., D'Agostino, S.L., Pilcher, K.C., Krieg, P.A., 2005. Wnt11-R, a protein closely related to mammalian Wnt11, is required for heart morphogenesis in Xenopus. Dev Biol 279, 179-192.

Garrod, D., 2010. Desmosomes in vivo. Dermatol Res Pract 2010, 212439.

Garrod, D., Chidgey, M., 2008. Desmosome structure, composition and function. Biochim Biophys Acta 1778, 572-587.

Garrod, D., Kimura, T.E., 2008. Hyper-adhesion: a new concept in cell-cell adhesion. Biochem Soc Trans 36, 195-201.

Garrod, D.R., 1993. Desmosomes and hemidesmosomes. Curr Opin Cell Biol 5, 30-40.

Garrod, D.R., Berika, M.Y., Bardsley, W.F., Holmes, D., Tabernero, L., 2005. Hyper-adhesion in desmosomes: its regulation in wound healing and possible relationship to cadherin crystal structure. J Cell Sci 118, 5743-5754.

Gasteiger, E., Gattiker, A., Hoogland, C., Ivanyi, I., Appel, R.D., Bairoch, A., 2003. ExPASy: The proteomics server for in-depth protein knowledge and analysis. Nucleic Acids Res 31, 3784-3788.

Gazel, A., Banno, T., Walsh, R., Blumenberg, M., 2006. Inhibition of JNK promotes differentiation of epidermal keratinocytes. J Biol Chem 281, 20530-20541.

Gerull, B., Heuser, A., Wichter, T., Paul, M., Basson, C.T., McDermott, D.A., Lerman, B.B., Markowitz, S.M., Ellinor, P.T., MacRae, C.A., Peters, S., Grossmann, K.S., Drenckhahn, J., Michely, B., Sasse-Klaassen, S., Birchmeier, W., Dietz, R., Breithardt, G., Schulze-Bahr, E., Thierfelder, L., 2004. Mutations in the desmosomal protein plakophilin-2 are common in arrhythmogenic right ventricular cardiomyopathy. Nat Genet 36, 1162-1164.

Gerwins, P., Blank, J.L., Johnson, G.L., 1997. Cloning of a novel mitogen-activated protein kinase kinase kinase, MEKK4, that selectively regulates the c-Jun amino terminal kinase pathway. J Biol Chem 272, 8288-8295.

Glise, B., Noselli, S., 1997. Coupling of Jun amino-terminal kinase and Decapentaplegic signaling pathways in Drosophila morphogenesis. Genes Dev 11, 1738-1747.

Godsel, L.M., Hsieh, S.N., Amargo, E.V., Bass, A.E., Pascoe-McGillicuddy, L.T., Huen, A.C., Thorne, M.E., Gaudry, C.A., Park, J.K., Myung, K., Goldman, R.D., Chew, T.L., Green, K.J., 2005. Desmoplakin assembly dynamics in four dimensions: multiple phases differentially regulated by intermediate filaments and actin. J Cell Biol 171, 1045-1059.

Goldie, K.N., Wedig, T., Mitra, A.K., Aebi, U., Herrmann, H., Hoenger, A., 2007. Dissecting the 3-D structure of vimentin intermediate filaments by cryo-electron tomography. J Struct Biol 158, 378-385.

Gonzalez-Mariscal, L., Dominguez-Calderon, A., Raya-Sandino, A., Ortega-Olvera, J.M., Vargas-Sierra, O., Martinez-Revollar, G., 2014. Tight junctions and the regulation of gene expression. Semin Cell Dev Biol 36, 213-223.

Goonesinghe, A., Luan, X.M., Hurlstone, A., Garrod, D., 2012. Desmosomal cadherins in zebrafish epiboly and gastrulation. BMC Dev Biol 12, 1.

Gottardi, C.J., Wong, E., Gumbiner, B.M., 2001. E-cadherin suppresses cellular transformation by inhibiting beta-catenin signaling in an adhesion-independent manner. J Cell Biol 153, 1049-1060.

Goujon, M., McWilliam, H., Li, W., Valentin, F., Squizzato, S., Paern, J., Lopez, R., 2010. A new bioinformatics analysis tools framework at EMBL-EBI. Nucleic Acids Res 38, W695-699.

Graf, J.D., Kobel, H.R., 1991. Genetics of Xenopus laevis. Methods Cell Biol 36, 19-34.

Graser, S., Stierhof, Y.D., Lavoie, S.B., Gassner, O.S., Lamla, S., Le Clech, M., Nigg, E.A., 2007. Cep164, a novel centriole appendage protein required for primary cilium formation. J Cell Biol 179, 321-330.

Green, K.J., Guy, S.G., Cserhalmi-Friedman, P.B., McLean, W.H., Christiano, A.M., Wagner, R.M., 1999. Analysis of the desmoplakin gene reveals striking conservation with other members of the plakin family of cytolinkers. Exp Dermatol 8, 462-470.

Green, K.J., Kowalczyk, A.P., Bornslaeger, E.A., Palka, H.L., Norvell, S.M., 1998. Desmosomes: integrators of mechanical integrity in tissues. Biol Bull 194, 374-376; discussion 376-377.

Green, K.J., Parry, D.A., Steinert, P.M., Virata, M.L., Wagner, R.M., Angst, B.D., Nilles, L.A., 1990. Structure of the human desmoplakins. Implications for function in the desmosomal plaque. J Biol Chem 265, 11406-11407.

Green, K.J., Simpson, C.L., 2007. Desmosomes: new perspectives on a classic. J Invest Dermatol 127, 2499-2515.

Green, K.J., Stappenbeck, T.S., Parry, D.A., Virata, M.L., 1992. Structure of desmoplakin and its association with intermediate filaments. J Dermatol 19, 765-769.

Gulmann, C., Sheehan, K.M., Conroy, R.M., Wulfkuhle, J.D., Espina, V., Mullarkey, M.J., Kay, E.W., Liotta, L.A., Petricoin, E.F., 3rd, 2009. Quantitative cell signalling analysis reveals down-regulation of MAPK pathway activation in colorectal cancer. J Pathol 218, 514-519.

Gumbiner, B., Stevenson, B., Grimaldi, A., 1988. The role of the cell adhesion molecule uvomorulin in the formation and maintenance of the epithelial junctional complex. J Cell Biol 107, 1575-1587.

Gupta, S., Barrett, T., Whitmarsh, A.J., Cavanagh, J., Sluss, H.K., Derijard, B., Davis, R.J., 1996. Selective interaction of JNK protein kinase isoforms with transcription factors. EMBO J 15, 2760-2770.

Hadj-Rabia, S., Baala, L., Vabres, P., Hamel-Teillac, D., Jacquemin, E., Fabre, M., Lyonnet, S., De Prost, Y., Munnich, A., Hadchouel, M., Smahi, A., 2004. Claudin-1 gene mutations in neonatal sclerosing cholangitis associated with ichthyosis: a tight junction disease. Gastroenterology 127, 1386-1390.

Hanakawa, Y., Schechter, N.M., Lin, C., Garza, L., Li, H., Yamaguchi, T., Fudaba, Y., Nishifuji, K., Sugai, M., Amagai, M., Stanley, J.R., 2002. Molecular mechanisms of blister formation in bullous impetigo and staphylococcal scalded skin syndrome. J Clin Invest 110, 53-60.

Hanakawa, Y., Selwood, T., Woo, D., Lin, C., Schechter, N.M., Stanley, J.R., 2003. Calcium-dependent conformation of desmoglein 1 is required for its cleavage by exfoliative toxin. J Invest Dermatol 121, 383-389.

Harland, R.M., Grainger, R.M., 2011. Xenopus research: metamorphosed by genetics and genomics. Trends Genet 27, 507-515.

Haslam, I.S., Roubos, E.W., Mangoni, M.L., Yoshizato, K., Vaudry, H., Kloepper, J.E., Pattwell, D.M., Maderson, P.F., Paus, R., 2014. From frog integument to human skin: dermatological perspectives from frog skin biology. Biol Rev Camb Philos Soc 89, 618-655.

Hatzfeld, M., 2007. Plakophilins: Multifunctional proteins or just regulators of desmosomal adhesion? Biochim Biophys Acta 1773, 69-77.

Hatzfeld, M., Haffner, C., Schulze, K., Vinzens, U., 2000. The function of plakophilin 1 in desmosome assembly and actin filament organization. J Cell Biol 149, 209-222.

Hatzfeld, M., Kristjansson, G.I., Plessmann, U., Weber, K., 1994. Band 6 protein, a major constituent of desmosomes from stratified epithelia, is a novel member of the armadillo multigene family. J Cell Sci 107 (Pt 8), 2259-2270.

Hatzfeld, M., Weber, K., 1990. The coiled coil of in vitro assembled keratin filaments is a heterodimer of type I and II keratins: use of site-specific mutagenesis and recombinant protein expression. J Cell Biol 110, 1199-1210.

Hayes, J.M., Kim, S.K., Abitua, P.B., Park, T.J., Herrington, E.R., Kitayama, A., Grow, M.W., Ueno, N., Wallingford, J.B., 2007. Identification of novel ciliogenesis factors using a new in vivo model for mucociliary epithelial development. Dev Biol 312, 115-130.

He, T., Stepulak, A., Holmstrom, T.H., Omary, M.B., Eriksson, J.E., 2002. The intermediate filament protein keratin 8 is a novel cytoplasmic substrate for c-Jun N-terminal kinase. J Biol Chem 277, 10767-10774.

Heasman, J., 2002. Morpholino oligos: making sense of antisense? Dev Biol 243, 209-214.

Hellsten, U., Khokha, M.K., Grammer, T.C., Harland, R.M., Richardson, P., Rokhsar, D.S., 2007. Accelerated gene evolution and subfunctionalization in the pseudotetraploid frog Xenopus laevis. BMC Biol 5, 31.

Hentula, M., Peltonen, J., Peltonen, S., 2001. Expression profiles of cell-cell and cell-matrix junction proteins in developing human epidermis. Arch Dermatol Res 293, 259-267.

Herrmann, H., Aebi, U., 1998. Structure, assembly, and dynamics of intermediate filaments. Subcell Biochem 31, 319-362.

Herrmann, H., Strelkov, S.V., Burkhard, P., Aebi, U., 2009. Intermediate filaments: primary determinants of cell architecture and plasticity. J Clin Invest 119, 1772-1783.

Higashi, T., Arnold, T.R., Stephenson, R.E., Dinshaw, K.M., Miller, A.L., 2016. Maintenance of the Epithelial Barrier and Remodeling of Cell-Cell Junctions during Cytokinesis. Curr Biol 26, 1829-1842.

Hirai, S., Katoh, M., Terada, M., Kyriakis, J.M., Zon, L.I., Rana, A., Avruch, J., Ohno, S., 1997. MST/MLK2, a member of the mixed lineage kinase family, directly phosphorylates and activates SEK1, an activator of c-Jun N-terminal kinase/stress-activated protein kinase. J Biol Chem 272, 15167-15173.

Hirsch, N., Zimmerman, L.B., Grainger, R.M., 2002. Xenopus, the next generation: X. tropicalis genetics and genomics. Dev Dyn 225, 422-433.

Hisano, Y., Sakuma, T., Nakade, S., Ohga, R., Ota, S., Okamoto, H., Yamamoto, T., Kawahara, A., 2015. Precise in-frame integration of exogenous DNA mediated by CRISPR/Cas9 system in zebrafish. Sci Rep 5, 8841.

Hobbs, R.P., Green, K.J., 2012. Desmoplakin regulates desmosome hyperadhesion. The Journal of investigative dermatology 132, 482-485.

Holbrook, K.A., 1983. The biology of human fetal skin at ages related to prenatal diagnosis. Pediatr Dermatol 1, 97-111.

Holbrook, K.A., Odland, G.F., 1975. The fine structure of developing human epidermis: light, scanning, and transmission electron microscopy of the periderm. J Invest Dermatol 65, 16-38.

Holbrook, K.A., Odland, G.F., 1980. Regional development of the human epidermis in the first trimester embryo and the second trimester fetus (ages related to the timing of amniocentesis and fetal biopsy). J Invest Dermatol 74, 161-168.

Hou, X.S., Goldstein, E.S., Perrimon, N., 1997. Drosophila Jun relays the Jun amino-terminal kinase signal transduction pathway to the Decapentaplegic signal transduction pathway in regulating epithelial cell sheet movement. Genes Dev 11, 1728-1737.

Houssin, N.S., Bharathan, N.K., Turner, S.D., Dickinson, A.J., 2017. Role of JNK during buccopharyngeal membrane perforation, the last step of embryonic mouth formation. Dev Dyn 246, 100-115.

Hsu, P.D., Lander, E.S., Zhang, F., 2014. Development and applications of CRISPR-Cas9 for genome engineering. Cell 157, 1262-1278.

Hu, W., Haamedi, N., Lee, J., Kinoshita, T., Ohnuma, S., 2013. The structure and development of Xenopus laevis cornea. Exp Eye Res 116, 109-128.

Huang, C., Rajfur, Z., Borchers, C., Schaller, M.D., Jacobson, K., 2003. JNK phosphorylates paxillin and regulates cell migration. Nature 424, 219-223.

Huen, A.C., Park, J.K., Godsel, L.M., Chen, X., Bannon, L.J., Amargo, E.V., Hudson, T.Y., Mongiu, A.K., Leigh, I.M., Kelsell, D.P., Gumbiner, B.M., Green, K.J., 2002. Intermediate filament-membrane attachments function synergistically with actin-dependent contacts to regulate intercellular adhesive strength. J Cell Biol 159, 1005-1017.

Hughes, M.K., Hughes, A.L., 1993. Evolution of duplicate genes in a tetraploid animal, Xenopus laevis. Mol Biol Evol 10, 1360-1369.

Hunt, D.M., Rickman, L., Whittock, N.V., Eady, R.A., Simrak, D., Dopping-Hepenstal, P.J., Stevens, H.P., Armstrong, D.K., Hennies, H.C., Kuster, W., Hughes, A.E., Arnemann, J., Leigh, I.M., McGrath, J.A., Kelsell, D.P., Buxton, R.S., 2001. Spectrum of dominant mutations in the desmosomal cadherin desmoglein 1, causing the skin disease striate palmoplantar keratoderma. Eur J Hum Genet 9, 197-203.

Ichijo, H., Nishida, E., Irie, K., ten Dijke, P., Saitoh, M., Moriguchi, T., Takagi, M., Matsumoto, K., Miyazono, K., Gotoh, Y., 1997. Induction of apoptosis by ASK1, a mammalian MAPKKK that activates SAPK/JNK and p38 signaling pathways. Science 275, 90-94.

Ingram, A.J., James, L., Ly, H., Thai, K., Scholey, J.W., 2000. Stretch activation of jun N-terminal kinase/stress-activated protein kinase in mesangial cells. Kidney Int 58, 1431-1439.

Iozumi, K., Hoganson, G.E., Pennella, R., Everett, M.A., Fuller, B.B., 1993. Role of tyrosinase as the determinant of pigmentation in cultured human melanocytes. J Invest Dermatol 100, 806-811.

Ip, Y.T., Davis, R.J., 1998. Signal transduction by the c-Jun N-terminal kinase (JNK)--from inflammation to development. Curr Opin Cell Biol 10, 205-219.

Irvine, A.D., Rugg, E.L., Lane, E.B., Hoare, S., Peret, C., Hughes, A.E., Heagerty, A.H., 2001. Molecular confirmation of the unique phenotype of epidermolysis bullosa simplex with mottled pigmentation. Br J Dermatol 144, 40-45.

Ishibashi, S., Love, N.R., Amaya, E., 2012. A simple method of transgenesis using I-SceI meganuclease in Xenopus. Methods Mol Biol 917, 205-218.

Ishii, K., Amagai, M., Hall, R.P., Hashimoto, T., Takayanagi, A., Gamou, S., Shimizu, N., Nishikawa, T., 1997. Characterization of autoantibodies in pemphigus using antigen-specific enzyme-linked immunosorbent assays with baculovirus-expressed recombinant desmogleins. J Immunol 159, 2010-2017.

Itoh, K., Yamashita, A., Kubota, H.Y., 1988. The expression of epidermal antigens in Xenopus laevis. Development 104, 1-14.

Ivanov, A.I., McCall, I.C., Parkos, C.A., Nusrat, A., 2004a. Role for actin filament turnover and a myosin II motor in cytoskeleton-driven disassembly of the epithelial apical junctional complex. Mol Biol Cell 15, 2639-2651.

Ivanov, A.I., Nusrat, A., Parkos, C.A., 2004b. Endocytosis of epithelial apical junctional proteins by a clathrin-mediated pathway into a unique storage compartment. Mol Biol Cell 15, 176-188.

Jackson, B.W., Grund, C., Winter, S., Franke, W.W., Illmensee, K., 1981. Formation of cytoskeletal elements during mouse embryogenesis. II. Epithelial differentiation and intermediate-sized filaments in early postimplantation embryos. Differentiation 20, 203-216.

Jefferson, J.J., Leung, C.L., Liem, R.K., 2004. Plakins: goliaths that link cell junctions and the cytoskeleton. Nat Rev Mol Cell Biol 5, 542-553.

Jinek, M., Chylinski, K., Fonfara, I., Hauer, M., Doudna, J.A., Charpentier, E., 2012. A programmable dual-RNA-guided DNA endonuclease in adaptive bacterial immunity. Science 337, 816-821.

Johnson, J.L., Najor, N.A., Green, K.J., 2014. Desmosomes: regulators of cellular signaling and adhesion in epidermal health and disease. Cold Spring Harb Perspect Med 4, a015297.

Jolly, P.S., Berkowitz, P., Bektas, M., Lee, H.E., Chua, M., Diaz, L.A., Rubenstein, D.S., 2010. p38MAPK signaling and desmoglein-3 internalization are linked events in pemphigus acantholysis. J Biol Chem 285, 8936-8941.

Jonas, E., Sargent, T.D., Dawid, I.B., 1985. Epidermal keratin gene expressed in embryos of Xenopus laevis. Proc Natl Acad Sci U S A 82, 5413-5417.

Jonkman, M.F., Pasmooij, A.M., Pasmans, S.G., van den Berg, M.P., Ter Horst, H.J., Timmer, A., Pas, H.H., 2005. Loss of desmoplakin tail causes lethal acantholytic epidermolysis bullosa. Am J Hum Genet 77, 653-660.

Jorgensen, K., Davidson, B., Florenes, V.A., 2006. Activation of c-jun N-terminal kinase is associated with cell proliferation and shorter relapse-free period in superficial spreading malignant melanoma. Mod Pathol 19, 1446-1455.

Joung, J.K., Sander, J.D., 2013. TALENs: a widely applicable technology for targeted genome editing. Nat Rev Mol Cell Biol 14, 49-55.

Kane, D.A., McFarland, K.N., Warga, R.M., 2005. Mutations in half baked/E-cadherin block cell behaviors that are necessary for teleost epiboly. Development 132, 1105-1116.

Kapprell, H.P., Owaribe, K., Franke, W.W., 1988. Identification of a basic protein of Mr 75,000 as an accessory desmosomal plaque protein in stratified and complex epithelia. J Cell Biol 106, 1679-1691.

Karin, M., Gallagher, E., 2005. From JNK to pay dirt: jun kinases, their biochemistry, physiology and clinical importance. IUBMB Life 57, 283-295.

Karnovsky, A., Klymkowsky, M.W., 1995. Anterior axis duplication in Xenopus induced by the over-expression of the cadherin-binding protein plakoglobin. Proc Natl Acad Sci U S A 92, 4522-4526.

Kartenbeck, J., Schmelz, M., Franke, W.W., Geiger, B., 1991. Endocytosis of junctional cadherins in bovine kidney epithelial (MDBK) cells cultured in low Ca2+ ion medium. J Cell Biol 113, 881-892.

Katsumi, A., Naoe, T., Matsushita, T., Kaibuchi, K., Schwartz, M.A., 2005. Integrin activation and matrix binding mediate cellular responses to mechanical stretch. J Biol Chem 280, 16546-16549.

Kennedy, A.E., Dickinson, A.J., 2012. Median facial clefts in Xenopus laevis: roles of retinoic acid signaling and homeobox genes. Dev Biol 365, 229-240.

Kharbanda, S., Saxena, S., Yoshida, K., Pandey, P., Kaneki, M., Wang, Q., Cheng, K., Chen, Y.N., Campbell, A., Sudha, T., Yuan, Z.M., Narula, J., Weichselbaum, R., Nalin, C., Kufe, D., 2000. Translocation of SAPK/JNK to mitochondria and interaction with Bcl-x(L) in response to DNA damage. J Biol Chem 275, 322-327.

Kim, K., Lake, B.B., Haremaki, T., Weinstein, D.C., Sokol, S.Y., 2012. Rab11 regulates planar polarity and migratory behavior of multiciliated cells in Xenopus embryonic epidermis. Dev Dyn 241, 1385-1395.

Kimmel, C.B., Ballard, W.W., Kimmel, S.R., Ullmann, B., Schilling, T.F., 1995. Stages of embryonic development of the zebrafish. Dev Dyn 203, 253-310.

Kimura, T.E., Merritt, A.J., Garrod, D.R., 2007. Calcium-independent desmosomes of keratinocytes are hyper-adhesive. J Invest Dermatol 127, 775-781.

Kimura, T.E., Merritt, A.J., Lock, F.R., Eckert, J.J., Fleming, T.P., Garrod, D.R., 2012. Desmosomal adhesiveness is developmentally regulated in the mouse embryo and modulated during trophectoderm migration. Dev Biol 369, 286-297.

Kitagawa, N., Inai, Y., Higuchi, Y., Iida, H., Inai, T., 2014. Inhibition of JNK in HaCaT cells induced tight junction formation with decreased expression of cytokeratin 5, cytokeratin 17 and desmoglein 3. Histochem Cell Biol 142, 389-399.

Klessner, J.L., Desai, B.V., Amargo, E.V., Getsios, S., Green, K.J., 2009. EGFR and ADAMs cooperate to regulate shedding and endocytic trafficking of the desmosomal cadherin desmoglein 2. Mol Biol Cell 20, 328-337.

Kljuic, A., Bazzi, H., Sundberg, J.P., Martinez-Mir, A., O'Shaughnessy, R., Mahoney, M.G., Levy, M., Montagutelli, X., Ahmad, W., Aita, V.M., Gordon, D., Uitto, J., Whiting, D., Ott, J., Fischer, S., Gilliam, T.C., Jahoda, C.A., Morris, R.J., Panteleyev, A.A., Nguyen, V.T., Christiano, A.M., 2003a. Desmoglein 4 in hair follicle differentiation and epidermal adhesion: evidence from inherited hypotrichosis and acquired pemphigus vulgaris. Cell 113, 249-260.

Kljuic, A., Gilead, L., Martinez-Mir, A., Frank, J., Christiano, A.M., Zlotogorski, A., 2003b. A nonsense mutation in the desmoglein 1 gene underlies striate keratoderma. Exp Dermatol 12, 523-527.

Koch, P.J., Mahoney, M.G., Ishikawa, H., Pulkkinen, L., Uitto, J., Shultz, L., Murphy, G.F., Whitaker-Menezes, D., Stanley, J.R., 1997. Targeted disruption of the pemphigus vulgaris antigen (desmoglein 3) gene in mice causes loss of keratinocyte cell adhesion with a phenotype similar to pemphigus vulgaris. J Cell Biol 137, 1091-1102.

Kockel, L., Zeitlinger, J., Staszewski, L.M., Mlodzik, M., Bohmann, D., 1997. Jun in Drosophila development: redundant and nonredundant functions and regulation by two MAPK signal transduction pathways. Genes Dev 11, 1748-1758.

Kofron, M., Heasman, J., Lang, S.A., Wylie, C.C., 2002. Plakoglobin is required for maintenance of the cortical actin skeleton in early Xenopus embryos and for cdc42-mediated wound healing. J Cell Biol 158, 695-708.

Kofron, M., Spagnuolo, A., Klymkowsky, M., Wylie, C., Heasman, J., 1997. The roles of maternal alpha-catenin and plakoglobin in the early Xenopus embryo. Development 124, 1553-1560.

Kok, F.O., Shin, M., Ni, C.W., Gupta, A., Grosse, A.S., van Impel, A., Kirchmaier, B.C., Peterson-Maduro, J., Kourkoulis, G., Male, I., DeSantis, D.F., Sheppard-Tindell, S., Ebarasi, L., Betsholtz, C., Schulte-Merker, S., Wolfe, S.A., Lawson, N.D., 2015. Reverse genetic screening reveals poor correlation between morpholino-induced and mutant phenotypes in zebrafish. Dev Cell 32, 97-108.

Kolly, C., Zakher, A., Strauss, C., Suter, M.M., Muller, E.J., 2007. Keratinocyte transcriptional regulation of the human c-Myc promoter occurs via a novel Lef/Tcf binding element distinct from neoplastic cells. FEBS Lett 581, 1969-1976.

Koster, M.I., Roop, D.R., 2007. Mechanisms regulating epithelial stratification. Annu Rev Cell Dev Biol 23, 93-113.

Kowalczyk, A.P., Bornslaeger, E.A., Borgwardt, J.E., Palka, H.L., Dhaliwal, A.S., Corcoran, C.M., Denning, M.F., Green, K.J., 1997. The amino-terminal domain of desmoplakin binds to plakoglobin and clusters desmosomal cadherin-plakoglobin complexes. J Cell Biol 139, 773-784.

Kowalczyk, A.P., Hatzfeld, M., Bornslaeger, E.A., Kopp, D.S., Borgwardt, J.E., Corcoran, C.M., Settler, A., Green, K.J., 1999. The head domain of plakophilin-1 binds to desmoplakin and

enhances its recruitment to desmosomes. Implications for cutaneous disease. J Biol Chem 274, 18145-18148.

Kowalczyk, A.P., Stappenbeck, T.S., Parry, D.A., Palka, H.L., Virata, M.L., Bornslaeger, E.A., Nilles, L.A., Green, K.J., 1994. Structure and function of desmosomal transmembrane core and plaque molecules. Biophys Chem 50, 97-112.

Kroger, C., Loschke, F., Schwarz, N., Windoffer, R., Leube, R.E., Magin, T.M., 2013. Keratins control intercellular adhesion involving PKC-alpha-mediated desmoplakin phosphorylation. J Cell Biol 201, 681-692.

Krylov, V., Kubickova, S., Rubes, J., Macha, J., Tlapakova, T., Seifertova, E., Sebkova, N., 2010. Preparation of Xenopus tropicalis whole chromosome painting probes using laser microdissection and reconstruction of X. laevis tetraploid karyotype by Zoo-FISH. Chromosome Res 18, 431-439.

Kuan, C.Y., Yang, D.D., Samanta Roy, D.R., Davis, R.J., Rakic, P., Flavell, R.A., 1999. The Jnk1 and Jnk2 protein kinases are required for regional specific apoptosis during early brain development. Neuron 22, 667-676.

Kuhl, M., 2002. Non-canonical Wnt signaling in Xenopus: regulation of axis formation and gastrulation. Semin Cell Dev Biol 13, 243-249.

Kukekov, N.V., Xu, Z., Greene, L.A., 2006. Direct interaction of the molecular scaffolds POSH and JIP is required for apoptotic activation of JNKs. J Biol Chem 281, 15517-15524.

Kupriyanov, S., Baribault, H., 1998. Genetic control of extraembryonic cell lineages studied with tetraploid<-->diploid chimeric concepti. Biochem Cell Biol 76, 1017-1027.

Kuwabara, T., Perkins, D.G., Cogan, D.G., 1976. Sliding of the epithelium in experimental corneal wounds. Invest Ophthalmol 15, 4-14.

Larre, I., Ponce, A., Franco, M., Cereijido, M., 2014. The emergence of the concept of tight junctions and physiological regulation by ouabain. Semin Cell Dev Biol 36, 149-156.

Lechler, T., Fuchs, E., 2005. Asymmetric cell divisions promote stratification and differentiation of mammalian skin. Nature 437, 275-280.

Lechler, T., Fuchs, E., 2007. Desmoplakin: an unexpected regulator of microtubule organization in the epidermis. J Cell Biol 176, 147-154.

Lee, M.H., Koria, P., Qu, J., Andreadis, S.T., 2009. JNK phosphorylates beta-catenin and regulates adherens junctions. FASEB J 23, 3874-3883.

Lei, K., Davis, R.J., 2003. JNK phosphorylation of Bim-related members of the Bcl2 family induces Bax-dependent apoptosis. Proc Natl Acad Sci U S A 100, 2432-2437.

Lei, K., Nimnual, A., Zong, W.X., Kennedy, N.J., Flavell, R.A., Thompson, C.B., Bar-Sagi, D., Davis, R.J., 2002. The Bax subfamily of Bcl2-related proteins is essential for apoptotic signal transduction by c-Jun NH(2)-terminal kinase. Mol Cell Biol 22, 4929-4942.

Lei, Y., Guo, X., Liu, Y., Cao, Y., Deng, Y., Chen, X., Cheng, C.H., Dawid, I.B., Chen, Y., Zhao, H., 2012. Efficient targeted gene disruption in Xenopus embryos using engineered transcription activator-like effector nucleases (TALENs). Proc Natl Acad Sci U S A 109, 17484-17489.

Leung, C.L., Green, K.J., Liem, R.K., 2002. Plakins: a family of versatile cytolinker proteins. Trends Cell Biol 12, 37-45.

Li, W., Cowley, A., Uludag, M., Gur, T., McWilliam, H., Squizzato, S., Park, Y.M., Buso, N., Lopez, R., 2015. The EMBL-EBI bioinformatics web and programmatic tools framework. Nucleic Acids Res 43, W580-584.

Liao, G., Tao, Q., Kofron, M., Chen, J.S., Schloemer, A., Davis, R.J., Hsieh, J.C., Wylie, C., Heasman, J., Kuan, C.Y., 2006. Jun NH2-terminal kinase (JNK) prevents nuclear beta-catenin accumulation and regulates axis formation in Xenopus embryos. Proc Natl Acad Sci U S A 103, 16313-16318.

Lifshitz, T., Levy, J., Cagnano, E., Halevy, S., 2004. Severe conjunctival and eyelid involvement in pemphigus vulgaris. Int Ophthalmol 25, 73-74.

Lin, A., Minden, A., Martinetto, H., Claret, F.X., Lange-Carter, C., Mercurio, F., Johnson, G.L., Karin, M., 1995. Identification of a dual specificity kinase that activates the Jun kinases and p38-Mpk2. Science 268, 286-290.

Liu, S., Zhang, H., Duan, E., 2013. Epidermal development in mammals: key regulators, signals from beneath, and stem cells. Int J Mol Sci 14, 10869-10895.

Lohr, J.L., Yost, H.J., 2000. Vertebrate model systems in the study of early heart development: Xenopus and zebrafish. Am J Med Genet 97, 248-257.

Lourenco, S.V., Kamibeppu, L., Fernandes, J.D., Sotto, M.N., Nico, M.M., 2008. Relationship of adhesion molecules expression with epithelial differentiation markers during fetal skin development. J Cutan Pathol 35, 731-737.

Magnuson, T., Demsey, A., Stackpole, C.W., 1977. Characterization of intercellular junctions in the preimplantation mouse embryo by freeze-fracture and thin-section electron microscopy. Dev Biol 61, 252-261.

Mahoney, M.G., Wang, Z., Rothenberger, K., Koch, P.J., Amagai, M., Stanley, J.R., 1999. Explanations for the clinical and microscopic localization of lesions in pemphigus foliaceus and vulgaris. J Clin Invest 103, 461-468.

Marcozzi, C., Burdett, I.D., Buxton, R.S., Magee, A.I., 1998. Coexpression of both types of desmosomal cadherin and plakoglobin confers strong intercellular adhesion. J Cell Sci 111 (Pt 4), 495-509.

Marsden, M.D., Collins, J.E., Greenwood, M.D., Adams, M.J., Fleming, T.P., Magee, A.I., Buxton, R.S., 1997. Cloning and transcriptional analysis of the promoter of the human type 2 desmocollin gene (DSC2). Gene 186, 237-247.

Mashal, R.D., Koontz, J., Sklar, J., 1995. Detection of mutations by cleavage of DNA heteroduplexes with bacteriophage resolvases. Nat Genet 9, 177-183.

Mathur, M., Goodwin, L., Cowin, P., 1994. Interactions of the cytoplasmic domain of the desmosomal cadherin Dsg1 with plakoglobin. J Biol Chem 269, 14075-14080.

Matsuda, Y., Uno, Y., Kondo, M., Gilchrist, M.J., Zorn, A.M., Rokhsar, D.S., Schmid, M., Taira, M., 2015. A New Nomenclature of Xenopus laevis Chromosomes Based on the Phylogenetic Relationship to Silurana/Xenopus tropicalis. Cytogenet Genome Res 145, 187-191.

Matsui, H., Fukuno, N., Kanda, Y., Kantoh, Y., Chida, T., Nagaura, Y., Suzuki, O., Nishitoh, H., Takeda, K., Ichijo, H., Sawada, Y., Sasaki, K., Kobayashi, T., Tamura, S., 2014. The expression of Fn14 via mechanical stress-activated JNK contributes to apoptosis induction in osteoblasts. J Biol Chem 289, 6438-6450.

Mattey, D.L., Garrod, D.R., 1986. Splitting and internalization of the desmosomes of cultured kidney epithelial cells by reduction in calcium concentration. J Cell Sci 85, 113-124.

Mayerson, P.L., Brumbaugh, J.A., 1981. Lavender, a chick melanocyte mutant with defective melanosome translocation: a possible role for 10 nm filaments and microfilaments but not microtubules. J Cell Sci 51, 25-51.

McCrea, P.D., Turck, C.W., Gumbiner, B., 1991. A homolog of the armadillo protein in Drosophila (plakoglobin) associated with E-cadherin. Science 254, 1359-1361.

McGrath, J.A., 2005. Inherited disorders of desmosomes. Australas J Dermatol 46, 221-229.

McGrath, J.A., McMillan, J.R., Shemanko, C.S., Runswick, S.K., Leigh, I.M., Lane, E.B., Garrod, D.R., Eady, R.A., 1997. Mutations in the plakophilin 1 gene result in ectodermal dysplasia/skin fragility syndrome. Nat Genet 17, 240-244.

McKoy, G., Protonotarios, N., Crosby, A., Tsatsopoulou, A., Anastasakis, A., Coonar, A., Norman, M., Baboonian, C., Jeffery, S., McKenna, W.J., 2000. Identification of a deletion in plakoglobin in arrhythmogenic right ventricular cardiomyopathy with palmoplantar keratoderma and woolly hair (Naxos disease). Lancet 355, 2119-2124.

McMahon, A., Reeves, G.T., Supatto, W., Stathopoulos, A., 2010. Mesoderm migration in Drosophila is a multi-step process requiring FGF signaling and integrin activity. Development 137, 2167-2175.

McMahon, A., Supatto, W., Fraser, S.E., Stathopoulos, A., 2008. Dynamic analyses of Drosophila gastrulation provide insights into collective cell migration. Science 322, 1546-1550.

McWilliam, H., Li, W., Uludag, M., Squizzato, S., Park, Y.M., Buso, N., Cowley, A.P., Lopez, R., 2013. Analysis Tool Web Services from the EMBL-EBI. Nucleic Acids Res 41, W597-600.

Melish, M.E., Glasgow, L.A., 1970. The staphylococcal scalded-skin syndrome. N Engl J Med 282, 1114-1119.

Mengistu, M., Brotzman, H., Ghadiali, S., Lowe-Krentz, L., 2011. Fluid shear stress-induced JNK activity leads to actin remodeling for cell alignment. J Cell Physiol 226, 110-121.

Mertens, C., Kuhn, C., Franke, W.W., 1996. Plakophilins 2a and 2b: constitutive proteins of dual location in the karyoplasm and the desmosomal plaque. J Cell Biol 135, 1009-1025.

Mertens, C., Kuhn, C., Moll, R., Schwetlick, I., Franke, W.W., 1999. Desmosomal plakophilin 2 as a differentiation marker in normal and malignant tissues. Differentiation 64, 277-290.

Messent, A.J., Blissett, M.J., Smith, G.L., North, A.J., Magee, A., Foreman, D., Garrod, D.R., Boulton, M., 2000. Expression of a single pair of desmosomal glycoproteins renders the corneal epithelium unique amongst stratified epithelia. Invest Ophthalmol Vis Sci 41, 8-15.

Miller, J.C., Holmes, M.C., Wang, J., Guschin, D.Y., Lee, Y.L., Rupniewski, I., Beausejour, C.M., Waite, A.J., Wang, N.S., Kim, K.A., Gregory, P.D., Pabo, C.O., Rebar, E.J., 2007. An improved zinc-finger nuclease architecture for highly specific genome editing. Nat Biotechnol 25, 778-785.

Miller, J.C., Tan, S., Qiao, G., Barlow, K.A., Wang, J., Xia, D.F., Meng, X., Paschon, D.E., Leung, E., Hinkley, S.J., Dulay, G.P., Hua, K.L., Ankoudinova, I., Cost, G.J., Urnov, F.D., Zhang, H.S., Holmes, M.C., Zhang, L., Gregory, P.D., Rebar, E.J., 2011. A TALE nuclease architecture for efficient genome editing. Nat Biotechnol 29, 143-148.

Milligan, J.F., Uhlenbeck, O.C., 1989. Synthesis of small RNAs using T7 RNA polymerase. Methods Enzymol 180, 51-62.

Miravet, S., Piedra, J., Castano, J., Raurell, I., Franci, C., Dunach, M., Garcia de Herreros, A., 2003. Tyrosine phosphorylation of plakoglobin causes contrary effects on its association with desmosomes and adherens junction components and modulates beta-catenin-mediated transcription. Mol Cell Biol 23, 7391-7402.

Miravet, S., Piedra, J., Miro, F., Itarte, E., Garcia de Herreros, A., Dunach, M., 2002. The transcriptional factor Tcf-4 contains different binding sites for beta-catenin and plakoglobin. J Biol Chem 277, 1884-1891.

Mitsuyama, K., Suzuki, A., Tomiyasu, N., Tsuruta, O., Kitazaki, S., Takeda, T., Satoh, Y., Bennett, B.L., Toyonaga, A., Sata, M., 2006. Pro-inflammatory signaling by Jun-N-terminal kinase in inflammatory bowel disease. Int J Mol Med 17, 449-455.

Mogensen, M.M., Malik, A., Piel, M., Bouckson-Castaing, V., Bornens, M., 2000. Microtubule minus-end anchorage at centrosomal and non-centrosomal sites: the role of ninein. J Cell Sci 113 (Pt 17), 3013-3023.

Moll, R., Moll, I., Wiest, W., 1982. Changes in the pattern of cytokeratin polypeptides in epidermis and hair follicles during skin development in human fetuses. Differentiation 23, 170-178.

Moody, S.A., 1987. Fates of the blastomeres of the 32-cell-stage Xenopus embryo. Dev Biol 122, 300-319.

Moody, S.A., Kline, M.J., 1990. Segregation of fate during cleavage of frog (Xenopus laevis) blastomeres. Anat Embryol (Berl) 182, 347-362.

Moriguchi, T., Toyoshima, F., Masuyama, N., Hanafusa, H., Gotoh, Y., Nishida, E., 1997. A novel SAPK/JNK kinase, MKK7, stimulated by TNFalpha and cellular stresses. EMBO J 16, 7045-7053.

Morita, H., Heisenberg, C.P., 2013. Holding on and letting go: cadherin turnover in cell intercalation. Dev Cell 24, 567-569.

Mueller, C.A., Seymour, R.S., 2011. The importance of perivitelline fluid convection to oxygen uptake of Pseudophryne bibronii eggs. Physiol Biochem Zool 84, 299-305.

Muhmer, M., Ditthardt, D., Jakel, J., Wischmann, V., Moll, R., Schmidt, A., 2014. An alternative promoter of the human plakophilin-3 gene controls the expression of the new isoform PKP3b. Cell Tissue Res 355, 143-162.

Mun, S.H., Kim, J.W., Nah, S.S., Ko, N.Y., Lee, J.H., Kim, J.D., Kim, D.K., Kim, H.S., Choi, J.D., Kim, S.H., Lee, C.K., Park, S.H., Kim, B.K., Kim, H.S., Kim, Y.M., Choi, W.S., 2009. Tumor necrosis factor alpha-induced interleukin-32 is positively regulated via the Syk/protein kinase Cdelta/JNK pathway in rheumatoid synovial fibroblasts. Arthritis Rheum 60, 678-685.

Nakayama, T., Fish, M.B., Fisher, M., Oomen-Hajagos, J., Thomsen, G.H., Grainger, R.M., 2013. Simple and efficient CRISPR/Cas9-mediated targeted mutagenesis in Xenopus tropicalis. Genesis 51, 835-843.

Nasevicius, A., Ekker, S.C., 2000. Effective targeted gene 'knockdown' in zebrafish. Nat Genet 26, 216-220.

Naydenov, N.G., Hopkins, A.M., Ivanov, A.I., 2009. c-Jun N-terminal kinase mediates disassembly of apical junctions in model intestinal epithelia. Cell Cycle 8, 2110-2121.

Niessen, C.M., 2007. Tight junctions/adherens junctions: basic structure and function. J Invest Dermatol 127, 2525-2532.

Niessen, C.M., Gottardi, C.J., 2008. Molecular components of the adherens junction. Biochim Biophys Acta 1778, 562-571.

Nieuwkoop, P., Faber, J., 1967. Normal table of Xenopus laevis (Daudin): a systematic and chronological survey of the development from the fertilized egg till the end of metamorphosis. North-Holland.

Nishifuji, K., Sugai, M., Amagai, M., 2008. Staphylococcal exfoliative toxins: "molecular scissors" of bacteria that attack the cutaneous defense barrier in mammals. J Dermatol Sci 49, 21-31.

Norgett, E.E., Hatsell, S.J., Carvajal-Huerta, L., Cabezas, J.C., Common, J., Purkis, P.E., Whittock, N., Leigh, I.M., Stevens, H.P., Kelsell, D.P., 2000. Recessive mutation in desmoplakin disrupts desmoplakin-intermediate filament interactions and causes dilated cardiomyopathy, woolly hair and keratoderma. Hum Mol Genet 9, 2761-2766.

Odegaard, E., Staff, A.C., Abeler, V.M., Kopolovic, J., Onsrud, M., Lazarovici, P., Davidson, B., 2007. The activated nerve growth factor receptor p-TrkA is selectively expressed in advanced-stage ovarian carcinoma. Hum Pathol 38, 140-146.

Ohga, R., Shida, M., Shida, H., 2004. Isolation of desmosomes from the epidermis of Xenopus laevis and immunochemical characterization of the Xenopus desmosomal cadherins. Cell Struct Funct 29, 17-26.

Oliver, J., 1944. New directions in renal morphology: A method, its results and its future. Harvey Lectures 40, 102-155.

Park, M.K., Lee, H.J., Shin, J., Noh, M., Kim, S.Y., Lee, C.H., 2011. Novel participation of transglutaminase-2 through c-Jun N-terminal kinase activation in sphingosylphosphorylcholine-induced keratin reorganization of PANC-1 cells. Biochim Biophys Acta 1811, 1021-1029.

Park, T.J., Mitchell, B.J., Abitua, P.B., Kintner, C., Wallingford, J.B., 2008. Dishevelled controls apical docking and planar polarization of basal bodies in ciliated epithelial cells. Nat Genet 40, 871-879.

Parker, A.E., Wheeler, G.N., Arnemann, J., Pidsley, S.C., Ataliotis, P., Thomas, C.L., Rees, D.A., Magee, A.I., Buxton, R.S., 1991. Desmosomal glycoproteins II and III. Cadherin-like junctional molecules generated by alternative splicing. J Biol Chem 266, 10438-10445.

Payne, A.S., Hanakawa, Y., Amagai, M., Stanley, J.R., 2004. Desmosomes and disease: pemphigus and bullous impetigo. Curr Opin Cell Biol 16, 536-543.

Pearl, E.J., Grainger, R.M., Guille, M., Horb, M.E., 2012. Development of Xenopus resource centers: the National Xenopus Resource and the European Xenopus Resource Center. Genesis 50, 155-163.

Peifer, M., Berg, S., Reynolds, A.B., 1994. A repeating amino acid motif shared by proteins with diverse cellular roles. Cell 76, 789-791.

Peifer, M., McCrea, P.D., Green, K.J., Wieschaus, E., Gumbiner, B.M., 1992. The vertebrate adhesive junction proteins beta-catenin and plakoglobin and the Drosophila segment polarity gene armadillo form a multigene family with similar properties. J Cell Biol 118, 681-691.

Pereira, A.M., Tudor, C., Kanger, J.S., Subramaniam, V., Martin-Blanco, E., 2011. Integrin-dependent activation of the JNK signaling pathway by mechanical stress. PLoS One 6, e26182.

Perrais, M., Chen, X., Perez-Moreno, M., Gumbiner, B.M., 2007. E-cadherin homophilic ligation inhibits cell growth and epidermal growth factor receptor signaling independently of other cell interactions. Mol Biol Cell 18, 2013-2025.

Pilichou, K., Nava, A., Basso, C., Beffagna, G., Bauce, B., Lorenzon, A., Frigo, G., Vettori, A., Valente, M., Towbin, J., Thiene, G., Danieli, G.A., Rampazzo, A., 2006. Mutations in desmoglein-2 gene are associated with arrhythmogenic right ventricular cardiomyopathy. Circulation 113, 1171-1179.

Pokutta, S., Weis, W.I., 2007. Structure and mechanism of cadherins and catenins in cell-cell contacts. Annu Rev Cell Dev Biol 23, 237-261.

Porteus, M.H., Baltimore, D., 2003. Chimeric nucleases stimulate gene targeting in human cells. Science 300, 763.

Potter, E., Braun, S., Lehmann, U., Brabant, G., 2001. Molecular cloning of a functional promoter of the human plakoglobin gene. Eur J Endocrinol 145, 625-633.

Pulverer, B.J., Kyriakis, J.M., Avruch, J., Nikolakaki, E., Woodgett, J.R., 1991. Phosphorylation of c-jun mediated by MAP kinases. Nature 353, 670-674.

Pummi, K., Malminen, M., Aho, H., Karvonen, S.L., Peltonen, J., Peltonen, S., 2001. Epidermal tight junctions: ZO-1 and occludin are expressed in mature, developing, and affected skin and in vitro differentiating keratinocytes. J Invest Dermatol 117, 1050-1058.

Quigley, I.K., Stubbs, J.L., Kintner, C., 2011. Specification of ion transport cells in the Xenopus larval skin. Development 138, 705-714.

Rice, P., Longden, I., Bleasby, A., 2000. EMBOSS: the European Molecular Biology Open Software Suite. Trends Genet 16, 276-277.

Riesgo-Escovar, J.R., Hafen, E., 1997. Drosophila Jun kinase regulates expression of decapentaplegic via the ETS-domain protein Aop and the AP-1 transcription factor DJun during dorsal closure. Genes Dev 11, 1717-1727.

Rogers, S.L., Gelfand, V.I., 1998. Myosin cooperates with microtubule motors during organelle transport in melanophores. Curr Biol 8, 161-164.

Roh, J.Y., Stanley, J.R., 1995. Plakoglobin binding by human Dsg3 (pemphigus vulgaris antigen) in keratinocytes requires the cadherin-like intracytoplasmic segment. J Invest Dermatol 104, 720-724.

Roop, D.R., Huitfeldt, H., Kilkenny, A., Yuspa, S.H., 1987. Regulated expression of differentiation-associated keratins in cultured epidermal cells detected by monospecific antibodies to unique peptides of mouse epidermal keratins. Differentiation 35, 143-150.

Roper, K., Gregory, S.L., Brown, N.H., 2002. The 'spectraplakins': cytoskeletal giants with characteristics of both spectrin and plakin families. J Cell Sci 115, 4215-4225.

Rosette, C., Karin, M., 1996. Ultraviolet light and osmotic stress: activation of the JNK cascade through multiple growth factor and cytokine receptors. Science 274, 1194-1197.

Rotzer, V., Hartlieb, E., Vielmuth, F., Gliem, M., Spindler, V., Waschke, J., 2015. E-cadherin and Src associate with extradesmosomal Dsg3 and modulate desmosome assembly and adhesion. Cell Mol Life Sci 72, 4885-4897.

Roux, K.J., Kim, D.I., Burke, B., 2013. BioID: a screen for protein-protein interactions. Curr Protoc Protein Sci 74, Unit 19 23.

Russell, D., Andrews, P.D., James, J., Lane, E.B., 2004. Mechanical stress induces profound remodelling of keratin filaments and cell junctions in epidermolysis bullosa simplex keratinocytes. J Cell Sci 117, 5233-5243.

Sabapathy, K., Hochedlinger, K., Nam, S.Y., Bauer, A., Karin, M., Wagner, E.F., 2004. Distinct roles for JNK1 and JNK2 in regulating JNK activity and c-Jun-dependent cell proliferation. Mol Cell 15, 713-725.

Sabapathy, K., Jochum, W., Hochedlinger, K., Chang, L., Karin, M., Wagner, E.F., 1999. Defective neural tube morphogenesis and altered apoptosis in the absence of both JNK1 and JNK2. Mech Dev 89, 115-124.

Saito, M., Stahley, S.N., Caughman, C.Y., Mao, X., Tucker, D.K., Payne, A.S., Amagai, M., Kowalczyk, A.P., 2012. Signaling dependent and independent mechanisms in pemphigus vulgaris blister formation. PLoS One 7, e50696.

Samak, G., Narayanan, D., Jaggar, J.H., Rao, R., 2011. CaV1.3 channels and intracellular calcium mediate osmotic stress-induced N-terminal c-Jun kinase activation and disruption of tight junctions in Caco-2 CELL MONOLAYERS. J Biol Chem 286, 30232-30243.

Sater, A.K., Moody, S.A., 2017. Using Xenopus to understand human disease and developmental disorders. Genesis 55.

Schempp, C., Emde, M., Wolfle, U., 2009. Dermatology in the Darwin anniversary. Part 1: Evolution of the integument. J Dtsch Dermatol Ges 7, 750-757.

Schett, G., Tohidast-Akrad, M., Smolen, J.S., Schmid, B.J., Steiner, C.W., Bitzan, P., Zenz, P., Redlich, K., Xu, Q., Steiner, G., 2000. Activation, differential localization, and regulation of the stress-activated protein kinases, extracellular signal-regulated kinase, c-JUN N-terminal kinase, and p38 mitogen-activated protein kinase, in synovial tissue and cells in rheumatoid arthritis. Arthritis Rheum 43, 2501-2512.

Schmelz, M., Franke, W.W., 1993. Complexus adhaerentes, a new group of desmoplakin-containing junctions in endothelial cells: the syndesmos connecting retothelial cells of lymph nodes. Eur J Cell Biol 61, 274-289.

Schmelz, M., Moll, R., Kuhn, C., Franke, W.W., 1994. Complexus adhaerentes, a new group of desmoplakin-containing junctions in endothelial cells: II. Different types of lymphatic vessels. Differentiation 57, 97-117.

Schmidt, A., Langbein, L., Rode, M., Pratzel, S., Zimbelmann, R., Franke, W.W., 1997. Plakophilins 1a and 1b: widespread nuclear proteins recruited in specific epithelial cells as desmosomal plaque components. Cell Tissue Res 290, 481-499.

Schmitt, S.M., Gull, M., Brandli, A.W., 2014. Engineering Xenopus embryos for phenotypic drug discovery screening. Adv Drug Deliv Rev 69-70, 225-246.

Sedzinski, J., Hannezo, E., Tu, F., Biro, M., Wallingford, J.B., 2016. Emergence of an Apical Epithelial Cell Surface In Vivo. Dev Cell 36, 24-35.

Sedzinski, J., Hannezo, E., Tu, F., Biro, M., Wallingford, J.B., 2017. RhoA regulates actin network dynamics during apical surface emergence in multiciliated epithelial cells. J Cell Sci 130, 420-428.

Session, A.M., Uno, Y., Kwon, T., Chapman, J.A., Toyoda, A., Takahashi, S., Fukui, A., Hikosaka, A., Suzuki, A., Kondo, M., van Heeringen, S.J., Quigley, I., Heinz, S., Ogino, H., Ochi, H., Hellsten, U., Lyons, J.B., Simakov, O., Putnam, N., Stites, J., Kuroki, Y., Tanaka, T., Michiue, T., Watanabe, M., Bogdanovic, O., Lister, R., Georgiou, G., Paranjpe, S.S., van Kruijsbergen, I., Shu, S., Carlson, J., Kinoshita, T., Ohta, Y., Mawaribuchi, S., Jenkins, J., Grimwood, J., Schmutz, J., Mitros, T., Mozaffari, S.V., Suzuki, Y., Haramoto, Y., Yamamoto, T.S., Takagi, C., Heald, R., Miller, K., Haudenschild, C., Kitzman, J., Nakayama, T., Izutsu, Y., Robert, J., Fortriede, J., Burns, K., Lotay, V., Karimi, K., Yasuoka, Y., Dichmann, D.S., Flajnik, M.F., Houston, D.W., Shendure, J., DuPasquier, L., Vize, P.D., Zorn, A.M., Ito, M., Marcotte, E.M., Wallingford, J.B., Ito, Y., Asashima, M., Ueno, N., Matsuda, Y., Veenstra, G.J., Fujiyama, A., Harland, R.M., Taira, M., Rokhsar, D.S., 2016. Genome evolution in the allotetraploid frog Xenopus laevis. Nature 538, 336-343.

Shah, A.N., Davey, C.F., Whitebirch, A.C., Miller, A.C., Moens, C.B., 2015. Rapid reverse genetic screening using CRISPR in zebrafish. Nat Methods 12, 535-540.

Shah, A.N., Moens, C.B., Miller, A.C., 2016. Targeted candidate gene screens using CRISPR/Cas9 technology. Methods Cell Biol 135, 89-106.

Sheu, H.M., Kitajima, Y., Yaoita, H., 1989. Involvement of protein kinase C in translocation of desmoplakins from cytosol to plasma membrane during desmosome formation in human squamous cell carcinoma cells grown in low to normal calcium concentration. Exp Cell Res 185, 176-190.

Shi, J., Wang, E., Milazzo, J.P., Wang, Z., Kinney, J.B., Vakoc, C.R., 2015a. Discovery of cancer drug targets by CRISPR-Cas9 screening of protein domains. Nat Biotechnol 33, 661-667.

Shi, Z., Wang, F., Cui, Y., Liu, Z., Guo, X., Zhang, Y., Deng, Y., Zhao, H., Chen, Y., 2015b. Heritable CRISPR/Cas9-mediated targeted integration in Xenopus tropicalis. FASEB J 29, 4914-4923.

Shimizu, T., Yabe, T., Muraoka, O., Yonemura, S., Aramaki, S., Hatta, K., Bae, Y.K., Nojima, H., Hibi, M., 2005. E-cadherin is required for gastrulation cell movements in zebrafish. Mech Dev 122, 747-763.

Shoji, M., Iwakami, N., Takeuchi, S., Waragai, M., Suzuki, M., Kanazawa, I., Lippa, C.F., Ono, S., Okazawa, H., 2000. JNK activation is associated with intracellular beta-amyloid accumulation. Brain Res Mol Brain Res 85, 221-233.

Sievers, F., Wilm, A., Dineen, D., Gibson, T.J., Karplus, K., Li, W., Lopez, R., McWilliam, H., Remmert, M., Soding, J., Thompson, J.D., Higgins, D.G., 2011. Fast, scalable generation of high-quality protein multiple sequence alignments using Clustal Omega. Mol Syst Biol 7, 539.

Simcha, I., Shtutman, M., Salomon, D., Zhurinsky, J., Sadot, E., Geiger, B., Ben-Ze'ev, A., 1998. Differential nuclear translocation and transactivation potential of beta-catenin and plakoglobin. J Cell Biol 141, 1433-1448.

Sirour, C., Hidalgo, M., Bello, V., Buisson, N., Darribere, T., Moreau, N., 2011. Dystroglycan is involved in skin morphogenesis downstream of the Notch signaling pathway. Mol Biol Cell 22, 2957-2969.

Sive, H.L., Grainger, R.M., Harland, R.M., 2000. Early development of Xenopus laevis: a laboratory manual.

Slanchev, K., Carney, T.J., Stemmler, M.P., Koschorz, B., Amsterdam, A., Schwarz, H., Hammerschmidt, M., 2009. The epithelial cell adhesion molecule EpCAM is required for epithelial morphogenesis and integrity during zebrafish epiboly and skin development. PLoS Genet 5, e1000563.

Sluss, H.K., Davis, R.J., 1997. Embryonic morphogenesis signaling pathway mediated by JNK targets the transcription factor JUN and the TGF-beta homologue decapentaplegic. J Cell Biochem 67, 1-12.

Smeal, T., Binetruy, B., Mercola, D.A., Birrer, M., Karin, M., 1991. Oncogenic and transcriptional cooperation with Ha-Ras requires phosphorylation of c-Jun on serines 63 and 73. Nature 354, 494-496.

Solnica-Krezel, L., Stemple, D.L., Mountcastle-Shah, E., Rangini, Z., Neuhauss, S.C., Malicki, J., Schier, A.F., Stainier, D.Y., Zwartkruis, F., Abdelilah, S., Driever, W., 1996. Mutations affecting cell fates and cellular rearrangements during gastrulation in zebrafish. Development 123, 67-80.

Song, S., Eckerle, S., Onichtchouk, D., Marrs, J.A., Nitschke, R., Driever, W., 2013. Pou5f1-dependent EGF expression controls E-cadherin endocytosis, cell adhesion, and zebrafish epiboly movements. Dev Cell 24, 486-501.

Spindler, V., Dehner, C., Hubner, S., Waschke, J., 2014. Plakoglobin but not desmoplakin regulates keratinocyte cohesion via modulation of p38MAPK signaling. J Invest Dermatol 134, 1655-1664.

Staehelin, L.A., Hull, B.E., 1978. Junctions between living cells. Sci Am 238, 140-152.

Stahley, S.N., Kowalczyk, A.P., 2015. Desmosomes in acquired disease. Cell Tissue Res 360, 439-456.

Stahley, S.N., Saito, M., Faundez, V., Koval, M., Mattheyses, A.L., Kowalczyk, A.P., 2014. Desmosome assembly and disassembly are membrane raft-dependent. PLoS One 9, e87809.

Stappenbeck, T.S., Bornslaeger, E.A., Corcoran, C.M., Luu, H.H., Virata, M.L., Green, K.J., 1993. Functional analysis of desmoplakin domains: specification of the interaction with keratin versus vimentin intermediate filament networks. J Cell Biol 123, 691-705.

Steinert, P.M., Marekov, L.N., Fraser, R.D., Parry, D.A., 1993. Keratin intermediate filament structure. Crosslinking studies yield quantitative information on molecular dimensions and mechanism of assembly. J Mol Biol 230, 436-452.

Stephenson, R.E., Miller, A.L., 2017. Tools for live imaging of active Rho GTPases in Xenopus. Genesis 55.

Sternberg, S.H., Redding, S., Jinek, M., Greene, E.C., Doudna, J.A., 2014. DNA interrogation by the CRISPR RNA-guided endonuclease Cas9. Nature 507, 62-67.

Stubbs, J.L., Davidson, L., Keller, R., Kintner, C., 2006. Radial intercalation of ciliated cells during Xenopus skin development. Development 133, 2507-2515.

Stubbs, J.L., Oishi, I., Izpisua Belmonte, J.C., Kintner, C., 2008. The forkhead protein Foxj1 specifies node-like cilia in Xenopus and zebrafish embryos. Nat Genet 40, 1454-1460.

Stubbs, J.L., Vladar, E.K., Axelrod, J.D., Kintner, C., 2012. Multicilin promotes centriole assembly and ciliogenesis during multiciliate cell differentiation. Nat Cell Biol 14, 140-147.

Sumigray, K.D., Lechler, T., 2012. Desmoplakin controls microvilli length but not cell adhesion or keratin organization in the intestinal epithelium. Mol Biol Cell 23, 792-799.

Syed, S.E., Trinnaman, B., Martin, S., Major, S., Hutchinson, J., Magee, A.I., 2002. Molecular interactions between desmosomal cadherins. Biochem J 362, 317-327.

Takahashi, H., Ibe, M., Nakamura, S., Ishida-Yamamoto, A., Hashimoto, Y., Iizuka, H., 2002. Extracellular regulated kinase and c-Jun N-terminal kinase are activated in psoriatic involved epidermis. J Dermatol Sci 30, 94-99.

Takekawa, M., Posas, F., Saito, H., 1997. A human homolog of the yeast Ssk2/Ssk22 MAP kinase kinase kinases, MTK1, mediates stress-induced activation of the p38 and JNK pathways. EMBO J 16, 4973-4982.

Tandon, P., Conlon, F., Furlow, J.D., Horb, M.E., 2017. Expanding the genetic toolkit in Xenopus: Approaches and opportunities for human disease modeling. Dev Biol 426, 325-335.

Thakur, A., Wang, X., Siedlak, S.L., Perry, G., Smith, M.A., Zhu, X., 2007. c-Jun phosphorylation in Alzheimer disease. J Neurosci Res 85, 1668-1673.

Thomason, H.A., Cooper, N.H., Ansell, D.M., Chiu, M., Merrit, A.J., Hardman, M.J., Garrod, D.R., 2012. Direct evidence that PKCalpha positively regulates wound re-epithelialization: correlation with changes in desmosomal adhesiveness. J Pathol 227, 346-356.

Thomason, H.A., Scothern, A., McHarg, S., Garrod, D.R., 2010. Desmosomes: adhesive strength and signalling in health and disease. Biochem J 429, 419-433.

Tournier, C., Dong, C., Turner, T.K., Jones, S.N., Flavell, R.A., Davis, R.J., 2001. MKK7 is an essential component of the JNK signal transduction pathway activated by proinflammatory cytokines. Genes Dev 15, 1419-1426.

Tournier, C., Hess, P., Yang, D.D., Xu, J., Turner, T.K., Nimnual, A., Bar-Sagi, D., Jones, S.N., Flavell, R.A., Davis, R.J., 2000. Requirement of JNK for stress-induced activation of the cytochrome c-mediated death pathway. Science 288, 870-874.

Tournier, C., Whitmarsh, A.J., Cavanagh, J., Barrett, T., Davis, R.J., 1997. Mitogen-activated protein kinase kinase 7 is an activator of the c-Jun NH2-terminal kinase. Proc Natl Acad Sci U S A 94, 7337-7342.

Trinkaus, J.P., Lentz, T.L., 1967. Surface specializations of Fundulus cells and their relation to cell movements during gastrulation. J Cell Biol 32, 139-153.

Troyanovsky, S.M., Troyanovsky, R.B., Eshkind, L.G., Leube, R.E., Franke, W.W., 1994. Identification of amino acid sequence motifs in desmocollin, a desmosomal glycoprotein, that are required for plakoglobin binding and plaque formation. Proc Natl Acad Sci U S A 91, 10790-10794.

Tselepis, C., Chidgey, M., North, A., Garrod, D., 1998. Desmosomal adhesion inhibits invasive behavior. Proc Natl Acad Sci U S A 95, 8064-8069.

Tsunoda, K., Ota, T., Aoki, M., Yamada, T., Nagai, T., Nakagawa, T., Koyasu, S., Nishikawa, T., Amagai, M., 2003. Induction of pemphigus phenotype by a mouse monoclonal antibody against the amino-terminal adhesive interface of desmoglein 3. J Immunol 170, 2170-2178.

Tucker, D.K., Stahley, S.N., Kowalczyk, A.P., 2014. Plakophilin-1 Protects Keratinocytes from Pemphigus Vulgaris IgG by Forming Calcium-Independent Desmosomes. Journal of Investigative Dermatology 134, 1033-1043.

Tuma, M.C., Zill, A., Le Bot, N., Vernos, I., Gelfand, V., 1998. Heterotrimeric kinesin II is the microtubule motor protein responsible for pigment dispersion in Xenopus melanophores. J Cell Biol 143, 1547-1558.

Tymowska, J., Kobel, H.R., 1972. Karyotype analysis of Xenopus muelleri (Peters) and Xenopus laevis (Daudin), Pipidae. Cytogenetics 11, 270-278.

Uno, Y., Nishida, C., Takagi, C., Ueno, N., Matsuda, Y., 2013. Homoeologous chromosomes of Xenopus laevis are highly conserved after whole-genome duplication. Heredity (Edinb) 111, 430-436.

Uttam, J., Hutton, E., Coulombe, P.A., Anton-Lamprecht, I., Yu, Q.C., Gedde-Dahl, T., Jr., Fine, J.D., Fuchs, E., 1996. The genetic basis of epidermolysis bullosa simplex with mottled pigmentation. Proc Natl Acad Sci U S A 93, 9079-9084.

van Tintelen, J.P., Entius, M.M., Bhuiyan, Z.A., Jongbloed, R., Wiesfeld, A.C., Wilde, A.A., van der Smagt, J., Boven, L.G., Mannens, M.M., van Langen, I.M., Hofstra, R.M., Otterspoor, L.C., Doevendans, P.A., Rodriguez, L.M., van Gelder, I.C., Hauer, R.N., 2006. Plakophilin-2 mutations are the major determinant of familial arrhythmogenic right ventricular dysplasia/cardiomyopathy. Circulation 113, 1650-1658.

Vasioukhin, V., Bowers, E., Bauer, C., Degenstein, L., Fuchs, E., 2001. Desmoplakin is essential in epidermal sheet formation. Nat Cell Biol 3, 1076-1085.

Virata, M.L., Wagner, R.M., Parry, D.A., Green, K.J., 1992. Molecular structure of the human desmoplakin I and II amino terminus. Proc Natl Acad Sci U S A 89, 544-548.

Walck-Shannon, E., Hardin, J., 2014. Cell intercalation from top to bottom. Nat Rev Mol Cell Biol 15, 34-48.

Wall, S.M., 2005. Recent advances in our understanding of intercalated cells. Curr Opin Nephrol Hypertens 14, 480-484.

Wallis, S., Lloyd, S., Wise, I., Ireland, G., Fleming, T.P., Garrod, D., 2000. The alpha isoform of protein kinase C is involved in signaling the response of desmosomes to wounding in cultured epithelial cells. Mol Biol Cell 11, 1077-1092.

Wan, H., South, A.P., Hart, I.R., 2007. Increased keratinocyte proliferation initiated through downregulation of desmoplakin by RNA interference. Exp Cell Res 313, 2336-2344.

Wang, F., Shi, Z., Cui, Y., Guo, X., Shi, Y.B., Chen, Y., 2015. Targeted gene disruption in Xenopus laevis using CRISPR/Cas9. Cell Biosci 5, 15.

Wang, Q., Margolis, B., 2007. Apical junctional complexes and cell polarity. Kidney Int 72, 1448-1458.

Wang, X., Chao, L., Li, X., Ma, G., Chen, L., Zang, Y., Zhou, G., 2010. Elevated expression of phosphorylated c-Jun NH2-terminal kinase in basal-like and "triple-negative" breast cancers. Hum Pathol 41, 401-406.

Wang, X.S., Diener, K., Jannuzzi, D., Trollinger, D., Tan, T.H., Lichenstein, H., Zukowski, M., Yao, Z., 1996. Molecular cloning and characterization of a novel protein kinase with a catalytic domain homologous to mitogen-activated protein kinase kinase kinase. J Biol Chem 271, 31607-31611.

Warkman, A.S., Krieg, P.A., 2007. Xenopus as a model system for vertebrate heart development. Semin Cell Dev Biol 18, 46-53.

Wasmeier, C., Hume, A.N., Bolasco, G., Seabra, M.C., 2008. Melanosomes at a glance. J Cell Sci 121, 3995-3999.

Watt, F.M., Mattey, D.L., Garrod, D.R., 1984. Calcium-induced reorganization of desmosomal components in cultured human keratinocytes. J Cell Biol 99, 2211-2215.

Wei, S.Y., Escudero, L.M., Yu, F., Chang, L.H., Chen, L.Y., Ho, Y.H., Lin, C.M., Chou, C.S., Chia, W., Modolell, J., Hsu, J.C., 2005. Echinoid is a component of adherens junctions that cooperates with DE-Cadherin to mediate cell adhesion. Dev Cell 8, 493-504.

Werner, M.E., Mitchell, J.W., Putzbach, W., Bacon, E., Kim, S.K., Mitchell, B.J., 2014. Radial intercalation is regulated by the Par complex and the microtubule-stabilizing protein CLAMP/Spef1. J Cell Biol 206, 367-376.

Weston, C.R., Wong, A., Hall, J.P., Goad, M.E., Flavell, R.A., Davis, R.J., 2004. The c-Jun NH2-terminal kinase is essential for epidermal growth factor expression during epidermal morphogenesis. Proc Natl Acad Sci U S A 101, 14114-14119.

Whittock, N.V., Ashton, G.H., Dopping-Hepenstal, P.J., Gratian, M.J., Keane, F.M., Eady, R.A., McGrath, J.A., 1999. Striate palmoplantar keratoderma resulting from desmoplakin haploinsufficiency. J Invest Dermatol 113, 940-946.

Whittock, N.V., Wan, H., Morley, S.M., Garzon, M.C., Kristal, L., Hyde, P., McLean, W.H., Pulkkinen, L., Uitto, J., Christiano, A.M., Eady, R.A., McGrath, J.A., 2002. Compound heterozygosity for non-sense and mis-sense mutations in desmoplakin underlies skin fragility/woolly hair syndrome. J Invest Dermatol 118, 232-238.

Wiedenheft, B., Sternberg, S.H., Doudna, J.A., 2012. RNA-guided genetic silencing systems in bacteria and archaea. Nature 482, 331-338.

Williamson, L., Raess, N.A., Caldelari, R., Zakher, A., de Bruin, A., Posthaus, H., Bolli, R., Hunziker, T., Suter, M.M., Muller, E.J., 2006. Pemphigus vulgaris identifies plakoglobin as key suppressor of c-Myc in the skin. EMBO J 25, 3298-3309.

Wilson, P., Keller, R., 1991. Cell rearrangement during gastrulation of Xenopus: direct observation of cultured explants. Development 112, 289-300.

Wilson, P.A., Hemmati-Brivanlou, A., 1995. Induction of epidermis and inhibition of neural fate by Bmp-4. Nature 376, 331-333.

Wood, A.J., Lo, T.W., Zeitler, B., Pickle, C.S., Ralston, E.J., Lee, A.H., Amora, R., Miller, J.C., Leung, E., Meng, X., Zhang, L., Rebar, E.J., Gregory, P.D., Urnov, F.D., Meyer, B.J., 2011. Targeted genome editing across species using ZFNs and TALENs. Science 333, 307.

Wu, X., Bowers, B., Rao, K., Wei, Q., Hammer, J.A., 3rd, 1998. Visualization of melanosome dynamics within wild-type and dilute melanocytes suggests a paradigm for myosin V function In vivo. J Cell Biol 143, 1899-1918.

Xu, H., Xiao, T., Chen, C.H., Li, W., Meyer, C.A., Wu, Q., Wu, D., Cong, L., Zhang, F., Liu, J.S., Brown, M., Liu, X.S., 2015. Sequence determinants of improved CRISPR sgRNA design. Genome Res 25, 1147-1157.

Xu, Z., Kukekov, N.V., Greene, L.A., 2005. Regulation of apoptotic c-Jun N-terminal kinase signaling by a stabilization-based feed-forward loop. Mol Cell Biol 25, 9949-9959.

Yamamoto, K., Ichijo, H., Korsmeyer, S.J., 1999. BCL-2 is phosphorylated and inactivated by an ASK1/Jun N-terminal protein kinase pathway normally activated at G(2)/M. Mol Cell Biol 19, 8469-8478.

Yamanaka, H., Moriguchi, T., Masuyama, N., Kusakabe, M., Hanafusa, H., Takada, R., Takada, S., Nishida, E., 2002. JNK functions in the non-canonical Wnt pathway to regulate convergent extension movements in vertebrates. EMBO Rep 3, 69-75.

Yan, M., Dai, T., Deak, J.C., Kyriakis, J.M., Zon, L.I., Woodgett, J.R., Templeton, D.J., 1994. Activation of stress-activated protein kinase by MEKK1 phosphorylation of its activator SEK1. Nature 372, 798-800.

Yang, L., Chen, Y., Cui, T., Knosel, T., Zhang, Q., Albring, K.F., Huber, O., Petersen, I., 2012. Desmoplakin acts as a tumor suppressor by inhibition of the Wnt/beta-catenin signaling pathway in human lung cancer. Carcinogenesis 33, 1863-1870.

Yang, L., Yang, J.L., Byrne, S., Pan, J., Church, G.M., 2014. CRISPR/Cas9-Directed Genome Editing of Cultured Cells. Curr Protoc Mol Biol 107, 31 31 31-17.

Yin, T., Getsios, S., Caldelari, R., Godsel, L.M., Kowalczyk, A.P., Muller, E.J., Green, K.J., 2005. Mechanisms of plakoglobin-dependent adhesion: desmosome-specific functions in assembly and regulation by epidermal growth factor receptor. J Biol Chem 280, 40355-40363.

You, H., Padmashali, R.M., Ranganathan, A., Lei, P., Girnius, N., Davis, R.J., Andreadis, S.T., 2013. JNK regulates compliance-induced adherens junctions formation in epithelial cells and tissues. J Cell Sci 126, 2718-2729.

Yu, C.C., Yu, C.H., Hsueh, C.H., Yang, C.T., Juang, J.M., Hwang, J.J., Lin, J.L., Lai, L.P., 2008. Arrhythmogenic right ventricular dysplasia: clinical characteristics and identification of novel desmosome gene mutations. J Formos Med Assoc 107, 548-558.

Yuan, L., Sakamoto, N., Song, G., Sato, M., 2012. Migration of human mesenchymal stem cells under low shear stress mediated by mitogen-activated protein kinase signaling. Stem Cells Dev 21, 2520-2530.

Zhou, F., Narasimhan, V., Shboul, M., Chong, Y.L., Reversade, B., Roy, S., 2015. Gmnc Is a Master Regulator of the Multiciliated Cell Differentiation Program. Curr Biol 25, 3267-3273.

Zhu, X., Raina, A.K., Rottkamp, C.A., Aliev, G., Perry, G., Boux, H., Smith, M.A., 2001. Activation and redistribution of c-jun N-terminal kinase/stress activated protein kinase in degenerating neurons in Alzheimer's disease. J Neurochem 76, 435-441.

Zhurinsky, J., Shtutman, M., Ben-Ze'ev, A., 2000. Plakoglobin and beta-catenin: protein interactions, regulation and biological roles. J Cell Sci 113 (Pt 18), 3127-3139.

Zihni, C., Balda, M.S., Matter, K., 2014. Signalling at tight junctions during epithelial differentiation and microbial pathogenesis. J Cell Sci 127, 3401-3413.

VITA

Navaneetha Krishnan Bharathan was born on January 12, 1990, in Doha, Qatar, and is an Indian citizen. He graduated from St. John's English School and Junior College, Chennai, India in 2007. He received his Bachelor of Technology in Genetic Engineering from SRM University, Chennai, India in 2011, where he was awarded the Gold Medal for his academic achievements. He was awarded the Roscoe D. Hughes Fellowship in 2016 and the Alpha Epsilon Lambda Award in 2017.